Table of Contents

List of Figures

List of Tables

CHAPTER I
INTRODUCTION

1.1: Background

Reinforced concrete structures all over the United States are deteriorating at an alarming rate. The estimated cost to fix all of these structures is between $1 and $3 trillion. Highway bridges are one such concrete structure and have an estimated repair cost of $50 billion. In fact, it has been reported that "over one-quarter of all bridges in the United States are either deficient or obsolete" with damaged bridge decks being the leading reason (Bedard 1992).

The primary reason for this structural deficiency is corrosion of the steel reinforcement within the concrete. This corrosion results in a large increase of volume of the metal, which in turn causes internal stresses in the concrete. These stresses are the cause of deterioration of the structure (Bradberry 2001). In concrete bridge decks, this corrosion is primarily due to either exposure to harsh environments such as high humidity climates and salt-water environments or direct application of de-icing salts and chemicals to the bridge deck (Khalifa et al. 1993).

Many different approaches have been taken to try to prevent this corrosion in bridge decks. They include: increased concrete cover, coated steel bars, concrete penetrating sealants, de-icing management, galvanized steel bars, stainless steel bars, cathodic protection systems, and concrete admixtures (Bradberry 2001). Another approach, which many researchers believe will be the answer, is the use of composite fiber-reinforced polymer (FRP) reinforcing bars which have excellent corrosion resistance. FRP composites have been around for years, initially used in the aerospace

industry and then adopted by many other industries such as the automobile and sporting goods industries. The high costs of these composites may initially seem unreasonable, but when compared with the additional costs of the aforementioned methods such as additional material price, construction time, maintenance, etc., the costs are very comparable to that of epoxy-coated steel (Bedard 1992).

These bars have many properties which differ significantly from these of steel bars. Some of these differences can be viewed as advantageous and some can be viewed as disadvantageous. On the positive side they are very light weight, high strength and, as mentioned above, are non-reactive to chlorides. However, their modulus of elasticity is significantly lower that that of steel and their stress-strain behavior is linear elastic up to failure, unlike steel which has a yield plateau to warn of failure. Because of these properties, many engineers and researchers believe that it will be most efficient to use the FRP bars as only the top mat of reinforcement in bridge decks and continue to use steel as the bottom mat.

The Virginia Department of Transportation, VDOT, has recently decided to replace a bridge on Rte. 668 over Gills Creek in Franklin County that is outdated and structurally deficient. The new bridge will consist of three simple spans, one of which will utilize Glass Fiber Reinforced Polymer, GFRP, reinforcing bars as the top mat of reinforcement and epoxy coated mild steel as the bottom mat of reinforcement. This bridge, in particular, was chosen for the project because of its rural location, just in case any unforeseen problems happen to arise with the use of the GFRP bars. The design for the span containing the GFRP bars was accomplished using the ACI 440 *Guide for the Design and Construction of Concrete Reinforced with FRP Bars* (2001) in conjunction

with the properties and recommendations reported by DeFreese (2001) in his thesis which investigated GFRP bars produced by three different manufacturers.

This project is sponsored by VDOT and the scope of it is to build a full-scale prototype of the GFRP span of the Rte. 668 bridge over Gills Creek. The prototype will then be tested to verify the design of the bridge before construction begins.

1.2: Objectives

1.2.1: Objective One

The primary objective of this project is to test a full-scale prototype of the actual bridge deck containing the GFRP bars. This is to verify that the design will resist the loads for which it was designed and to provide VDOT engineers with assurance that they have a good design that will not unexpectedly fail due to the use of this new material. Within this scope, it will be determined if the design is conservative or unconservative and the behavior of the bridge and deck will be examined. The aspects of behavior to be examined are failure load, failure mode, cracking load, crack widths, deflections, and internal stresses. The behavior of the bridge deck at service loads will also be examined.

To accomplish these objectives, a full-scale prototype of the bridge deck was constructed in the Virginia Tech Structures and Materials Laboratory; which included the design and construction of the bridge supports and form work. The bridge was instrumented with strain gauges on various GFRP and steel reinforcing bars and wires pots were attached to the deck and girders at designated locations to measure deflections. Four different tests were then performed on the bridge deck. For each test, a loading scheme was devised and a load frame was designed and constructed to carry the

predetermined loads. Data for each test were recorded using a data acquisition system and the deck was inspected at various load increments for cracks and crack widths. Finally, the data was reduced, analyzed, and compared to calculated theoretical values.

1.2.2: Objective Two

The secondary objective of the project is to comment on the construction of a bridge deck reinforced with GFRP bars and to note any concerns or possible advantages in the construction process along with a critique of the state-of-the-art of designing bridge decks that utilize FRP reinforcement.

To accomplish this objective, as the prototype bridge deck was constructed by the researcher, observations and comments on the construction were noted. To critique the state-of-the-art of designing these decks, design procedures and guidelines were reviewed and used in the analysis of the data.

1.3: Thesis Organization

Chapter 2 presents more detail on the mechanical and material properties of GFRP as well as previous research and tests that have been conducted along the same lines. Chapter 3 presents the properties of the materials used during testing. Chapter 3 also goes into detail about the test setup, test instrumentation, and test procedures. Chapter 4 presents the results from the tests that were conducted which are accompanied by theoretical data and a discussion of the findings. Finally, in Chapter 5, the overall findings of the project are presented with recommendations for further action to be taken.

CHAPTER II
LITERATURE REVIEW

2.1: Material Properties

FRP reinforcing bars are a composite material consisting of high modulus fibers that run the length of the bar held together in a resin matrix material. The fibers can be either carbon, aramid, glass, or a combination of any of the three. The bars are manufactured through a process known as pultrusion. In this process, fibers are bundled together and drawn through a resin bath. Next they are run through a shaping die to obtain the reinforcing bar's shape. Finally, they are put in a curing chamber where the resin hardens, after which the bars are ready for use (Nanni 1993). Most bars have some kind of exterior deformation or coating, such as sand, to promote bonding to the concrete.

Of the different fiber types mentioned above, glass is the most widely used for reinforcing bars, even though it is the lowest performing of the three. The reason that the glass fibers are used is because their properties are adequate and they are substantially cheaper than the other two. The two main types of glass fibers used are E-glass and S-glass. E-glass fibers have resistance to attack by water and mild chemicals while S-glass fibers are higher strength and are used in high performance applications (Hyer 1998).

The resin matrix material is usually of a polymer which can be classified as either thermoplastic or thermosetting. Thermoplastic polymers can be reshaped with the application of heat and pressure, where as thermosetting polymers cannot be reshaped once cured. Most resin matrices are thermosetting polymers. The most commonly used are polyester, vinyl ester, and epoxy. Currently, vinyl ester is the most favored of these three because of its ability to resist chemicals and high temperatures. The role of the

resin matrix material is to hold the fibers together in the desired shape, transfer load to the fibers, and protect the fibers from physical and environmental damage (TTI 2000).

2.2: Mechanical Properties

The mechanical properties of FRP reinforcing bars are substantially different than those of steel. In fact, the mechanical properties of FRP bars can vary greatly between different manufacturers which adds a challenge to the design engineers job (Bradberry 2001). FRP bars are very light weight, with a specific gravity of 1.25 to 2.0 which is about a quarter of steel's which is 7.9. This property can be advantageous in that it takes less time to place and is cheaper to ship (TTI 2000).

Glass FRP bars (GFRP) can have a tensile strength of up to two times that of steel. The larger the diameter the bar, the smaller the tensile strength due to a phenomenon know as shear lag. On the other hand, the tensile modulus of GFRP bars is only about twenty-five percent that of steel. This can lead to increased deflections and crack widths. The shear strength of GFRP bars, which is largely dependent on the matrix properties, is also only about twenty-five percent that of steel (TTI 2000).

The coefficient of thermal expansion (CTE) of GFRP in the longitudinal direction is very close to that of concrete which is good, however the CTE in the transverse direction is much higher which could cause internal stresses in the concrete in hot environments (Erki and Rizkalla 1993). Another potential problem is that bent FRP bars are found to fail at the bend at a strength well below their design strength which makes it hard to use in certain application where bent bars are required (Bradberry 2001).

One of the most interesting properties of FRP bars is their tensile failure mode. Unlike steel, FRP bars do not yield, therefore their stress-strain curve is linear elastic up

to failure. It was found that the typical moment-deflection curve for GFRP reinforced concrete is composed of two straight lines. The first straight line, like steel, is of higher slope and represents the uncracked section. The second straight line, unlike steel because of its linear elastic properties, represents the behavior of the cracked section up to failure (Nanni 1993). This property is a major concern for design engineers because it can lead to non-ductile brittle failures with no advanced warning.

2.3: Experimental Results and Designs

Rahman et al. (2000) tested a 6 m by 6 m concrete slab reinforced with CFRP grids for both the top and bottom mats. The deck thickness was chosen as 185 mm which was governed by punching shear. To represent true service load conditions, a monotonic load was applied to the slab to induce cracking. The deck was next cyclically loaded to represent fifty years of traffic. It was found that the behavior of the slab was satisfactory under these service conditions. To be more specific, only small deflections of less than the recommended value of L/800 were observed and the maximum stress in the reinforcing was found to be only seven percent of the ultimate strength. The slab was next tested to failure and was found to have considerable reserve capacity. The deck failed in punching shear and the load to fail it was five times the design wheel load. Overall, it was concluded that the CFRP grid was suitable.

Hassan et al. (2000) tested a 7.2 m by 3.0 m 200 mm thick concrete slab reinforced with GFRP in the top mat and epoxy coated steel in the bottom mat. It was found that the deck failed only by punching shear and that deflections were very small under service loads. Analytical models were then made using this test result and other test results. From the model, Hassan et al. (2000) recommends that when reinforcing a

slab with only GFRP that the reinforcement ratio of the top layer be 1.2 percent in the transverse direction and that the bottom layer have a ratio of 0.6 percent in the transverse direction for slabs with a span to depth ratio of between nine and fifteen. It was also found that using GFRP as top mat reinforcement has a negligible effect on punching shear capacity and that the GFRP in the bottom mat only experiences tensile stress of twenty percent of ultimate tensile strength under service loads. Overall, it was found that the strength of the slab reinforced with GFRP is 1.6 times what is required by the code.

A bridge deck utilizing GFRP as both top and bottom mats of reinforcement was designed and built in West Virginia. The bridge was completed in 1996 and had a deck thickness of 9 in. with the top cover being only 1 ½ in., presumably reduced from the typical 2 in. because of the GFRP's resistance to de-icing salts. After completion, the bridge was tested by placing trucks at position that caused maximum positive and negative moment in the deck (Thippeswamy et al. 1998). Thippeswamy et al. (1998) found during the tests that observed stress in the GFRP reinforcement was only three percent of the ultimate tensile strength of the bars. It was also found that the deflection of the deck was approximately L/1500, well within the AASHTO limits for the area. Overall, it was concluded that the GFRP was 'attractive' for the construction because of its lightweight and that it is satisfactory for deflection and stress limits.

Brown and Bartholomew (1993) conducted tests on six 6 in. by 6 in. by 30 in. concrete beams reinforced with one FRP bar. They found that the beams behaved similarly to the anticipated behavior of beams reinforced with steel. On average, they found that the ultimate moment was 2.37 times larger than the cracking moment. It was also observed that the FRP beams had more cracking than what would be expected in a

steel reinforced beam. The midspan deflections were recorded and were found to be three to four times higher than the calculated deflection for a similar steel reinforced beam. They also observed that the beams failed in a ductile manner, even though the FRP bars did not yield. It was concluded that the FRP bars are adequate and may be a good alternative to steel in harsh environments.

Tannous and Saadatmanesh (1998) tested ten 8 in. by 16 in. by 8 ft long beams reinforced with GFRP rebars, five of which utilized polyester resin and five of which utilized vinylester resin. The two types of GFRP bars were initially tested for ultimate tensile strength for later comparison. The beams were under-reinforced and contained steel shear reinforcement to guarantee that the beams failed due to tensile rupture. One beam of each type of reinforcement was tested after a year of just being in the concrete. Neither of the two rebars lost more than four percent of their strength. Two other beams of each type were tested after exposure to two different types of de-icing chemicals for periods of one and two years. After two years of exposure, the maximum amount of strength lost was found to be 12.8 percent by a polyester bar. Tannous and Saadatmanesh (1998) concluded that concrete cover depth and limiting crack widths plays a vital role in protecting the bars from exposure to chemicals that may degrade the strength of the bars. They also concluded that vinylester resin shows better resistance to chemicals than polyester.

Shear is another major problem for FRP reinforced concrete. Currently, ACI (ACI 318 1999) recommends the following formula for shear strength of non-prestressed reinforced concrete members subject to only flexure and shear:

$$V_c = 2\sqrt{f_c'}b_w d \quad (in.-lb) \qquad \textbf{(2.1)}$$

However, this formula was developed for steel-reinforced concrete. Michaluk et al. (1998) tested five different one-way slabs reinforced with steel, CFRP, and GFRP. The slabs were tested to failure and all but the GFRP slabs failed in flexure. The GFRP slabs failed in shear at a strength lower that the design flexural capacity. They attributed this shear failure to the fact that the cracks were wider and deeper than expected and that full aggregate interlock was not achieved. They proposed multiplying equation (2.1) by the ratio of FRP modulus of elasticity to steel modulus of elasticity:

$$V_c = \frac{E_f}{E_s}\left(2\sqrt{f_c'}b_w d\right)\ (in.-lb) \qquad \textbf{(2.2)}$$

Dietz et al. (1999) tested four concrete decks reinforced with only GFRP and another eight concrete decks reinforced with GFRP and the top mat and epoxy-coated steel and the bottom mat to represent a bridge deck. The GFRP decks failed in diagonal-tension under one-way flexural loading. They found equation (2.2) to be overly conservative and proposed the following equation:

$$V_c = 3\frac{E_f}{E_s}\left(2\sqrt{f_c'}b_w d\right)\ (in.-lb) \qquad \textbf{(2.3)}$$

Yost et al. (2001) believe that in bridge decks, the shear strength is provided solely by the concrete because of lack of shear reinforcement. They tested seven different reinforced beams, 3 of each type. Six of the beams were reinforced with GFRP, all with different reinforcement ratios, and one beam was reinforced with steel. All of

the GFRP beams failed in shear similar to the failure of the steel reinforced beam, but at lower loads. Also, all the GFRP beams failed within loads close enough to one another to conclude that the amount of longitudinal GFRP reinforcement has negligible effects on shear capacity and therefore empirical equations can be used to calculate shear strength. With this in mind, Yost et al. (2001) compared the shear capacity of the beams with the shear capacity predicted by equations (2.1), (2.2), and (2.3). They found that (2.1) did a good job of predicting shear strength of the steel reinforced beam but that it was very unconservative for the GFRP reinforced beams. They also found that (2.2) was overly conservative and would not be economical. However, they found (2.3) to be an acceptable lower bound design equation for concrete reinforcement with GFPR and with no shear reinforcement.

Bradberry (2001) designed a bridge deck for the Texas Department of Transportation that utilized GFRP as the top mat of reinforcement and epoxy-coated steel as the bottom mat of reinforcement. The slab is 8 in. thick and was designed as a one-ft strip continuous over knife-edged supports. Three of the major challenges Bradberry ran into were the design of maximum crack widths, ensuring ductile failure, and design strength of GFRP bars. With no guidance on crack widths, Bradberry chose the limiting width to be 0.02 in. based upon previous projects in Canada. To ensure ductile failure, he made sure that the section was over-reinforced so that the concrete crushes before the bars rupture. As for the strength of the GFRP bar, Bradberry chose a strength that represented the strength of the bar after 50 years in service based upon manufacturer data. This would hopefully ensure that the deck would fail in a ductile manner even at the end of its service life. Of all these factors, crack widths controlled the design of the GFRP

bars and strength and allowable stress limit states were not even approached. Bradberry concluded that GFRP bars are a good option in harsh environments and that his deck is conservative, but that there is still much unknown about GFRP bars, especially their long-term durability and ductility issues.

In May of 2001, ACI Committee 440 (ACI 440.1R 2001) published the first copy of design guidelines for use of FRP as reinforcement in concrete. The committee set no standard for crack width and recommended that the maximum crack width allowance should be up to the engineer's judgment. The committee did however recommend that the tensile strength of an FRP rebar be reduced by an environmental reduction factor that reflects the type of bar and its exposure condition. Those factors range from 0.7 to 1.0. It is also recommended that the calculated nominal moment capacity of the section be reduced by between 30 and 50 percent depending on the amount of reinforcement to ensure concrete crushing occurs first as a warning for failure. ACI 440.1R (2001) also has recommended that the following equation be used for shear strength:

$$V_c = \frac{A_f E_f}{A_s E_s}\left(2\sqrt{f_c'}\, b_w d\right)\ (in.-lb) \qquad \textbf{(2.4)}$$

2.4: Conclusions and Recommendations

From previous experimental data, it can be concluded that the use of FRP reinforcing bars in concrete is a good option for bridge decks subjected to harsh environments and de-icing salts. However, many questions still remain. Some of those major questions are:

- What should be the crack width limit?
- What concrete cover depth should be used?
- How should long-term durability issues be handled?
- What is the shear strength of an FRP reinforced concrete section?
- What type of bar, fiber and polymer type, should be used?
- How can ductile failure be ensured?

With all these questions still to be answered, more research in the area of concrete reinforced with FRP is needed. The goal of this thesis is to try to address all of the above questions, except type of bar, polymer and fiber to be used.

CHAPTER III
METHODS AND MATERIALS

3.1: Bridge Prototype

The prototype of the bridge was built to full scale with a few modifications. Table 3.1 shows a comparison between the prototype bridge deck and the proposed actual bridge deck. The prototype is only three girders wide with an overhang on each side as opposed to six girders wide with an overhang on each side. The overall width of the bridge deck is 17 ft 4 in. and the length is 24 ft. The deck also has four 1 ft by 2 ft block outs, two on either side, to accommodate the columns for a load frame (Figure 3.1).

Table 3.1: Bridge Deck Design Comparison

	Prototype Bridge Deck	Actual Bridge Deck
Overall width	17 ft-4 in.	30 ft-4 in.
Overall length	24 ft	45 ft
No. of spans/type	3/continuous	1/simple
No. of girders	3	5
Type of girders	W27x94	W27x94
Spacing between girders	6 ft-6 in.	6 ft-6 in.
No. of overhangs	2	2
Width of overhangs	2 ft-2 in.	2 ft-2 in.
Top mat reinforcement	GFRP	GFRP
Bot. mat reinforcement	bare steel	epoxy-coated steel
Trans. rebar size, top mat	No. 5	No. 6
Long. rebar size, top mat	No. 6	No. 6
Trans. rebar size, bot. mat	No. 6	No. 6
Long. rebar size, bot. mat	No. 4	No. 4
Rebar spacing	identical for both	
Min. concrete strength	4000 psi	4000 psi
Depth of slab between girders	7.5 in.	8.0 in.*
Depth of slab at overhangs	8.5 in.	9.0 in.*

*Includes 1/2 in. sacrificial wearing surface

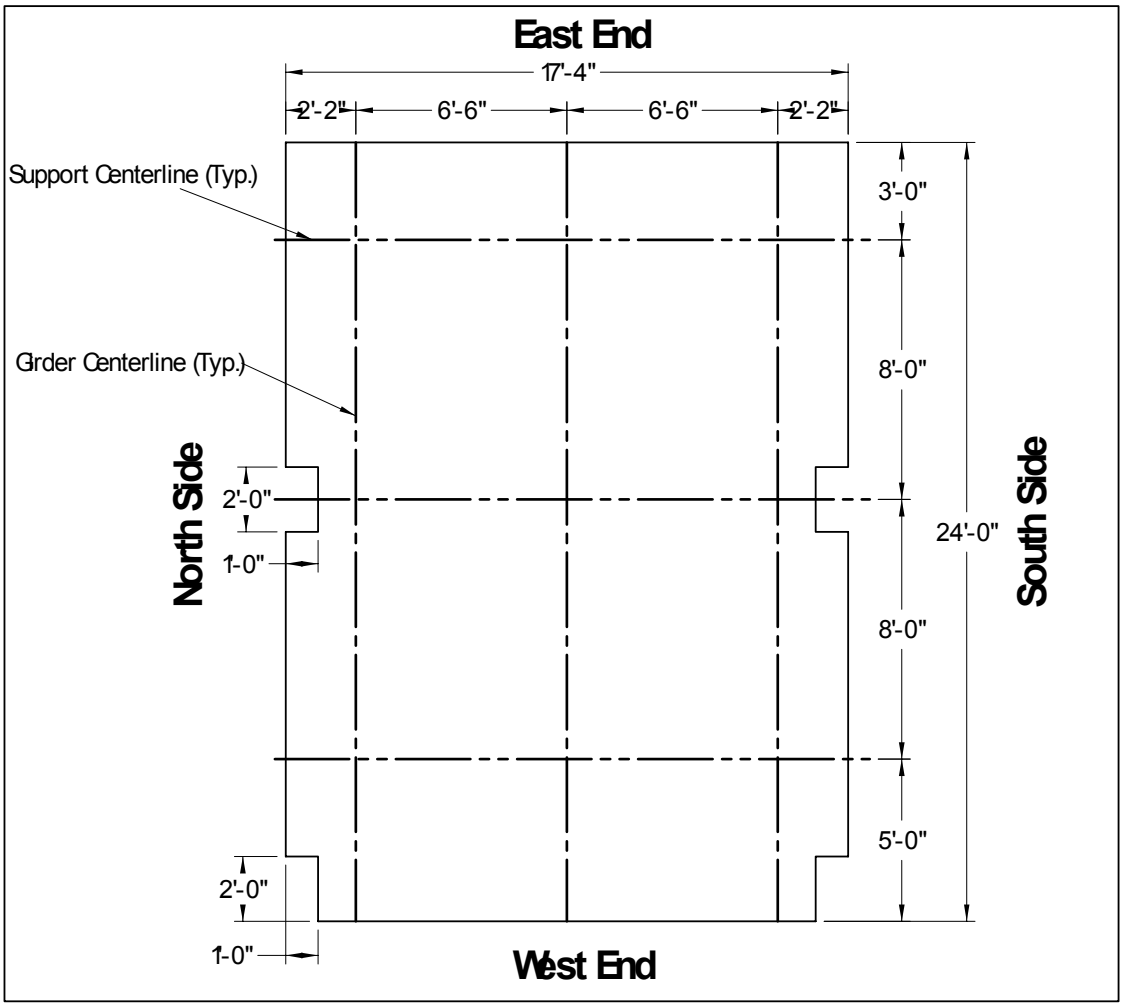

Figure 3.1: Plan View of Prototype Bridge Deck

3.1.1: Girders

The girders for the prototype bridge were W 27x94 Grade 50 hot rolled sections. They were spaced at 6 ft 6 in. on center and were supported at 3 ft, 11 ft, and 19 ft from the East end (Figure 3.1). The support at 19 ft from the East end was a rocker type (Figure 3.2) and the other two supports were bolted. The supports at 3 ft were bolted to a support beam which rested on the strong floor and was bolted to three reaction beams. At the interior support at 11 ft the center girder support was bolted to the reaction floor beams and the outside girder supports rested on, but were not bolted to, the reaction floor (Figure 3.3). Each beam had 6 in. long ¾ in. diameter shear studs welded to the top flange to create full composite action with the deck. Pairs of studs were spaced 6 in. on center to 8 ft 9 in. from the West end and to 3 ft 3 in. from the East end, and were spaced 8 in. on center in-between. The girders also had stiffeners welded on either side of the web at each support to prevent web buckling (Figure 3.2).

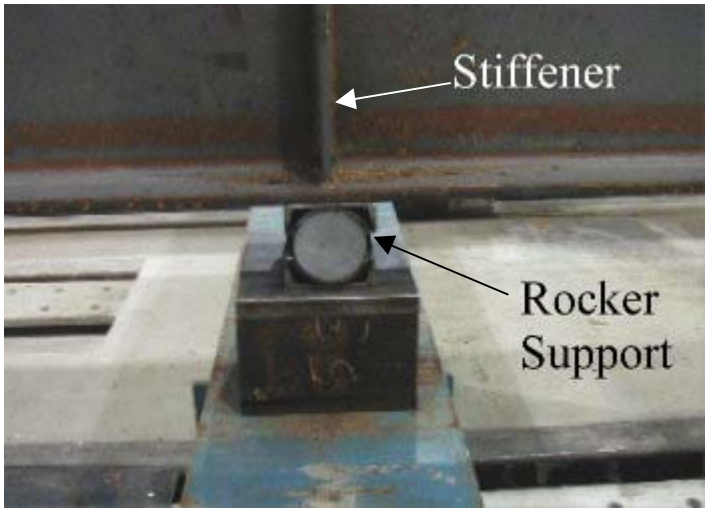

Figure 3. 2: Rocker Support

3.1.2: Reinforcing Bars

As mentioned before, the top mat of reinforcement for the deck consisted of GFRP bars and the design called for epoxy coated mild steel in the bottom mat, but bare steel was used instead because corrosion is not an issue with this project. The steel bars

were No. 6 in the transverse direction and No. 4 in the longitudinal direction. The GFRP bars used

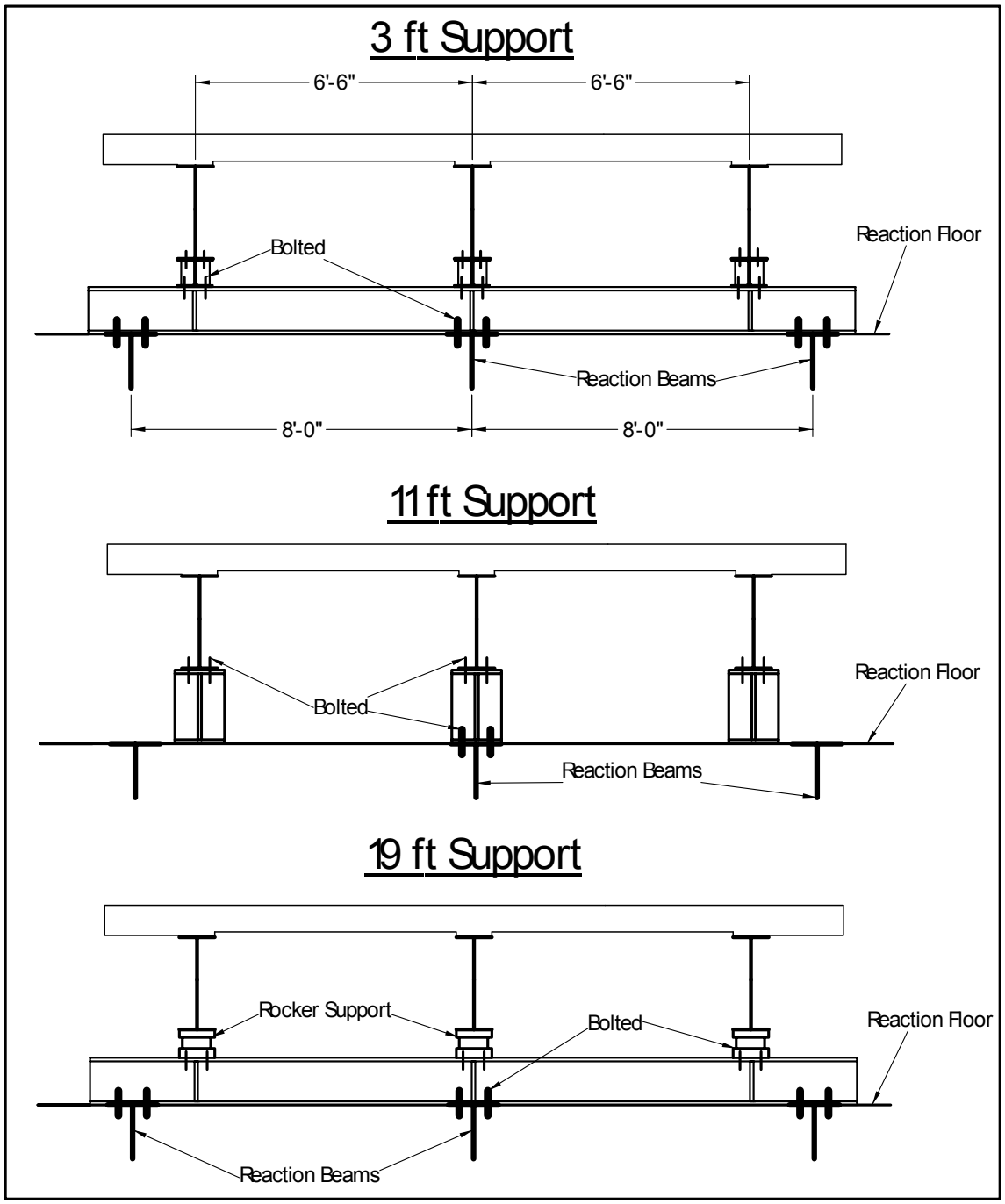

Figure 3.3: Prototype Bridge Girder Supports

were manufactured by Hughes Brothers Inc. and are denoted by a helical wrap and a mild sand impregnation. The design called for No. 6 GFRP bars in both the longitudinal and transverse directions. However, smaller diameter bars were used in the prototype to account for the fact that GFRP bars lose strength with time in a concrete environment.

ACI 440.1R (2001) recommends that GFRP bars in concrete exposed to earth and weather have an environmental reduction factor, CE, of 0.7 applied to their guaranteed tensile strength to yield the design tensile strength. The design tensile strength, f_{fu}, is the estimated tensile strength of the bar after fifty years. The area of a No. 5 bar (0.31 in^2) is approximately equal to seventy percent of the area of a No. 6 bar (0.44 in^2). Therefore, No. 5 transverse bars were used in the prototype to model the strength of the transverse bars in the actual bridge after fifty years of service.

3.1.2.1: Steel Reinforcement Layout

The No. 6 mild steel bars were spaced 8 in. on center in the transverse direction (Figure 3.4). They had a cover depth of 1 in. between girders and 2 in. on the overhangs. The longitudinal No. 4 steel bars were laid on top of the transverse bars. From the centerline of the exterior girder to 2 in. from the edge of the overhang, there were five equal spaces and the bars are spaced approximately 4 $^4/_5$ in. on center with no bar placed over the girder. From the centerline of the exterior girder to a distance 1 ft. 7 ½ in. towards the interior, there is one bar over the edge of the girder and two equal spaces of 7 ¼ in., and this is the same spacing for the interior girder towards the exterior with no bar over the girder. The 3 ft 3 in. in-between is divided into eight equal spaces corresponding to bars placed 4 $^7/_8$ in. on center (Figure 3.5). The spacing is the same on both sides of the interior girder.

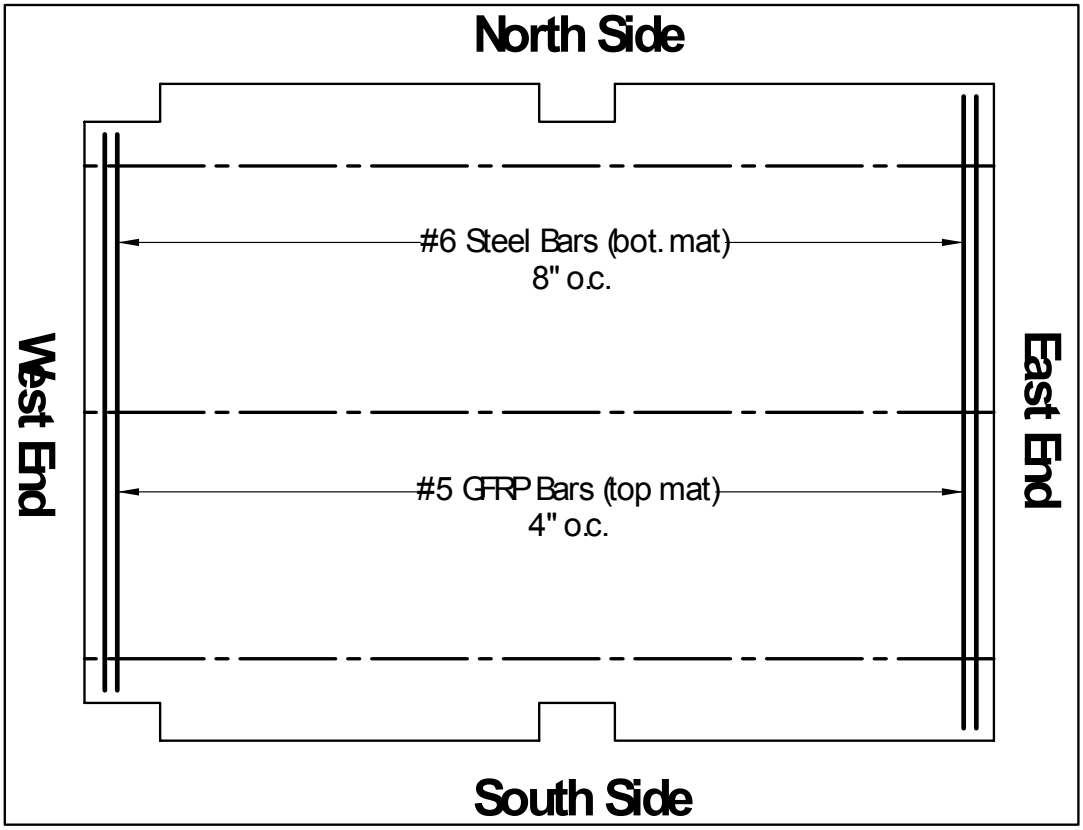

Figure 3. 4: Transverse Reinforcement Layout

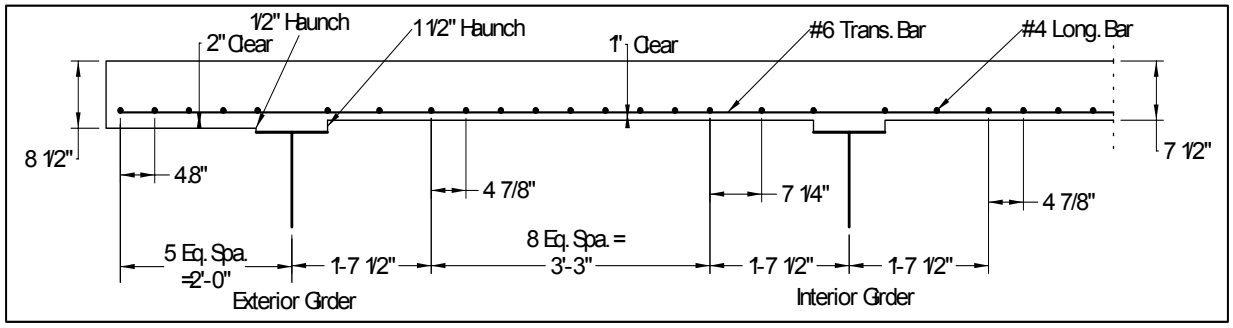

Figure 3.5: Longitudinal Steel Rebar

3.1.2.1: GFRP Reinforcement Layout

The No. 5 GFRP bars are spaced 4 in. on center in the transverse direction (Figure 3.4). They have a cover depth of 2 in. everywhere except the East half of the North

overhang where they have a cover depth of 2 $^{1}/_{8}$ in. We attempted to make this cover depth 2 ½ in. by using shorter chairs, but the bars pulled the chairs up off the form work resulting in a cover depth of only 2 $^{1}/_{8}$ in. The No. 6 longitudinal bars are spaced at 6 in. on center between the interior and exterior girders. From the centerline of the exterior girder to 2 in. from the edge of the overhang, there are five equal spaces and the bars are spaced at approximately 4 $^{4}/_{5}$ in. on center (Figure 3.6).

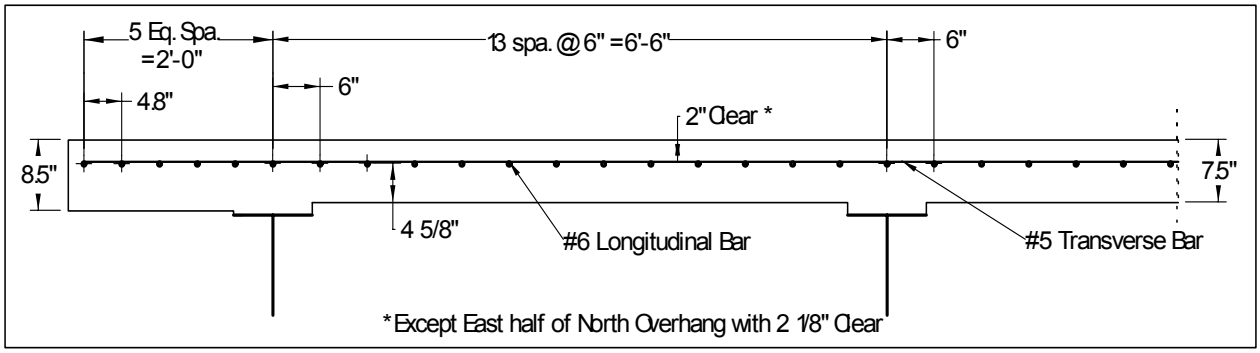

Figure 3. 6: Longitudinal GFRP Bars

3.2: Bridge Deck Construction

3.2.1: Formwork

The girders, with their shear studs previously welded on, were positioned using overhead cranes. Strippable formwork constructed out of plywood and 2x4's was used to form the deck. It was positioned in such a manner that a ½ in. haunch was obtained at the overhang slabs and a 1 ½ in. haunch was created at the interior slabs. This made the overhang slabs 8 ½ in. deep and the interior slabs 7 ½ in. deep. The plywood forms were supported on the floor by wood shoring towers (Figure 3.7).

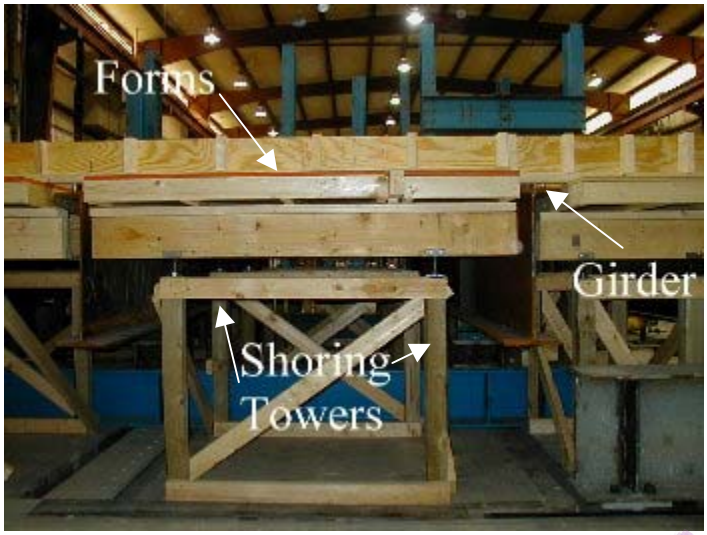

Figure 3. 7: Formwork Shoring Towers

3.2.2: Steel Reinforcing Bars

One inch steel bar chairs were laid parallel to the girders between the girders, and two inch chairs were used on the overhang. The transverse steel was laid down and tied to the chairs. The longitudinal steel was then laid on top of and tied to the transverse steel (Figure 3.8).

Figure 3. 8: Bottom Steel Mat Tie

3.2.3: GFRP Reinforcing Bars

The GFRP reinforcing bars require a special chair and tie wire in order to prevent them from being damaged during construction. The chairs used for this project were plastic chairs and the wire was epoxy-coated steel (Figure 3.9). The chairs were

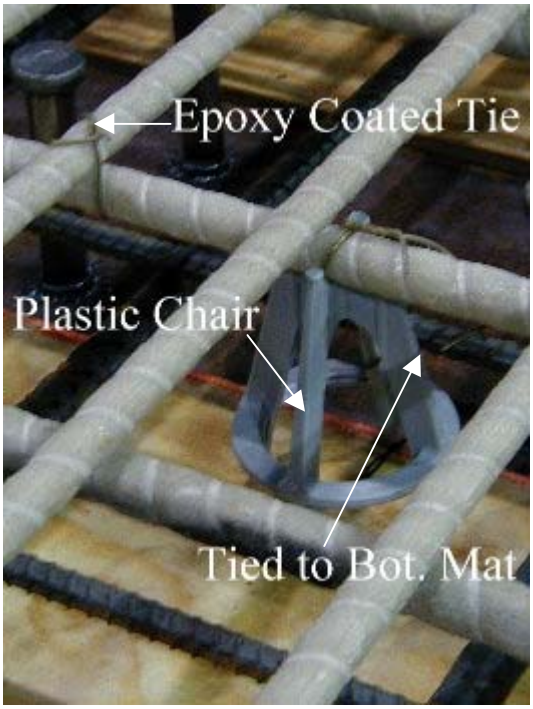

positioned as close as possible to their desired locations. Some of the chairs were not positioned exactly where they needed to be because they could not sit over top of the steel bars. On the interior slabs, 4 ¼ in. chairs were used, on the South and West half of the North overhang, 5 ¼ in. chairs were used, and on the East half of the North overhang, 4 ¾ in. chairs were used.

Figure 3. 9: GFRP Bar Chair

Some of the longitudinal bars were placed on the chairs. They were tied to the chairs and the chairs were then tied to the bottom mat of steel (Figure 3.9). This was done to keep the GFRP bars from floating because the density of the concrete is greater that the density of the GFRP bars. The transverse bars were then positioned and tied to the longitudinal bars. The remaining longitudinal bars were then positioned and tied to the transverse bars. The bars supported on chairs were spaced between 2 ½ ft and 3 ft on center between the girders and 1 ft on center over the girders. The bars were very flexible to stand on at first. As more bars were tied together, the mat got stiffer until the entire mat was tied and it was pretty stiff, with the ability to hold a 250 lb. man with little flexure.

3.2.3: Placing the Concrete

The concrete was placed using a ¾ cubic yard bucket. The concrete was vibrated as it was placed to ensure that all voids were filled and that no honeycombing took place.

A screed rail was placed along the width of the deck at approximately 11 ft from the North end so that the deck could be poured using two separate pours and concrete batches. Two separate pours had to be made with two separate concrete batches because of equipment limitations: the limited screed length and the concrete truck capacity. The total amount of concrete used was approximately 11 cubic yards, but the maximum truck capacity is about 7 cubic yards, so two separate trucks with batches of 6 and 5 cubic yards were used. After both pours were complete, the screed rail was removed and the void was filled in with concrete. The surface was then finished and 4 in. diameter cylinders were made for each batch of concrete to measure the strength gain over time.

The deck was covered with plastic sheeting and watered for seven days to obtain a seven day moist cure. The cylinders were match cured to the deck. The formwork was stripped after 12 days.

3.3: Materials

3.3.1: Concrete

The type of concrete used for the deck was a VDOT A4 mix, which is a standard mix for bridge decks. The A4 mix is a 4000 psi mix that has ¾ in. aggregate, a water-cement ratio of 0.45, typical slump of 2 in. to 4 in., and air content of 6.5% ± 1.5%. As aforementioned, 4 in. diameter compressive test cylinders were made for both of the batches used in the bridge deck. Batch 1 was placed in the East half of the slab and batch 2 was placed in the West half of the slab. As shown in Table 3.1, both batches exceeded their 4000 psi minimum strength and batch 2 had a higher strength than batch 1.

Table 3.2: Concrete Compressive Strengths

Compressive Cylinder Strengths				
	Batch 1		Batch 2	
Day	f'_c (psi)	Avg. (psi)	f'_c (psi)	Avg. (psi)
7	3064	3060	3482	3570
7	3064		3661	
21	4496	4600	5133	5090
21	4695		5053	
28	5252	5150	5769	5550
28	5053		5332	
34	5133	5010	5849	5730
34	4894		5610	
61	5332	5270	6127	6270
61	5212		6406	

3.3.2: Steel Reinforcing Bars

The steel reinforcing bars used were mild steel with a specified yield strength of 60 ksi. Both the No. 4 and No. 6 bars were tested according to ASTM standards in a SATEC Universal Testing Machine, UTM. A clip on extensometer with a 2 in. gauge length was used to measure the strain in the bar, and the computer recorded the stresses. Stress-strain curves were produced for each test (Figure 3.10) and from them a modulus of elasticity, E, and a yield strength, f_y, were acquired. The average modulus of elasticity for the bars was 29,100 ksi (Table 3.2), and the average yield strength was 70.6 ksi (Table 3.3).

Table 3.3: Modulus of Steel Bars

		Modulus of elasticity, E (ksi)	Average E
Bar Size	Test #	Extensometer	(ksi)
#4	424	28800	28400
	425	28000	
#6	426	28900	29800
	428	30600	

Average (ksi)	29100
Std. Dev., s (ksi)	1094
COV (%)	3.76
Low (ksi)	28000
High (ksi)	30600

Table 3.4: Yield Strength of Steel Bars

		Measured Yield Strength, f_y, (psi)	Average f_y
Bar Size	Test #	Extensometer	(ksi)
#4	424	72700	72.0
	425	71300	
#6	426	69100	69.2
	428	69300	

Average (ksi)	70.6
Std. Dev., s (ksi)	1.7
COV (%)	2.43
Low (ksi)	69.1
High (ksi)	72.7

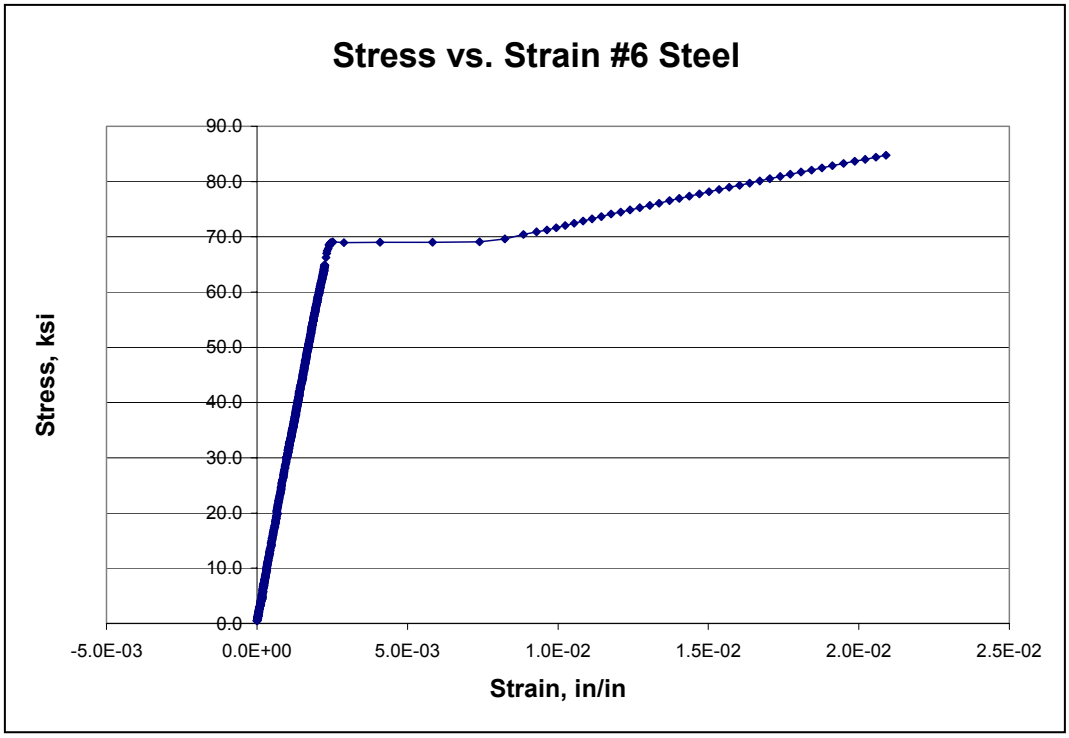

Figure 3.10 : Typical Steel Stress-Strain Curve

3.3.3 GFRP Reinforcing Bars

As aforementioned, the GFRP bars used were manufactured by Hughes Brothers Inc. and are helically wrapped with a mild sand impregnation (Figure 3.11). They are 73 percent fiber and 27 percent resin by volume. The fiber type is E-glass and the resin type

is vinyl ester. The bars were tested in the SATEC UTM using the same procedures and standards as used by DeFreese (2001). The clip on extensometer with a 2 in. gauge length was also used for this test to record the strains, and the computer recorded the stresses. Stress-strain curves were produced using the data. The stress-strain curves are linear-elastic up to failure, however, the extensometer was taken off before failure to prevent damage.

Figure 3.11: GFRP Bar

The No. 5 bars had a straight line stress-strain plot and the modulus of elasticity was calculated using a best fit line (Figure 3.12). However, the data jumped around on the No. 6 bar tests, due to extensometer slip or local fiber failure at the extensometer location (Figure 3.13). Therefore, the modulus was calculated for each of the straight line portions of each graph and then averaged to obtain a modulus for that particular test. The average tensile strength was 106 ksi for the No. 5 bars and 89.3 ksi for the No. 6 bars (Table 3.4). The average modulus of elasticity for the bars was 6210 ksi (Table 3.5), but

Table 3.5 : GFRP Bar Ultimate Tensile Strength

Bar Size	Measured Tensile Strength, (psi)					Average (ksi)	COV (%)
#5	Test 435	Test 436	Test 437	Test 438	Test 439		
	100960	110864	104288	99658	115298	106	6.29
#6	Test 429	Test 430	Test 431	Test 433	Test 434		
	92823	93406	*	87007	84033	89.3	5.10

* Test accidentally aborted before failure

a modulus of 6300 ksi was used in analysis because Defreese (2001) found this to be the average modulus. DeFreese (2001) tested three different sizes of Hughes Brothers bars with each size being tested five times. Three different types of instrumentation measured the strain in the bars; two strain gauges, an extensometer with a 2 in. gauge length, and three LVDTs with a 7.5 in. gauge length.

Table 3.6: GFRP Bar Modulus

		Modulus of elasticity, E (ksi)	Average E
Bar Size	Test #	Extensometer	(ksi)
#5	435	6013	6120
	436	6320	
	437	6034	
	438	6146	
	439	6102	
#6	429	6461	6300
	430	6388	
	431	6145	
	433	6309	
	434	6208	
		Average (ksi)	6210
		Std. Dev., s (ksi)	151.40
		COV (%)	2.44
		Low (ksi)	6013
		High (ksi)	6461

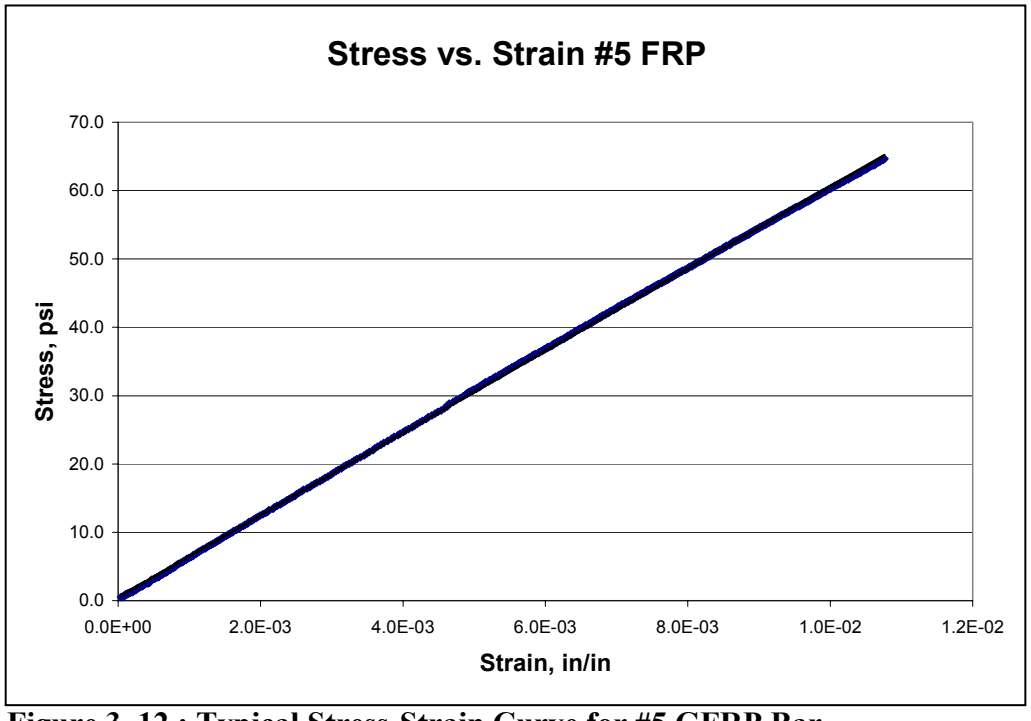

Figure 3. 12 : Typical Stress-Strain Curve for #5 GFRP Bar

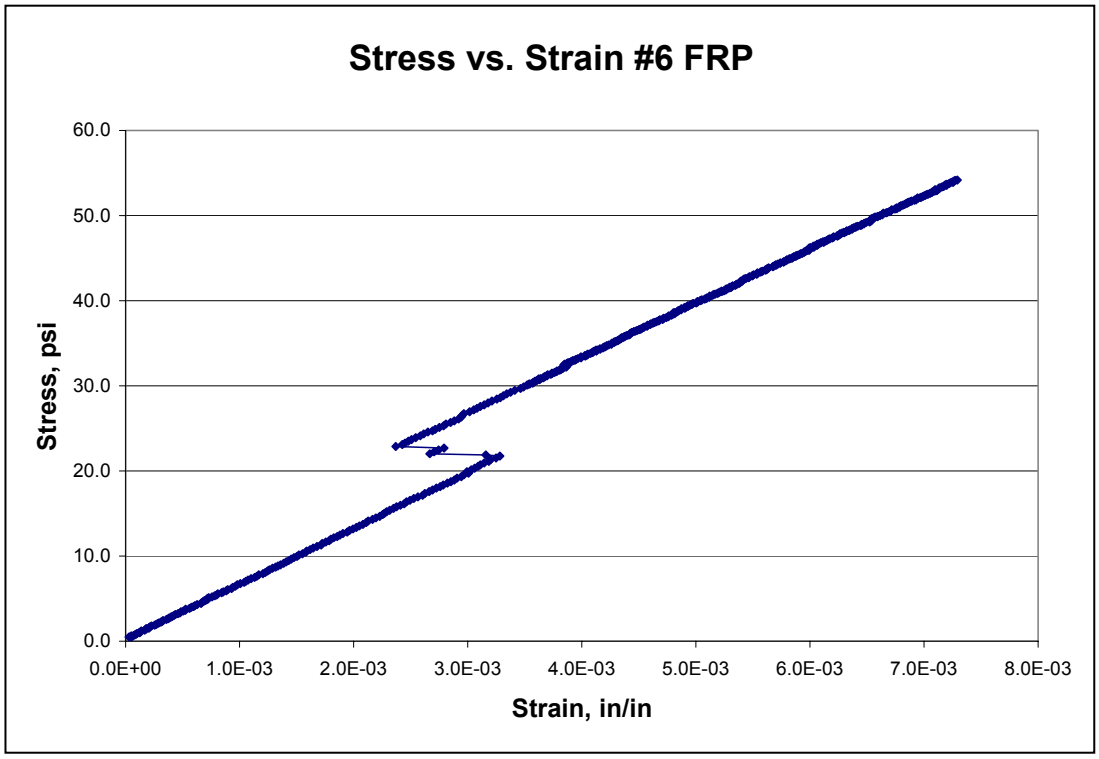

Figure 3. 13: Typical Stress-Strain Curve for #6 GFRP Bar

3.4: Instrumentation and Test Setup

3.4.1: Overhang Tests #1 & #2

Overhang Tests #1 and #2 were designed to simulate a typical AASHTO design truck tire on the edge of the overhang, which would create a negative moment in the deck over the exterior girder. This load is harsher than reality, because the bridge will have a barrier rail on the overhang that will prevent a wheel load from being applied to the overhang. The instrumentation and test setup for overhang tests #1 (South side) and #2 (North side) were almost identical. The only difference between the two were slight differences in strain gauge locations. These differences were no more than ½ in. and were due to human error in placing the bars.

3.4.1.1: Instrumentation

Each of the two overhang tests had eight No. 5 transverse GFRP bars strain gauged and four No. 6 transverse steel bars strain gauged. Both the GFRP and steel strain gauges were positioned along the outer edge of the exterior girder's flange. This distance measured 21 in. from the North and South sides for tests #1 and #2, respectively. For Overhang test #1, North side, the gauges were positioned as shown in Figure 3.14, and all the gauges were 2 $^{3}/_{8}$ in. from the top of the slab. For Overhang test #2, South side, the gauges gauges were positioned as shown in Figure 3.14, and all the gauges were 2 ½ in. from the top of the slab. The steel gauges were positioned as shown in Figure 3.15 the slab, and were 2 ¼ in. from the bottom of the slab for both tests. All of the strain gauges for all of the tests were oriented along the length of the particular bar that they were affixed to.

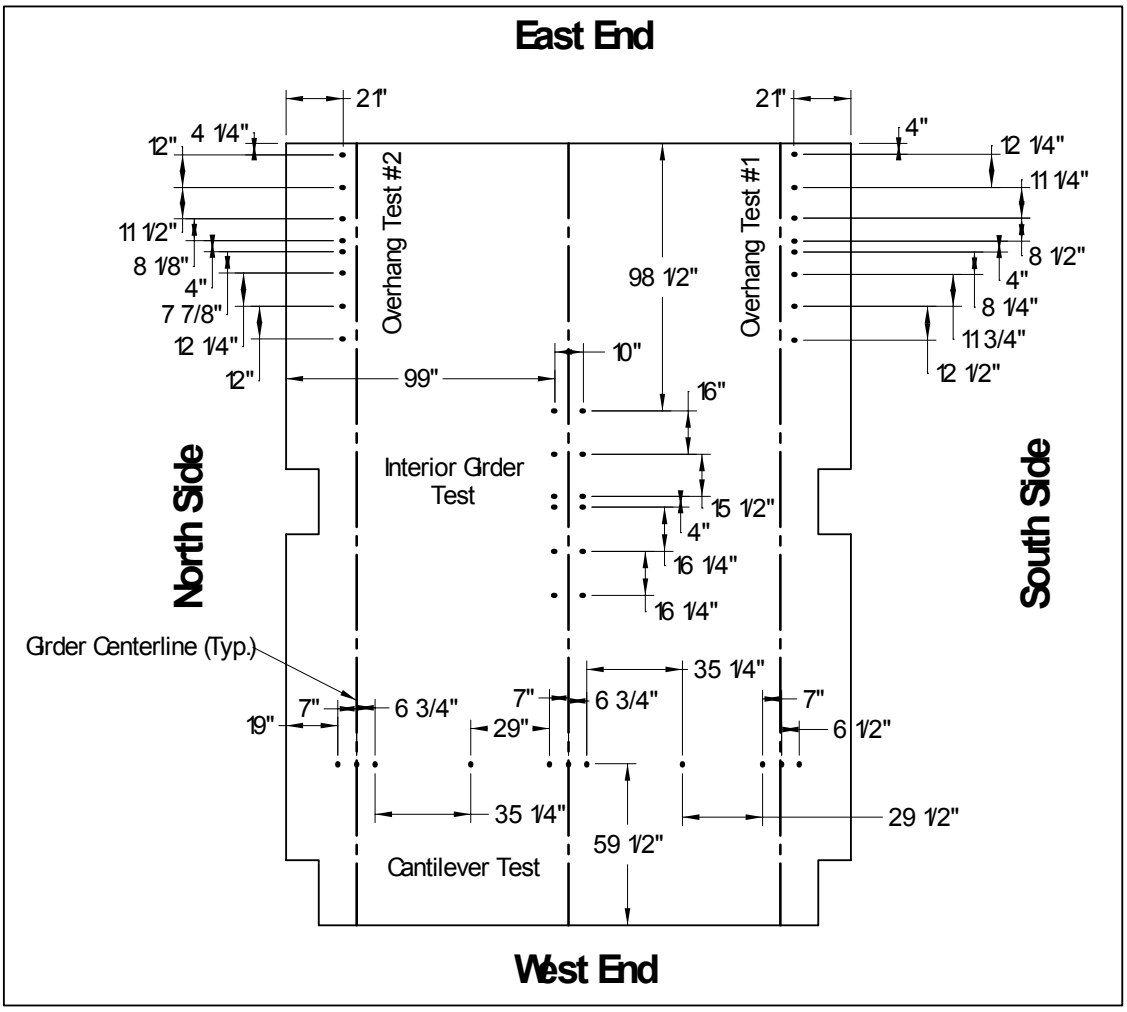

Figure 3.14: GFRP Strain Gauge Locations

The wire pots used to measure deflections were in the same locations for both tests. They were anchored to the bottom of the slab at ½ in. from the edge. The first pot was located 8 in. from the East end of the slab, and the other five were positioned 12 in. on center from the first (Figure 3.16).

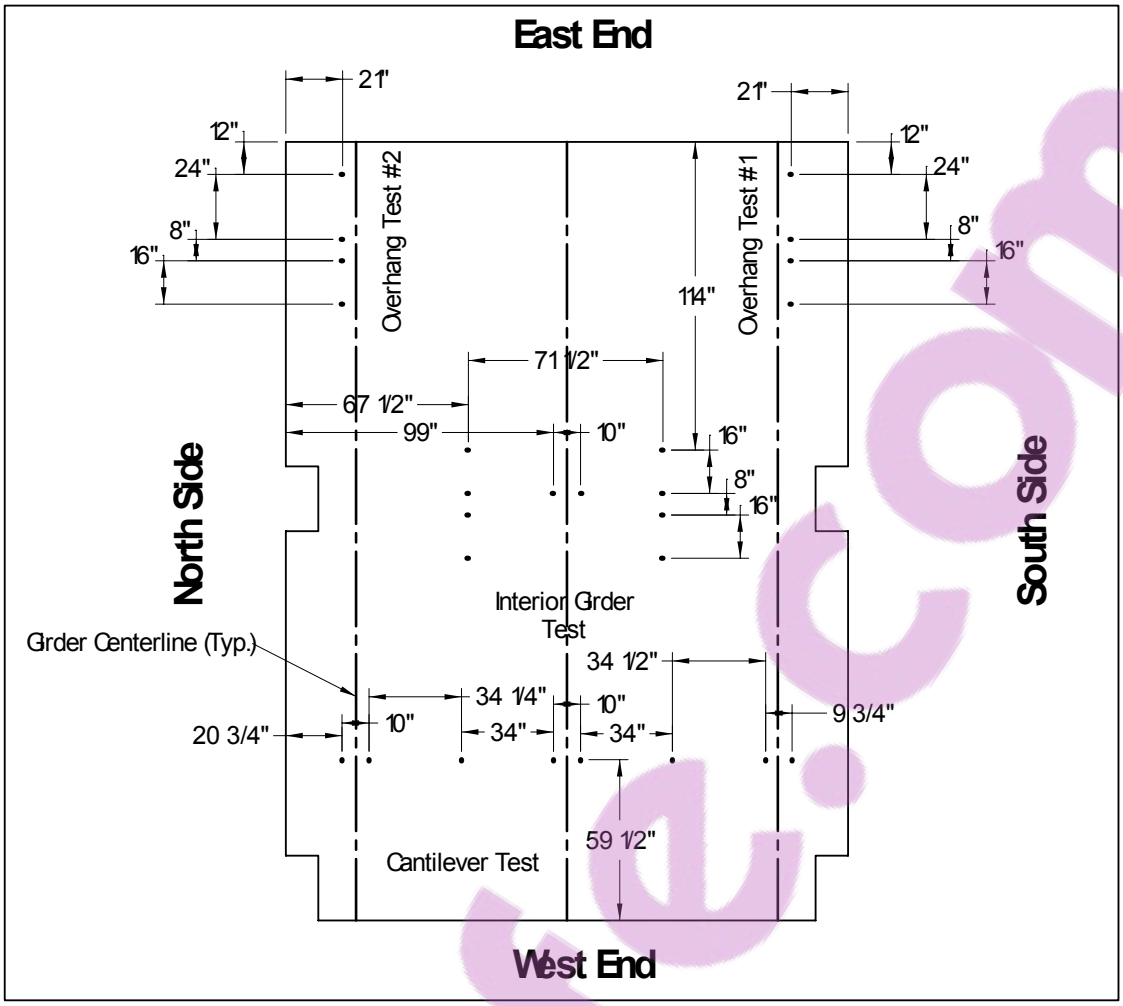

Figure 3.15: Steel Strain Gauge Locations

Whittemore gauge points were placed 4 in. on either side of the outer edge of the exterior girder for a total gauge length of 8 in. Test #1 had eight points while test #2 only had seven points. The first set of gauges were located 8 in. on from the East edge of the slab (Figure 3.17), and all other were 12 in. on center from the first.

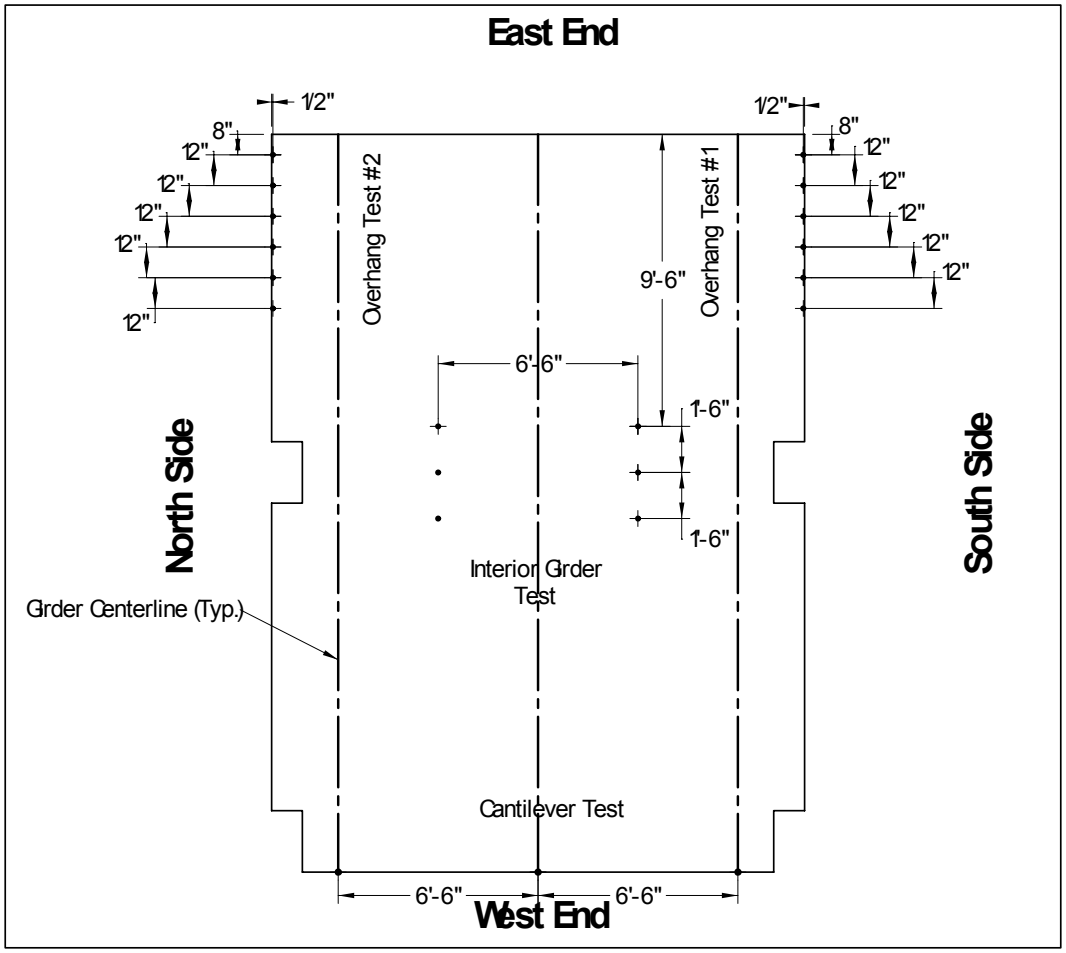

Figure 3.16 : Wire Pot Locations

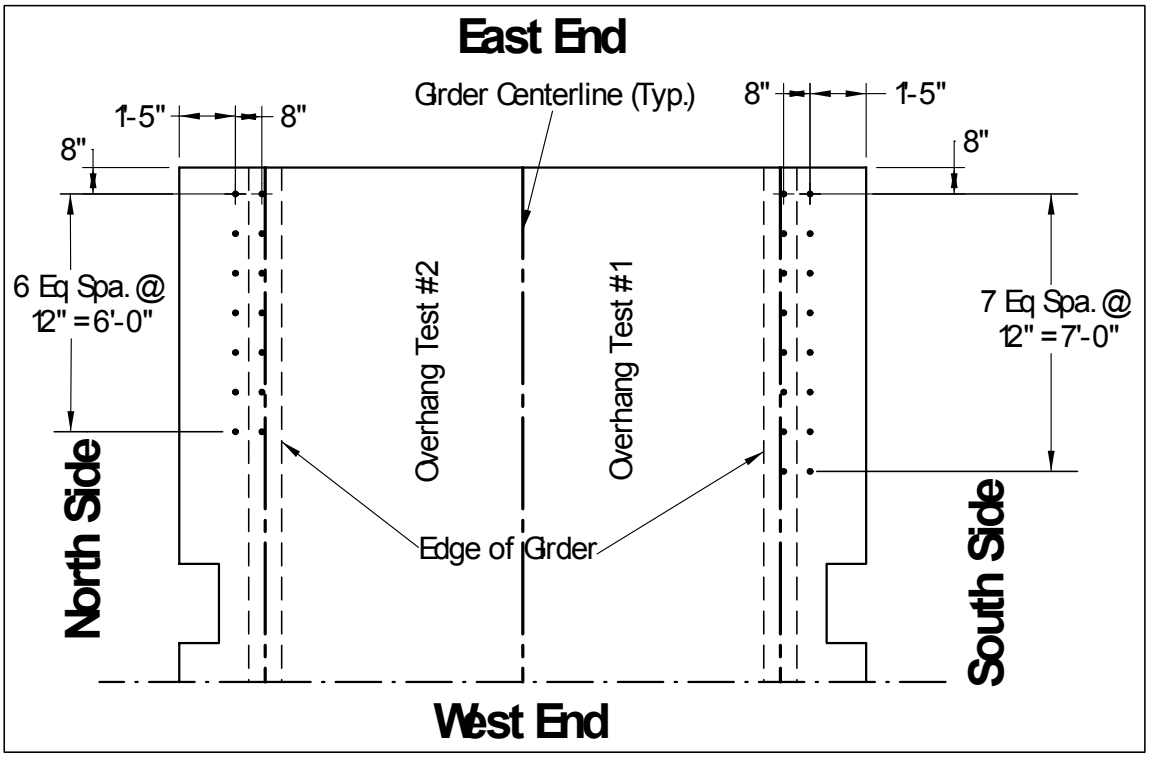

Figure 3.17: Whittemore Gauge Locations

3.4.1.2: Test Setup

The load frame ran parallel to the bridge girders with one column placed in the notched out section at mid-span, and the other column placed in front of the East end of the deck. The columns for the load frame were bolted down to the reaction floor beam and a crossbeam was bolted to their flanges. The crossbeam had a moment end plate on both ends and a stiffener located at the load point. A 120 kip capacity hydraulic load ram was hung from the crossbeam with a 200 kip capacity load cell placed between the ram and crossbeam to measure the loads.

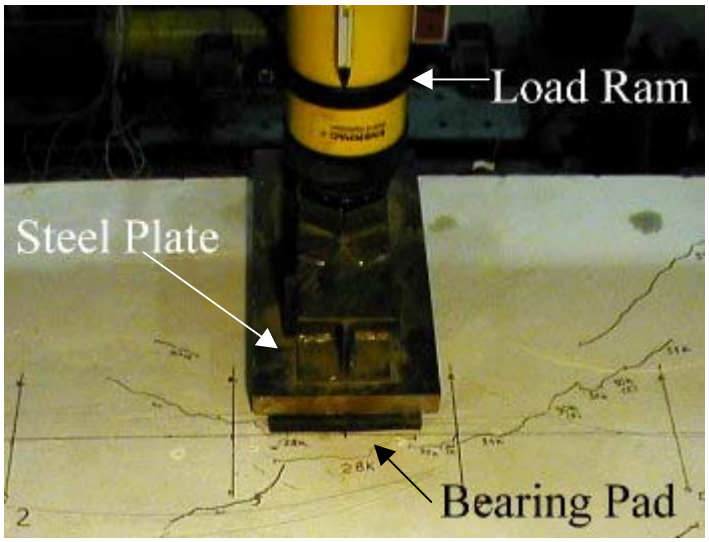

Figure 3. 18: Load Ram and Patch Load

The load was applied to the overhang by an 8 in. by 20 in. patch load, to resemble a truck tire patch. These patch dimensions were calculated using Equation 3.1 as presented in AASHTO LRFD (1994).

$$Tire\,Width = \frac{P}{0.8} \qquad \textbf{(3. 1)}$$

$$Tire\ Length = 6.4 \cdot \gamma \cdot \left(1 + \frac{IM}{100}\right)$$

Where : P = wheel load, kips
γ = load factor
IM = impact factor, percent

With a wheel load of 16 kips, a load factor of 1.0, and an impact factor of 30 percent, the width and length were calculated to be 20 in. and 8.3 in., respectively. However, a patch of 20 in. by 8 in. was used instead because it was easier to manufacture. The 8 in. dimension ran along the length of the bridge and the 20 in. dimension ran along the width of the bridge. A neoprene pad was placed directly on the concrete and a modified steel plate was placed on top of the pad. The ram applied load to

the modified steel plate (Figure 3.18). The center of the patch load was positioned 3 ft 2 in. from the East end, and the edge of the pad and steel plate were flush with the edge of the deck (Figure 3.19).

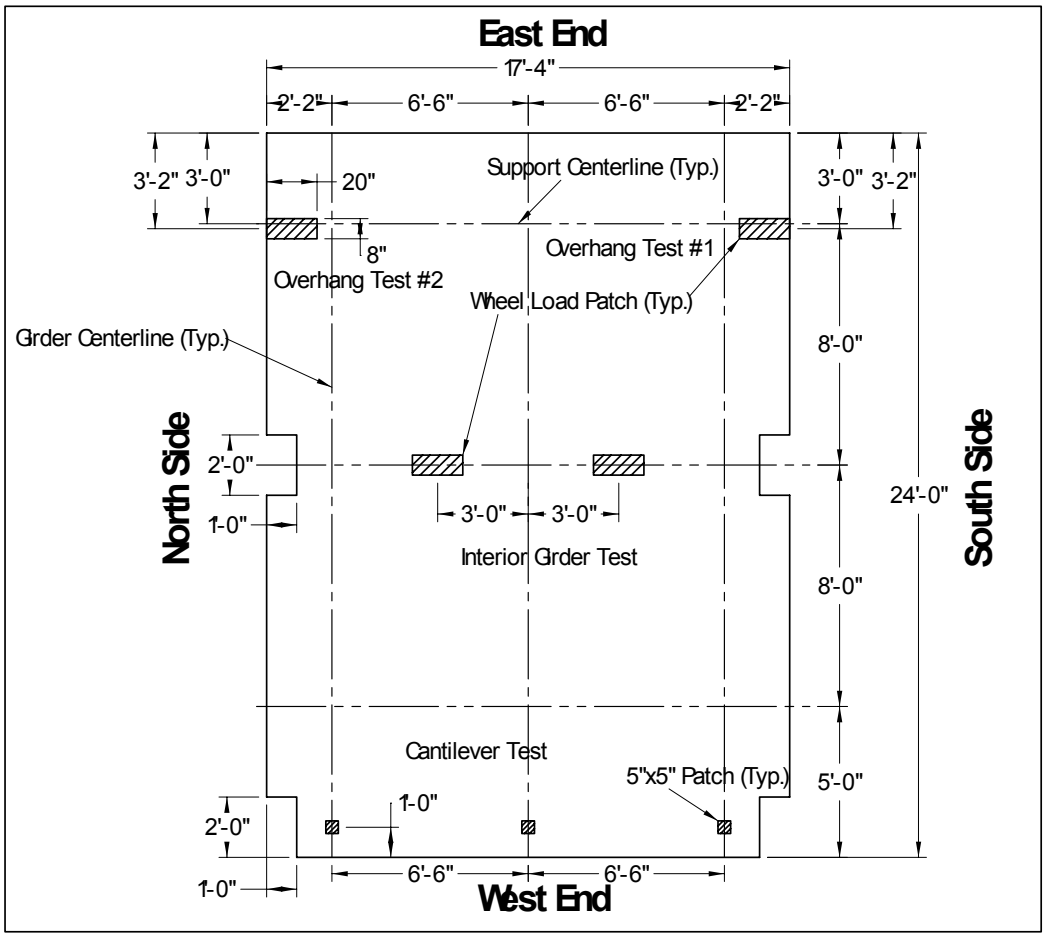

Figure 3.19: Load Positions and Patch Sizes

3.4.2: Interior Girder Test

The interior girder test was performed to simulate a typical AASHTO design truck traveling over the center of an interior girder with its axle perfectly straddling the girder. This creates a maximum negative moment over the interior girder.

3.4.2.1: Instrumentation

This test utilized ten steel strain gauges and twelve GFRP gauges, all of which were located on transverse bars. Six GFRP bars were gauged, with two gauges on each bar. The gauges were 10 in. apart and the bars were positioned so that the gauges were on either edge of the interior girders top flange. The distance to the gauges measured 99 in. from the South side to the first gauge and an additional 10 in. to the second gauge, a total of 109 in. The gauges were also set up to straddle the middle support with three equally spaced rows on either side. The rows of two gauges were positioned as shown in Figure 3.14. All of the GFRP gauges were approximately 2 $^{3}/_{8}$ in. from the top of the slab.

Two of the steel strain gauges were positioned similarly to the GFRP gauges in that they were placed on either edge of the interior girder's top flange. They were located 130 in. from the East end. The remaining eight were on four different bars, two per bar. They measured 67 ½ in. and 139 in. from the North side of the slab, respectively. This placed the gauges under the load points to measure stresses at the location of maximum positive moment. The pairs were positioned as shown in Figure 3.15. All of the gauges were 1 ¼ in. from the bottom of the slab.

The wire pots used to measure deflections were in the same locations on both sides of the interior girder. They were anchored to the bottom of the slab at 3 ft. 3 in. from the centerline of the interior girder to either side. The first pot on either side was located 9 ½ ft from the East end of the slab, and the other two on either side were positioned 18 in. on center from the first (Figure 3.16).

3.4.2.2: Test Setup

The two columns for the load frame were placed in the notched out sections of the slab 11 ft from the East end. The columns were bolted to the reaction floor beams and the crossbeams were bolted to the columns. A 400 kip capacity hydraulic ram and a 500 kip capacity load cell were hung from the crossbeams directly over the interior girder. The load was applied to the slab through two 8 in. by 20 in. neoprene pads with steel plates placed on top of them. The centers of the pads were placed 3 ft to either side of the centerline of the interior girder and 11 ft from the East end. A spreader beam was placed on top of both load plates running along the width of the slab. The ram applied load to the center of the spreader beam, which applied two equal loads to the patches (Figure 3.19).

3.4.3: Cantilever Test

The cantilever test was performed to simulate negative moments over interior supports in continuous span structures. Even though the actual design comprises simple spans, this test was performed to examine the behavior of GFRP reinforced decks in continuous spans.

3.4.3.1: Instrumentation

This test utilized eleven GFRP strain gauges, eight steel strain gauges on reinforcing bars, and six steel strain gauges on the girders. Of the eleven GFRP strain gauges, three were positioned on longitudinal bars over the centers of each girder, six were positioned on longitudinal bars on either edge of the top flange of each girder, and the other two were positioned on longitudinal bars halfway between the three girders.

They were positioned as shown in Figure 3.14. They all measured 59 ½ in. from the West edge of the slab and 2 $^{7}/_{8}$ in. from the top of the slab.

Of the eight steel reinforcing bar strain gauges, six were positioned on longitudinal bars on either edge of the top flange of each girder, and the other two were positioned on longitudinal bars halfway between the three girders. They were positioned as shown in Figure 3.15. They all measured 59 ½ in. from the West edge of the slab and 1 $^{7}/_{8}$ in. from the bottom of the slab. All of the six steel strain gauges on the webs of the three girders measured approximately 58 in. from the West end of the girders. On each girder, one gauge was located approximately 3 $^{7}/_{16}$ in. from the bottom of the girder, and one was located approximately 3 $^{7}/_{16}$ in. from the top of the girder.

The three wire pots used on this test were attached to the bottoms of each girder with a magnet. The pots were positioned right on the West end of each of the girders (Figure 3.16).

3.4.3.2: Test Setup

The two columns for the load frame were placed in the notched out sections of the slab at the West end. The columns were bolted to the reaction floor beams and the crossbeams were bolted to the columns. Three 400 kip capacity hydraulic load rams were used for this test. One was hung over each of the girders. The two rams over the exterior girders were hung with 200 kip capacity load cells and the ram over the interior girder was hung with a 500 kip capacity load cell. Load was applied to the slab through 5 in. by 5 in. neoprene pads with steel plates on top of them. The pads were located over the top of each girder and they were all 1 ft from the West end (Figure 3.19).

3.5: Test Procedures

All of the instrumentation devices; the strain gauges, wire pots, and load cells, were connected to the System 6000 data acquisition system. The Strain Smart software program was used to record the data. All the channels of the data acquisition system were zeroed and an online display of all the channels and their readings was created so the data could be monitored during testing.

3.5.1: Overhang Tests #1 & #2

A preload of 5 kips was applied to the overhangs to allow the structure to settle and the overhangs were then unloaded. Load was applied to the overhangs in 2 kip increments and data was recorded at each increment. This was continued until it was determined that the section was cracked, 30 kips for test #1 and 32 kips for test #2. The overhangs were then unloaded and reloaded up to a service wheel load times an impact factor, 21 kips. This was done three times to represent the cycling of traffic the bridge would see and data was recorded at each load stage.

The overhangs were loaded again from the previous load in 2 kip increments until a total load of approximately 40 kips was on the overhang. At this point, the load increments were increased to 4 kips up to failure, and data was still recorded at each increment.

Throughout the entire process, the overhang was continuously checked for cracks and the crack widths were measured using crack cards. The Whittemore gauge readings were also taken at various loads throughout the testing.

During test #1, after a load of 65 kips had been reached, it was discovered that the ram was putting a torque on the crossbeam. This was in turn was putting a torque on the entire frame and causing the columns to bend. The test was stopped and the columns were braced. The test was started again and loaded in 10 kip increments up to the previous load of 65 kips. The overhang was then loaded up to failure in 5 kip increments.

3.5.2 Interior Girder Test

A preload of 10 kips was applied to the spreader beam, 5 kips per patch load, to allow the structure to settle and then the deck was unloaded. The load was applied to the spreader beam in 10 kip increments up to a load of 160 kips and data was recorded at each increment. The increments were then increased to 20 kips up to failure.

The deck was continuously checked for cracks throughout the test. Once cracking occurred, some of the cracks were labeled and their widths were measured at various loads using a crack microscope.

3.5.3: Cantilever Test

The two exterior hydraulic load rams for this test were connected in series and the interior ram was connected separately. The loads were kept about equal on each ram by using the online display of the loads as measure by the load cells.

A preload of 10 kips was applied to each ram to allow the structure to settle and then the bridge was unloaded. Load was applied to the cantilever through each ram in 10 kip increments and data was recorded at each increment. This was done until it was determined that the section was significantly cracked, 110 kips on each ram. The cantilever was then unloaded to 10 kips and loaded up to a service load, about 80 kips.

This was done five times to represent the cycling of traffic the bridge would see and data was recorded at each load stage. The load was taken back up to 110 kips and continued in 10 kip increments until a load of 140 kips was reached. The section was not failed due to inadequate capacity of the load cells and load frames.

The deck was continuously checked for cracks throughout the test. Once cracking occurred, some of the cracks were labeled and their widths were measured at almost all load increments, including the service cycling, using a crack microscope.

CHAPTER IV
RESULTS AND DISCUSSION

4.1: Overhang Tests #1 & #2

4.1.1: Introduction

The tests of the bridge deck overhangs were performed to obtain deflection information, GFRP reinforcing bar stresses, cracking loads, crack widths, and failure load and type. These tests were completed by following the procedures as presented in Chapter 3. This section presents the results of these two tests.

4.1.2: Deflections

4.1.2.1: Overhang Test #1

For both overhangs, the deflections were measured using wire pots that were anchored to the bottom of the deck. The collected data was used to create load vs. deflection graphs for each wire pot. Figure 4.1 presents the load vs. deflection data series for wire pots ST 1 and ST 31 on overhang test #1. The graph also contains two theoretical data series for the overhang test #1, which are an attempt to predict the deflection values based on current design guides and equations.

The data series labeled 'Theoretical' was the more basic of the two theoretical models. The effective width of the overhang was calculated using Equation 4.1 as presented in Table 4.6.2.1.3-1 of the AASHTO LRFD Bridge Design Specifications

$$EW_{overhang} = 45'' + 0.833X \quad \textbf{(4. 1)}$$

Where : $EW_{overhang}$ = effective width of overhang

X = distance from load to point of support, in.

(1994). The effective width was calculated to be 4 ½ ft using an X of 11 in. The deck was modeled as a 12 in. wide strip in the analysis program RISA-2D (1993) with the girders modeled as pin supports. For the exterior girder closest to the overhang test, the exterior edge of the girder was modeled as a pin support. The load was applied to the beam at a distance of 11 in. from the exterior edge of the girder. The loads applied in the analysis were the actual test loads divided by the effective width of the overhang, to obtain an 'effective load' on the section.

Transformed moments of inertia, I_t, of 443.4 in.^{4} and 629.9 in.^{4} were used for the interior slab and overhang portions, respectively. Sample calculations of cross-sectional properties are located in Appendix B. Once the estimated cracking load of 26 kips, 5.78 kips effective load, was reached, a cracked moment of inertia, I_{cr}, of 47.9 in.^{4} was used to model the overhang portion of the slab. The loads and their corresponding deflections were recorded and plotted.

The data series labeled 'Theo. I_{eff}' was modeled and calculated exactly the same way as 'Theoretical' except an effective moment of inertia, I_e, was used for the overhang portion of the slab. Equations 4.2 and 4.3, as presented by ACI 440 (2001), were used to calculate the effective moment of inertia. Equation 4.2 is only valid for values of $M_a > M_{cr}$.

$$I_e = \left(\frac{M_{cr}}{M_a}\right)^3 \beta_d I_g + \left[1 - \left(\frac{M_{cr}}{M_a}\right)^3\right] I_{cr} \leq I_g \qquad \textbf{(4. 2)}$$

Where : I_e = effective moment of inertia, in^4

M_{cr} = cracking moment, in. - k

M_a = max moment in a member at particular load, in. - k

I_g = gross moment of inertia, in^4

β_d = reduction coefficient

I_{cr} = cracked moment of inertia, in^4

$$\beta_d = \alpha_b \left[\frac{E_f}{E_s} + 1 \right] \quad \textbf{(4. 3)}$$

Where : α_b = bond dependent coefficient, 0.5
E_s = modulus of elasticity of steel, 29,000 ksi
E_f = modulus of elasticity of FRP, 6,300 ksi

In Equation 4.2, the transformed moment of inertia, I_t, was used in place of the gross moment of inertia, I_g. The difference between the two is very small, but the use of the transformed moment of inertia is more accurate and will yield better results.

M_a was calculated by multiplying the effective load by 11 in., the distance from the load point to the edge of the girder. Equation 4.4 was used to calculate the cracking moment M_{cr}.

$$M_{cr} = \frac{f_t I_t}{y} \quad \textbf{(4. 4)}$$

Where : I_t = transformed moment of inertia, in^4
M_{cr} = cracking moment, in. - k
$f_t = 7.5\sqrt{f_c'}$, concrete tensile strength, psi
f_c' = concrete compressive strength, psi
y = distance to centroid from surface, in.

For the RISA-2D (1993) analysis, I_e was equal to I_t up until the load of 32.1 kips was reached. At this load, the effective load was calculated to be 8.02 kips and M_a was 7.35 ft-kips, which exceeded the value of M_{cr}, 6.47 ft-kips. The value of f_c' used was 5010 psi. This was the 34 day batch 1 average. Both overhangs were poured with batch 1 and were tested about 34 days after the pour.

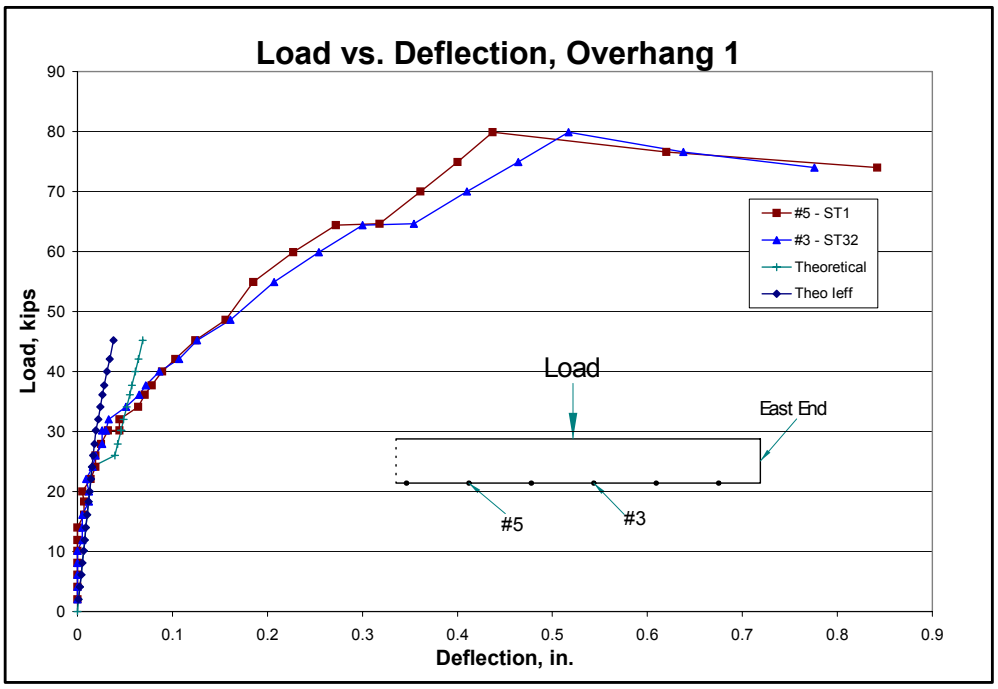

Figure 4.1: Load vs. Deflection Plot for Overhang Test #1

As shown in Figure 4.1, both theoretical approaches predict the measured deflections well up to a load of about 26 kips. Actually, both of the theoretical data series have identical deflection values up to a load of 26 kips, because they are both using I_t for the moment of inertia of the overhang. At around 24 kips, there is a slight slope change in the measured value data series, indicating that the section has become less stiff and non-visible cracking may be occurring. Cracking doesn't occur in the 'Theoretical' data series until a load of 26 kips is reached and I_{cr} is used as opposed to I_t. This causes a noticeable jump in the data, whereas the measured data series has more of a gradual slope change during cracking. The jump can be attributed to the fact that the section is assumed to be completely cracked at a load of 26 kips, when in fact the change in I is probably more of a gradual process up until the section becomes completely cracked. When the section is completely cracked, the cracks in the section have propagated as deep and as wide as they will go.

On the other hand, the 'Theo. I_{eff}' data series accurately models this gradual slope change, but the change occurs at a much higher load, 32 kips to be exact, than is shown by the measured data. This can be attributed to the fact that I_{eff} is formulated to constantly decrease with increased moment, starting at the predicted cracking moment. Because I_e is constantly decreasing, the slope is constantly decreasing as well until a totally cracked section exists and the slope ceases to change. This is a more accurate representation of what actually happens as shown by the experimental data, because when a concrete section starts to crack, it does not instantly become completely cracked. The cracking is gradual with increased load until the section is completely cracked.

A second and more major slope change occurs in the experimental data around a load of 32 kips. This slope change is not seen at all in the theoretical data series. One contributor to these increased deflections may be shear deflections, which are not accounted for in the theoretical models. Deflections in short spans are known to be dominated by shear, especially at higher loads, as it the case here. Other contributors may include support deflection (at the girder flange), which was not measured, the fact that the East end was a cantilever that was allowed to deflect during the test, and the fact that the concrete has gone non-linear at the higher loads, above 40 kips.

4.1.2.2: Overhang Test #2

Overhang test #2 was performed and data was collected in exactly the same manner as it was for test #1, and Figure 4.2 was created the same way, only this time using wire pots ST 3 and ST 4. The theoretical data calculations were identical with the exception of a few different numbers. I_t for overhang #2 was 629.6 $in.^4$, I_{cr} was 46.2 $in.^4$, but M_{cr} remained 6.47 ft-kips. For the 'Theoretical' data series, the estimated crack load

was lowered to 20 kips, 4.44 kips effective, based on observations and other data. Therefore, at 20 kips, the deflections in the overhang section were calculated using I_{cr} as opposed to I_t. For the 'Theo. I_{eff}' data series, I_e was equal to I_t up to a load of 32 kips.

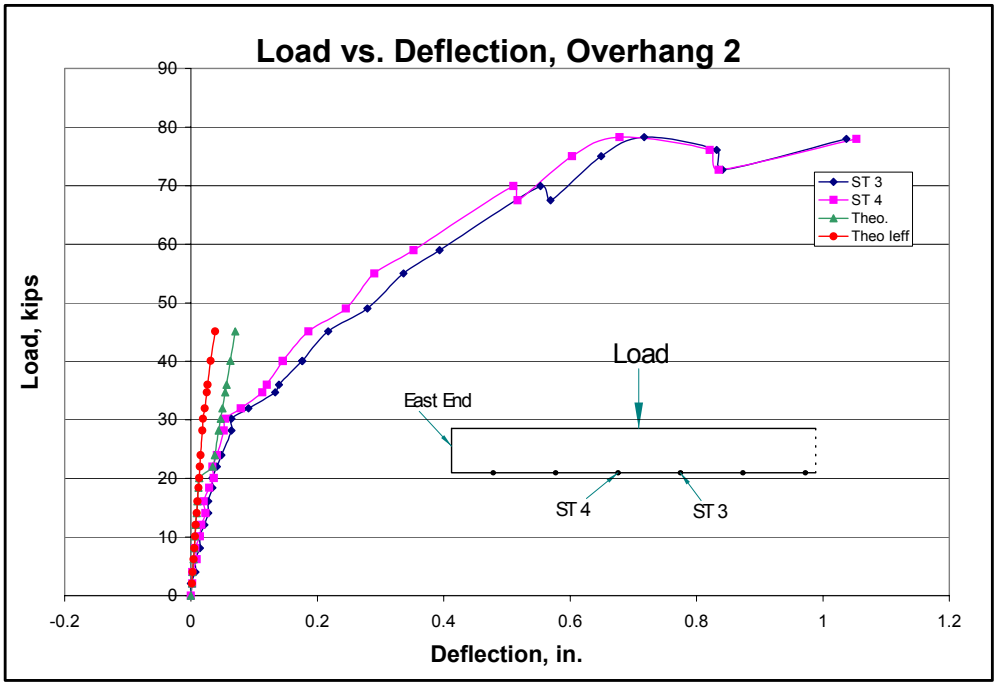

Figure 4. 2: Load vs. Deflection Plot for Overhang #2

Again in Figure 4.2, the theoretical deflections predict the measured values reasonable well, but this time only up to a load of about 16 kips. At this point, the slope gradually begins to decrease in the measured values, once again indicating possible cracking. At about 20 kips, this slope change is a little more obvious and the 'Theoretical' data series is now modeled as fully cracked and is predicting the measured deflections well, where it is expected that it would possibly over-predict the deflections. This may be due to the fact that the measured deflections may already be including shear deflections. The 'Theo I_{eff}' data series is once again not accurately predicting deflections after cracking because of its high modeled cracking load of 32 kips. It is, however,

modeling the gradual slope change well. As in the test #1 graph, the measured deflections begin to increase more rapidly at a load of about 32 kips, and are not modeled at all by the theoretical data series. This can once again be attributed to shear deflections, support deflections, and East end cantilever deflections.

4.1.3: Reinforcing Strains and Stresses

4.1.3.1: Overhang Test #1

The strain gauge data was acquired by the System 6000 and reduced into micro strains. Load vs. strain plots were then created for both the steel and GFRP gauges. Below, Figure 4.3 is a plot of load vs. steel reinforcing bar strains. Steel gauge #1 on the plot has a fairly constant negative slope up to a load of 46 kips, indicating that the bar is below the neutral axis and is in compression. At a load of 49 kips, the stain takes a large jump and becomes positive, indicating that the bar is now above the neutral axis and in

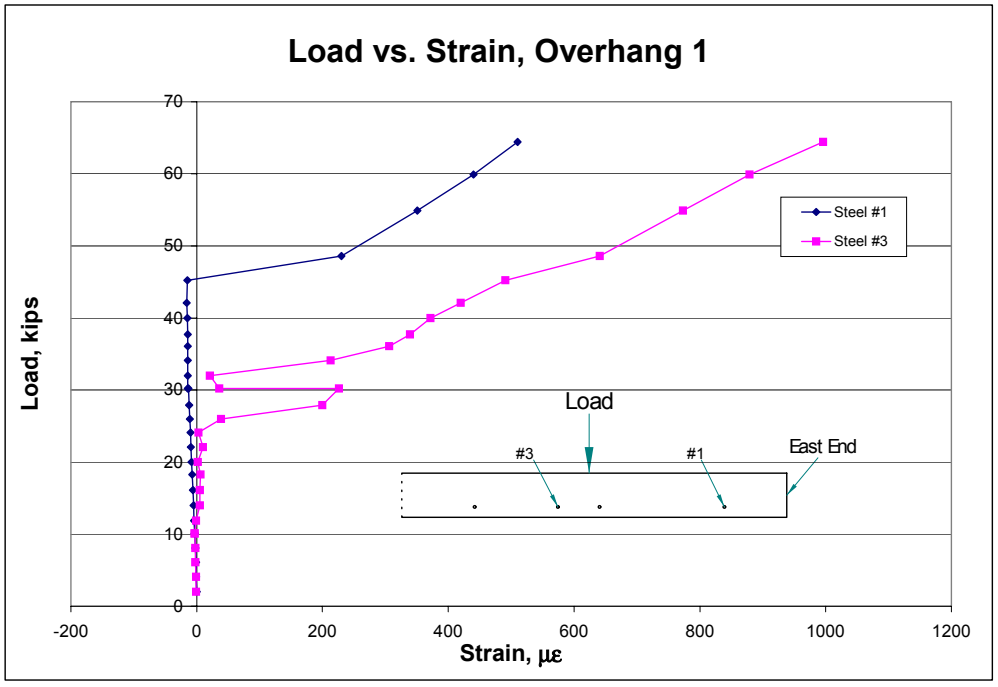

Figure 4.3: Load vs. Strain Plot for Overhang #1, Steel Gauges

tension. The change in neutral axis location is due to cracking in the concrete above the bar. Calculations of I_{cr} also indicate the neutral axis to be below the steel after cracking.

Steel gauge #3 follows the same pattern as gauge #1, only the strains are constant and hover around zero up to a load of 24 kips. This would indicate that the bar is fairly close to the neutral axis. At a load of 26 kips, the strains make a large increase into the tension region. This once again indicates that a crack in the concrete has opened up and the neutral axis has dropped below the bar, causing it to go into tension. This happens at 26 kips as opposed to 49 kips because gauge #1 is closer to the load and cracking occurred there first.

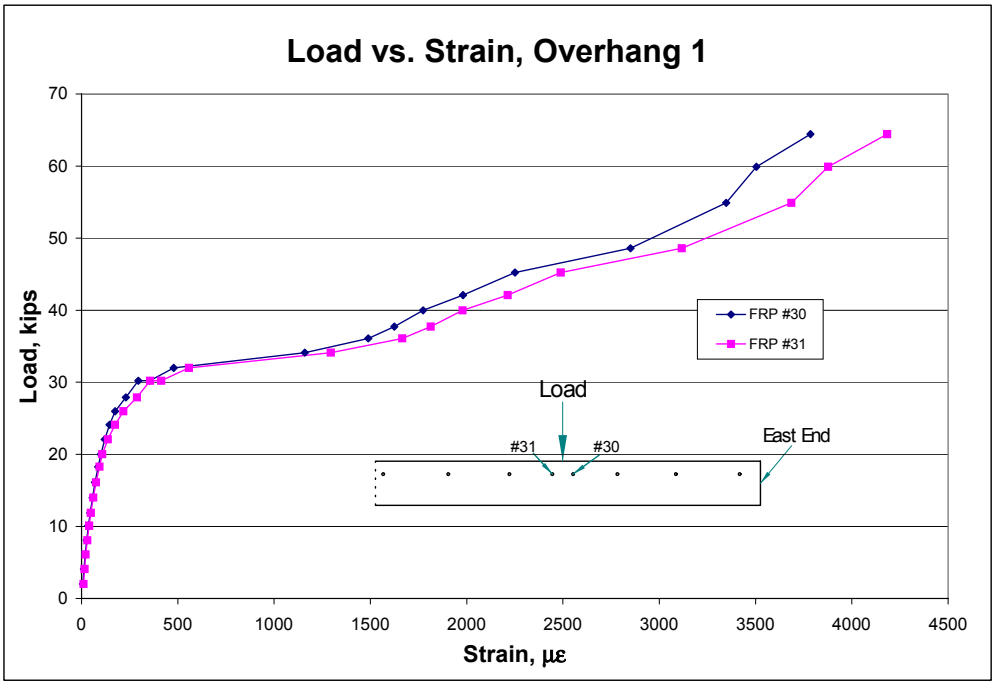

Figure 4.4: Load vs. Strain Plot for Overhang #1, GFRP Gauges

Figure 4.4 is a load vs. strain plot for GFRP gauges #30 and #31 which were located 2 in. to either side of the load. The plot shows both gauges having approximately

the same values, which is expected because they are approximately the same distance away from the load. They both have a relatively constant positive slope up to a load of about 22 kips. This indicates that they were both located above the neutral axis and were in tension. At a load of 24 kips, the slope starts to decrease indicating that the section has cracked, the neutral axis has been lowered, and therefore strains in the bars are increasing more for the same load increment. The slope continues to decrease up to a load of about 32 kips, where it almost reaches zero slope, and then increases again at 36 kips at which point it stays pretty constant, indicating that the section is fully cracked.

The stresses in the GFRP bars were obtained by multiplying the recorded strains by the modulus of elasticity of the GFRP bars, 6300 ksi. Stress profile curves were then created at various loads. These plots showed the stress in each bar relative to its distance from the load point. Figure 4.5 is a stress profile plot for loads of 16 kips and 20 kips. As can be seen and as expected, the stresses are highest closer to the load and taper off as

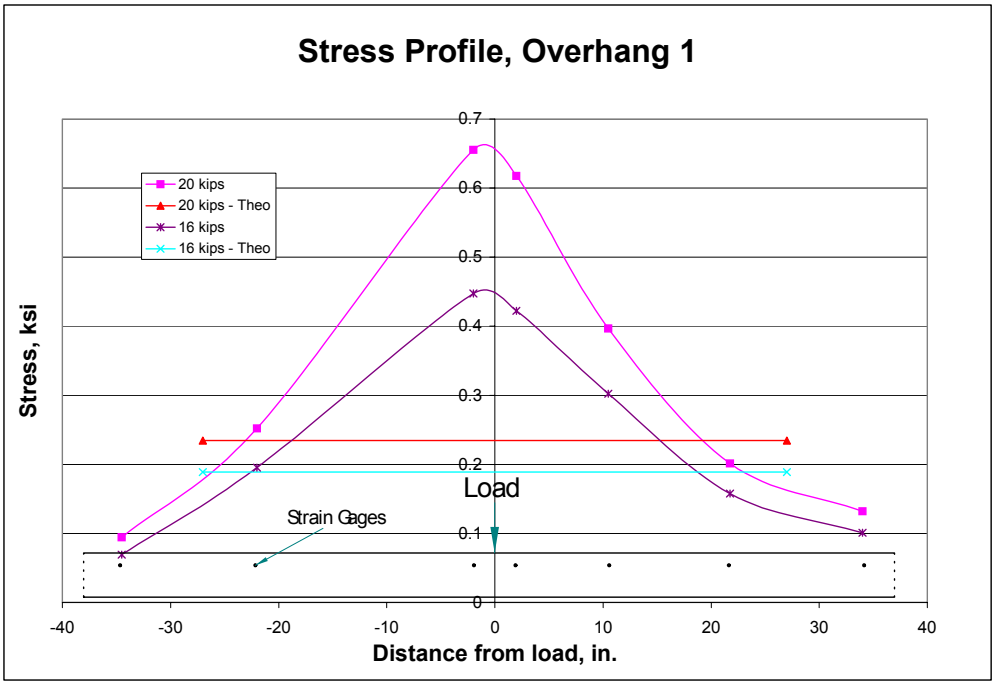

Figure 4.5: Stress Profile of Overhang #1, Pre-Cracking

gauges get further away from the load.

Figure 4.5 also contains calculated theoretical values for the stresses in the bars. These were calculated by multiplying the effective load by a moment arm of 11 in. to obtain an effective moment. Since the section was not cracked at these two loads, the moment was multiplied by y, the distance from the bar to the neutral axis, 1.935 in., and then divided by the transformed moment of inertia, I_t. The theoretical stress is plotted over the 4 ½ ft effective width, and should match the peak stresses in the measured data, but it is significantly less. As can be seen, with the load increased from 16 kips to 20 kips, the predicted value becomes more unconservative. Therefore, it is doing a better job of predicting stresses at lower loads before cracking, but is still unconservative at the low loads.

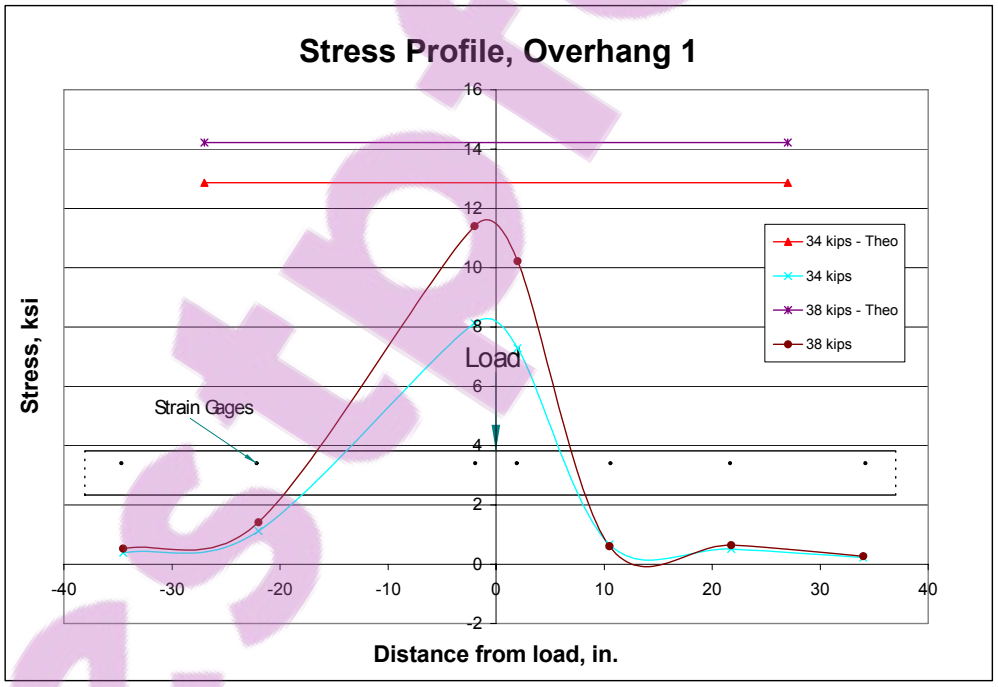

Figure 4.6: Stress Profile for Overhang #1, Post Cracking

Figure 4.6 is the same type of stress profile, only at higher loads of 34 kips and 38 kips. This is considered to be after the section had cracked based on observations and data. The same pattern of higher stresses closer to the loads is again seen in this plot. The theoretical stresses were calculated in the same manner as before, only this time, the cracked moment of inertia, I_{cr}, was used and the y value increased to 4.735 in. Now, the theoretical values are conservative and over-predicting the measured stresses. The theoretical stresses are however becoming less conservative with increased load. This is because the theoretical stresses are being calculated assuming that the section is completely cracked, when it is not. The section is only beginning to crack and as the load increases, the section will become more and more cracked and the measured values will begin to approach the theoretical values.

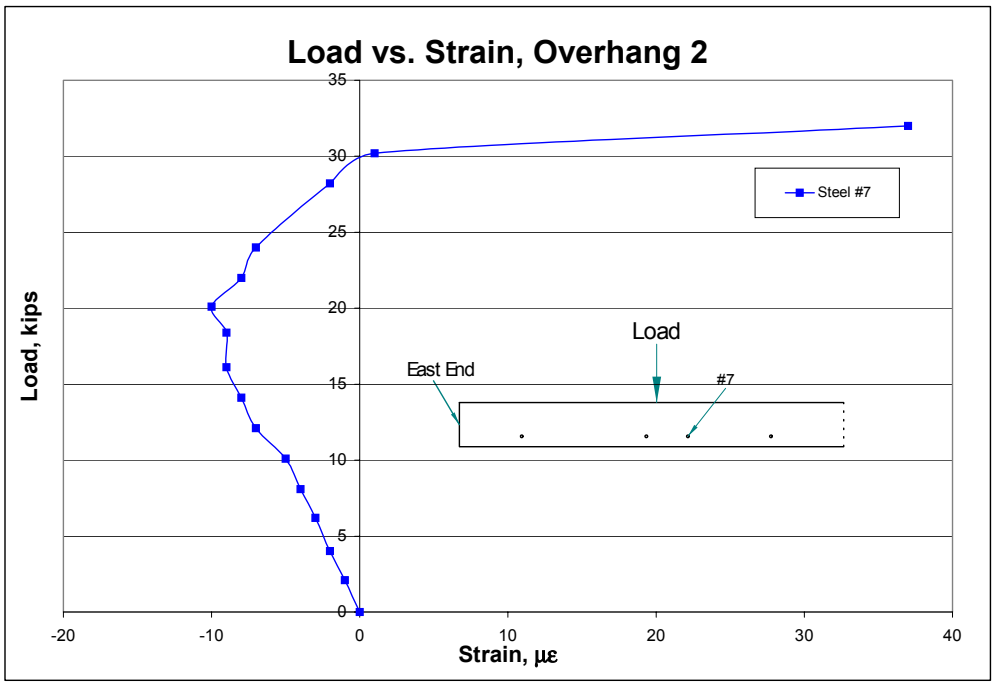

Figure 4.7: Load vs. Strain Plot for Overhang #2, Steel Gauge

4.1.3.2: Overhang #2

Figure 4.7 shows the load vs. strain plot for steel gauge #7. The plot starts out with a constant negative slope up to a load of 20 kips. At 22 kips, the slope becomes positive and gradually works its way into tension. This shows that the bar was initially below the neutral axis and in compression. At 22 kips, the section cracked, lowering the neutral axis and the compressive force in the bar decreased. The bar eventually went into tension, at which point the neutral axis was below the bar.

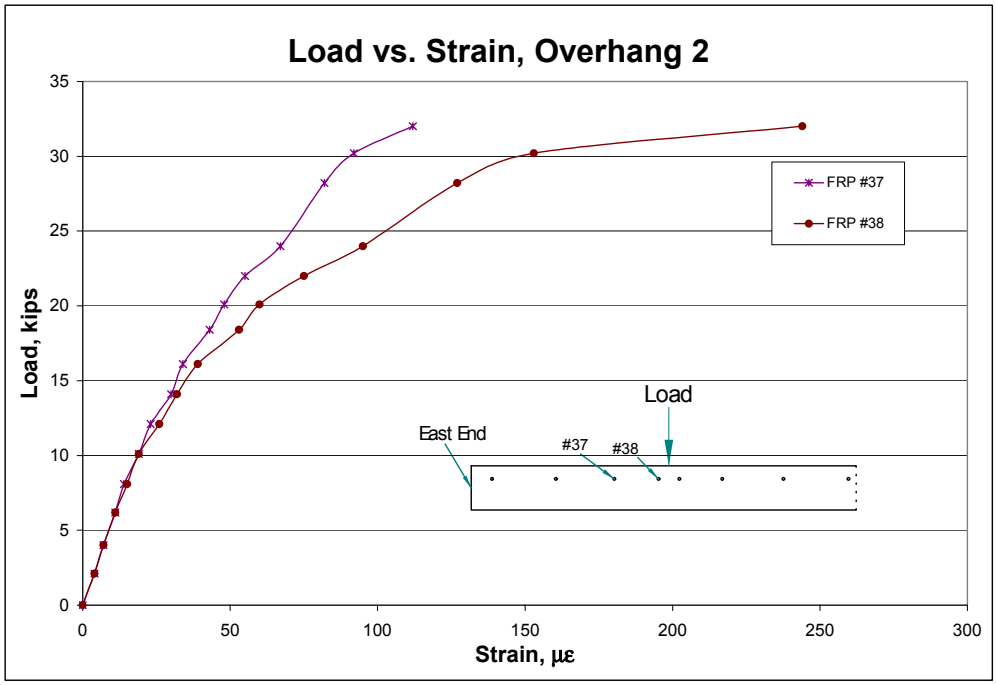

Figure 4.8: Load vs. Strain Plot for Overhang #2, GFRP bars

Figure 4.8 is a load vs. strain plot for GFRP gauges #37 and #38. Both gauges act very similarly, but #38 has higher strains as the load increases which is expected because it is closer to the load. They both have the same slope up to about 10 kips, where the slope of #38 changes slightly. Both slopes decrease slightly again at about 16 kips and then again more noticeably at 22 kips. This would correspond to some possible micro

cracking of the section and then visible cracking around 22 kips. The slope changes again around 32 kips, this time it is a very drastic change, as the section has become more cracked.

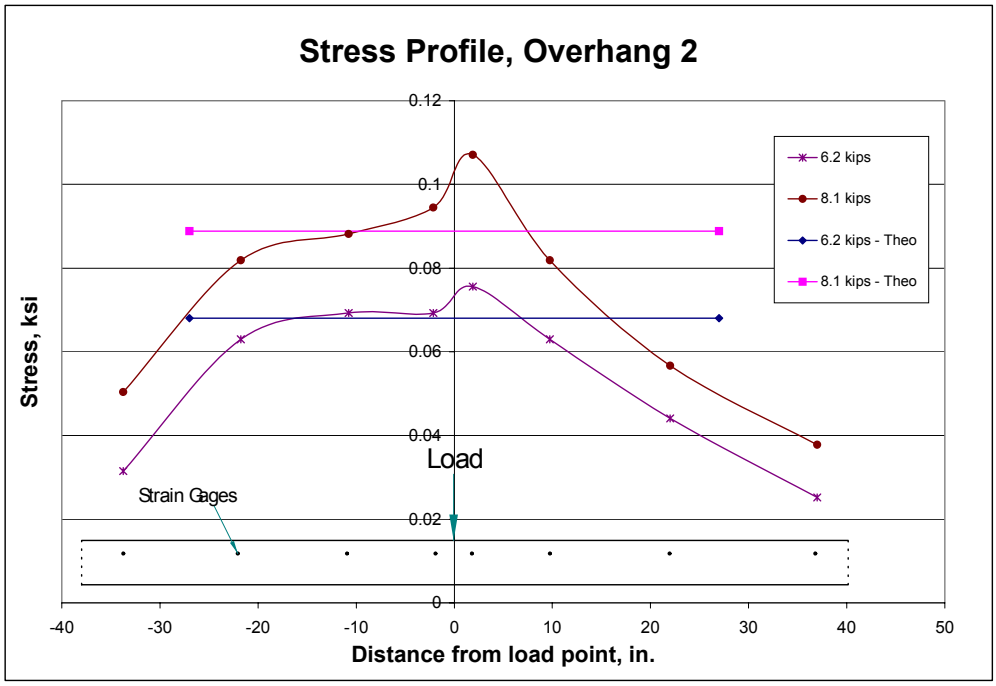

Figure 4.9: Stress Profile of Overhang #2, Pre-Cracking

The stresses were again calculated by multiplying the strains by the modulus of elasticity. Stress profile plots were made similar to those of overhang #1. Figure 4.9 is a plot of the stresses at loads of 6.2 kips and 8.1 kips. The plot has the same trend as the plots for overhang #1, with the stresses being higher closer to the load and tapering off with increased distance from the load. The theoretical stresses were calculated in the same manner, and were plotted over the same effective width of 4 ½ ft. The effective moment was multiplied by a y of 1.81 in. and then divided by I_t, because the section was not considered to be cracked yet. These loads in Figure 4.9 are lower than those presented for overhang #1, and the theoretical values predict the peak stresses quite well.

However, as in overhang #1, as the load increased, the theoretical values became more unconservative.

Figure 4.10 is the same type of stress profile plot, only the section is cracked at the loads of 34 kips and 40 kips. Again, higher stresses exist closer to the load and fall off with increased distance. The theoretical stresses were calculated using I_{cr} and a value of 4.62 in. for y. As seen in the plot, the theoretical stresses over-predict the measured values; therefore, these values are considered to be conservative. The theoretical stresses are, however, becoming less conservative with increased load. This is because the theoretical stresses are being calculated assuming that the section is completely cracked, when it is not. The section is only beginning to crack and as the load increases, the cracks in the section will propagate deeper and wider at which point the measured values will begin to approach the theoretical values.

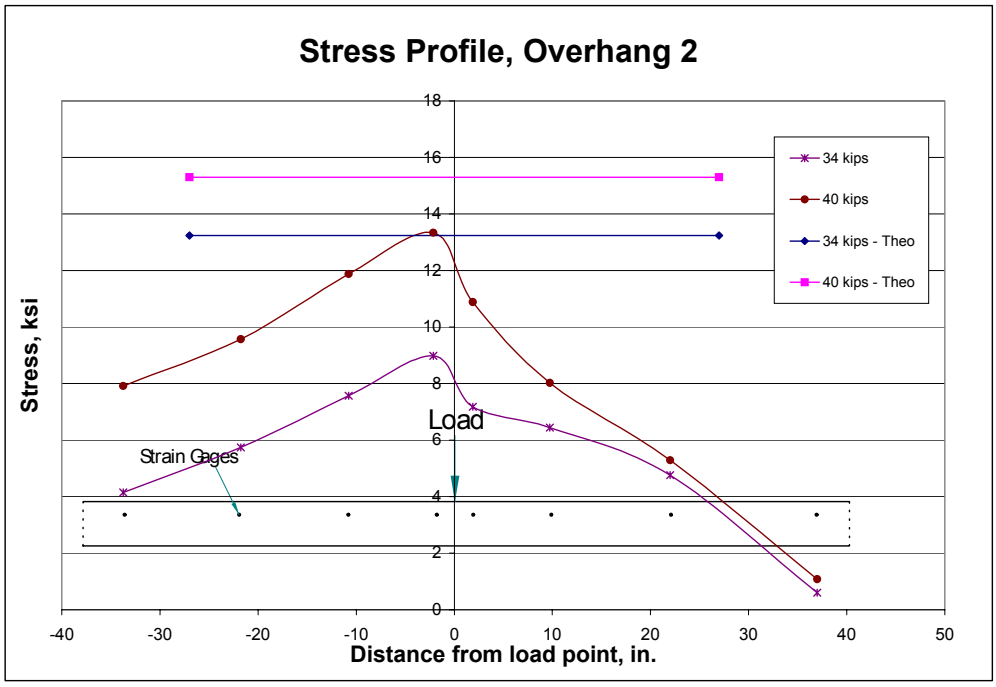

Figure 4.10: Stress Profile for Overhang #2, Post Cracking

4.1.4: Crack Widths and Cracking Loads

The first visible cracks occurred at loads of 28 kips for overhang #1 and 26 kips for overhang #2. Cracking of the two overhangs then progressed in a very similar manner. Figure 4.11 and 4.12 are crack maps of overhang #1 and overhang #2, respectively.

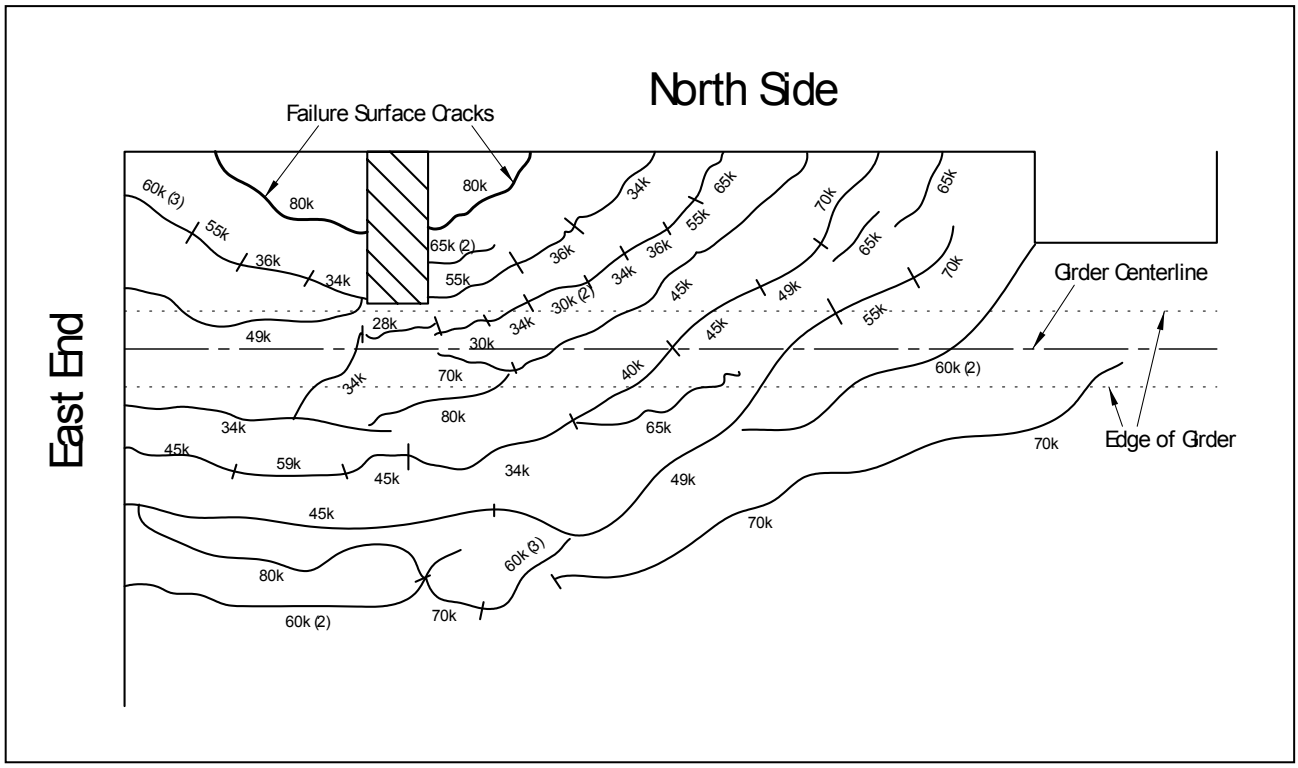

Figure 4.11: Crack Map for Overhang #1

For overhang #1, cracking started near the load and gradually progressed outwards in a semicircular pattern. The first few cracks in overhang #2 started further away from the load when compared to the first cracks for overhang #1, but the pattern and progression was virtually the same.

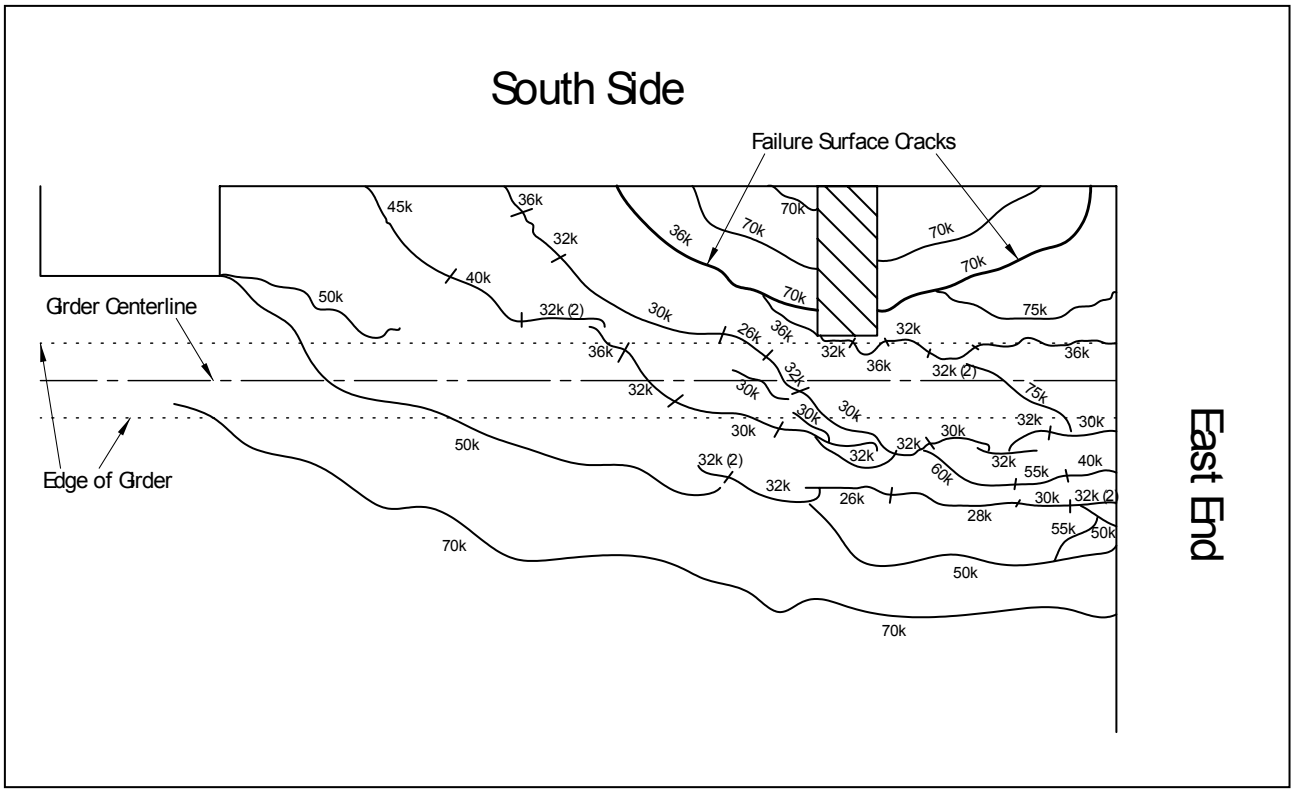

Figure 4.12: Crack Map for Overhang #2

As mentioned above, the first visible crack in overhang #1 was seen at a load of 28 kips. This is fairly consistent with the strain and deflection data which indicated cracking at about 24 kips to 26 kips. The AASHTO LRFD effective width for overhangs and the cracking moment were used in conjunction to try to predict this first cracking load. With the cracking moment, M_{cr}, previously calculated as 6.47 ft-kips and the effective width calculated as 4 ½ ft, the applied load needed to crack the section was calculated by multiplying M_{cr} by the effective width and then dividing by the moment arm of 11 in. This yielded an estimated cracking load of 31.8 kips, which over-predicts the actual load of 24 kips to 26 kips obtained from the strain and deflection data.

Another possible method instead of using the effective width would be to use influence surfaces. Influence surfaces are basically influence lines put into a two-dimensional setting, such as a plate or slab. Pucher (1977) created influence surface

maps for given situations, in this case a restrained edge of a cantilever (see Figure A.1 in Appendix A). The load is then placed on the map and the value of the influence surface is interpolated. This value is then divided by 8π and multiplied by the load to obtain the moment. In this case, the moment to be found is at the edge of the girder and the cantilever length is 21 in. The load is applied 11 in. from the edge of the girder corresponding to a value of 9.1 on the influence map. With a calculated cracking moment of 6.47 ft-kips, the load to crack the section can be calculated by multiplying M_{cr} by 8π and dividing by 9.1. This yields a cracking load of 17.9 kips, which is lower than the observed cracking load of 24 kips to 26 kips.

Table 4.1: Crack Widths for Overhang Tests

Overhang #1 Crack Widths			Overhang #2 Crack Widths			
Load	Measured*	Theoretical		Measured		
kips	in.	in.	Load	Crack Card	Whittemore	Theoretical
28	0.002	0.0279	kips	in.	in.	in.
30	0.002	0.0302	30	*	0.0014	0.0320
34	0.01	0.0341	32	0.013	#	0.0342
36	0.013	0.0362	36	0.016	0.0136	0.0385
38	0.013	0.0378	40	0.02	0.0188	0.0427
40	0.016	0.0401	45	0.02	#	0.0482
45	0.016	0.0453	50	0.04	0.0328	0.0534
49	0.02	0.0487	55	0.05	#	0.0587
55	0.03	0.0550	60	0.05	0.0558	0.0641
59	0.03	0.0600	*Too small to measure			

*Measured with crack card #Measurements not taken

Visible cracks didn't appear on overhang #2 until a load of 26 kips was reached. This is in contrast with the strain and deflection data which shows that cracking probably occurred at a load of 22 kips. The cracks in the deck at a load of 22 kips were probably too small for the human eye to observe, and therefore, the deck is considered cracked at 22 kips. The AASHTO LRFD and influence surface methods both yield the same cracking loads as for overhang #1 of 31.8 kips and 17.9 kips, respectively. These

numbers once again over-predict and under-predict the actual cracking load of 22 kips. However, for overhang #2, the influence surface method was closer to the actual value.

The measured and theoretical crack widths for overhangs #1 and #2 are presented in Table 4.1. The crack widths for overhang #1 were only measured by using a crack card, whereas the crack widths for overhang #2 were measured using a crack card and a Whittemore gauge, if a crack existed across the gauge length. The theoretical values were calculated using Equation 4.5, the ACI 440 (2001) modified semi-emperical Gergely-Lutz equation as shown below.

$$w = \frac{2200}{E_f}\beta k_b f_f \sqrt[3]{d_c A} \qquad \textbf{(4. 5)}$$

Where : w = crack width, in.

E_f = modulus of elasticity of GFRP, 6300 ksi

β = ratio of the distance from the neutral axis to extreme tension fiber to the distance from the neutral axis to the center of the tensile reinforcement

k_b = bond - dependent coefficient, 1.3 (from DeFreese (2001))

f_f = calculated stress in the GFRP reinforcing bars, ksi

d_c = thickness of the concrete cover measured from extreme tension fiber to center of bar closest thereto, in.

A = effective tension area of concrete, $in.^2$

As can be seen in Table 4.1, the ACI 440 equation for crack widths over-predicts the measured values, proving the equation to be extremely conservative. One factor that may make the equation so conservative is f_f. This stress in the GFRP bars is calculated using the AASHTO LRFD effective width. Previously in Section 4.1.3, it has been shown that this method over-predicts the stresses. This would and does appear to lead to the crack widths being over-predicted as well.

4.1.5: Ultimate Load and Failure Mode

The failure mode of both overhang tests was two-way shear, commonly referred to as punching shear. Overhang test #1 failed at a load of 86 kips, while overhang test #2 failed at a slightly lower load of 78 kips. This failure mode and load were not predictable with calculations. The predicted failure mode was one-way shear. Equation 4.6, as presented in ACI 440 (2001), for the shear strength of concrete reinforced with FRP is shown below.

$$V_{c,\,f} = \frac{\rho_f E_f}{90\beta_1 f_c'} 2\sqrt{f_c'} b_w d \qquad \textbf{(4. 6)}$$

Where : $V_{c,\,f}$ = nominal shear strength provided by concrete with FRP flexural reinforcement, k

ρ_f = FRP reinforcement ratio, $\frac{A_f}{b_w d}$

A_f = area of FRP reincorcement, in.^{2}

E_f = modulus of elasticity of FRP, psi

f_c' = compressive strength of concrete, psi

b_w = effective width of concrete block, in.

d = depth to tension reinforcement from surface, in.

β_1 = concrete factor equal to .80 for f_c' = 5000 psi

With an A_f of 0.93 in.^{2}, E_f of 6,300,000 psi, f_c' of 5010 psi, b_x of 12 in., and a d of 6.125 in., the shear capacity of overhang #1 was calculated to be 2.3 kips per foot. This multiplied by the effective width of 4.5 ft yields a load of 10.3 kips. All of the numbers were the same for overhang #2 except d was 6 in., which still yielded a shear failure load of 10.3 kips for overhang #2. Because the section did not fail in one-way shear as expected, the accuracy of this equation cannot be validated or disproved, but it does

appear to be very conservative. This is probably a combination of the actual equation being conservative, and the effective width equation being slightly conservative.

With both overhangs having failed in punching shear, Equation 4.7 from ACI 318 (1999) was used to calculate the two-way shear capacity of the overhangs.

$$V_c = \left(2 + \frac{4}{\beta_c}\right)\sqrt{f_c'}\, b_o d \qquad \textbf{(4. 7)}$$

Where : V_c = nominal shear strength provided by concrete, lb
f_c' = compressive strength of concrete, psi
b_o = perimeter of critical section for slabs, in.
d = depth to tension reinforcement from surface, in.
β_c = ratio of long side to short side of concentrated load

With a β_c of 2.5, b_o of 56.125 in., d of 6.125 in., and f_c' still equal to 5010 psi, the two-way shear strength of overhang #1 was calculated to be 87.7 kips, which is very close to the actual failure load of 86 kips. For overhang #2, with b_o now equal to 56 in. and a d of 6 in., the shear strength was calculated to be 85.7 kips. This is still relatively close to the actual failure load of 78 kips. Overall, it appears that the equation for punching shear predicts the failure loads for both overhangs reasonably well, even though they were expected to fail in one-way shear.

4.1.6: Design Criteria

Table 4.2: Design Criteria Comparison

	Overhang #1 Values			Overhang #2 Values		
Design Criteria	Allowable	Measured	Calculated	Allowable	Measured	Calculated
Stresses, ksi	12.1	1.87	7.92	12.1	3.55	8.01
Crack Widths, in.	0.02	< 0.001	0.021	0.02	< 0.001	0.022
Deflections, in.	0.07	0.048	0.032	0.07	0.073	0.033
Nominal Moment Capacity, ft-k	-	78.8*	121.1	-	71.5*	117.2

*Failed in punching shear prior to flexural capacity

Table 4.2 shows a comparison between allowable, calculated, and measured values for various design criteria.

The allowable stresses were calculated in accordance with the ACI 440 (2001) guidelines. For cyclic stress limits in FRP reinforcement, the allowable stress is 20 percent of the design tensile strength, f_{fu}. The design tensile strength, f_{fu}, is equal to the guaranteed tensile strength, f^*_{fu}, times an environmental reduction factor, C_E, which is equal to 0.7 for GFRP bars. The guaranteed tensile strength, f^*_{fu}, is equal to the tested average, 106 ksi for the No. 5 bars, minus three standard deviations of 6.68 ksi. This yielded a design value of 12.1 ksi. The measured values were taken at service load, 16 kips plus an impact factor of 30 percent, for a total load of 21 kips on the overhang. As can be seen in the table, the measured values for both overhangs are well below the allowable design value. This indicates that the design is conservative.

The calculated values for the crack widths were obtained using Equation 4.5, which was presented in Section 4.1.4. The load used for the calculation was 21 kips, service load of 16 kips plus a 30 percent impact factor. ACI 440 (2001) recommends a maximum crack width of 0.02 in. In the two overhang tests, the slab was not even cracked at a load of 21 kips. After the slab became cracked and a load of 21 kips was applied, the cracks were too small to measure and were less that 0.001 in. when compared to a crack card. This indicates that the design method is conservative.

AASHTO LRFD Bridge Design Specifications (1994) set the recommended, not mandatory, allowable deflections at service loads of an overhang section as the length of the overhang section divided by 300. Overhangs #1 and #2 had a cantilever length of 21 in. leading to an allowable deflection of 0.07 in. at a service load of 21 kips. The

measured data for overhang #1 was well below the allowable, while the measured value for overhang #2 was slightly higher. Overhang #1 indicates that the design is conservative, but overhang #2 indicates that the design is neither conservative nor unconservative.

The nominal moment capacity of the section was calculated using Equations 4.8, 4.9, and 4.10, as presented in ACI 440 (2001).

$$M_n = A_f f_f \left(d - \frac{a}{2} \right) \qquad \textbf{(4. 8)}$$

Where : M_n = nominal moment capacity of section, in. - lb
A_f = area of FRP reinforcement, in.^{2}
f_f = stress in the FRP reinforcement in tension, psi
d = depth to the tension reinforcement from surface, in.
a = depth of equivalent rectangular stress block, in.

$$a = \frac{A_f f_f}{0.85 f_c' b} \qquad \textbf{(4. 9)}$$

Where : f_c' = compressive strength of concrete, psi
b = effective width of concrete, in.

$$f_f = \left(\sqrt{\frac{(E_f \varepsilon_{cu})^2}{4} + \frac{0.85 \beta_1 f_c'}{\rho_f} E_f \varepsilon_{cu}} - 0.5 E_f \varepsilon_{cu} \right) \leq f_{fu} \qquad \textbf{(4. 10)}$$

Where : E_f = modulus of elasticity of FRP, psi
ε_{cu} = ultimate strain of concrete, 0.003
ρ_f = FRP reinforcement ratio
β_1 = concrete factor equal to .80 for f_c' = 5000 psi
f_c' = compressive strength of concrete, psi
f_{fu} = design tensile strength of FRP, psi

The measured nominal moment capacity is not the true nominal moment capacity because the section did not fail in flexure, it failed in punching shear. It is simply the ultimate load on the section multiplied by the moment arm of 11 in. As can be seen, the section failed well before the nominal moment capacity was reached. Therefore, the flexure design of the overhang does not control.

4.2: Interior Girder Test

4.2.1: Introduction

The test of the bridge deck over the interior girder was performed to obtain deflection information, GFRP reinforcing bar stresses, cracking loads, crack widths, and failure load and type. This test was completed by following the procedures as presented in Chapter 3. The results of this test are presented in Section 2 of this chapter.

4.2.2: Deflections

With the wire pots anchored to the bottom of the slab, the deflections were measured at various load intervals. The data was collected and load vs. deflection plots were made. Figure 4.13, below, is a plot that contains the load vs. deflection data series for two of the wire pots and one theoretical data series. The location of the two wire pots is shown on the figure. They were both under the patch load 3 ft 3in. on either side of the interior girder.

The theoretical data series was calculated in a very similar manner to the 'Theo. I_{eff}' data series for overhangs #1 and #2. The effective width for this case was calculated using Equation 4.11 as presented in Table 4.6.2.1.3-1 of the AASHTO LRFD Bridge Design Specifications (1994).

$$EW_{neg.mom.} = 48'' + 0.25S \quad \textbf{(4.11)}$$

Where : $EW_{neg.mom.}$ = effective width of negative moment region, in.

S = spacing of supporting components (girders), in.

The effective width was found to be 5 ft 7 ½ in. The deck was again modeled as a 12 in. wide strip in the analysis program RISA-2D (1993) with the girders modeled as pin supports. The overhang portions were not included in the analysis because they have very little to no effect on the deflection. Two equal loads were applied, one 3 ft on either side of the interior girder. The loads applied in the analysis were the actual test loads divided by the effective width of the overhang, to obtain an 'effective load' at each point.

The analysis was performed using an effective moment, I_e, over the whole section. This effective moment of inertia was a combination of two moments of inertia, the midspan effective moment of inertia, $I_{e(m)}$, and the support effective moment of inertia, $I_{e(1)}$. Both of these were calculated using Equations 4.2 and 4.3 in Section 4.1.2.1, again using the transformed moment of inertia, I_t, as opposed to the gross moment of inertia I_g. They were combined using Equation 4.12 for beams continuous on one end only as prescribed by ACI 435 (1995).

$$I_e = 0.85\, I_{e(m)} + 0.15 I_{e(1)} \quad \textbf{(4.12)}$$

Where : I_e = effective moment of inertia, in^4

$I_{e(m)}$ = effective moment of inertia at midspan, in^4

$I_{e(1)}$ = effective moment of inertia at the support, in^4

Each effective moment of inertia had a different M_{cr} and M_a. The M_a for each was calculated using the same RISA-2D (1993) analysis program mentioned previously.

M_{cr} for each was calculated using Equation 4.4, with f_c' being 5770 psi. This was the average compressive strength of batch 1 and 2 combined at 64 days. This was used because the test contained batches 1 and 2 and was tested just before the 64 day break. $M_{cr(m)}$ was calculated as 5.75 k-ft per ft and $M_{cr(1)}$ was calculated as 5.48 k-ft per ft. I_e for the section was equal to I_t, 443.3 in.^{4}, up the load of 50 kips. At this load, $M_{a(1)}$ exceeded $M_{cr(1)}$, so the section was assumed to be cracked at the interior support. $I_{e(m)}$ was equal to I_t up to a load of 80 kips. So at 80 kips, the section was assumed to be cracked over the support and at midspan.

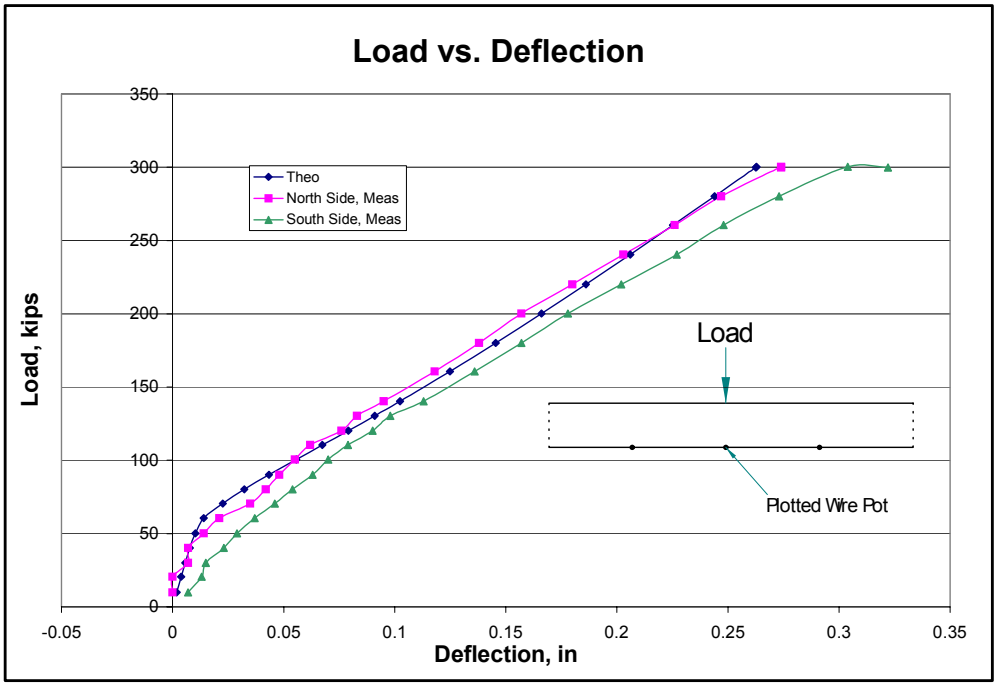

Figure 4.13: Load vs. Deflection Plot for Interior Girder Test

As shown in Figure 4.13, the theoretical value predicts the measured deflections of both wire pots very well. The theoretical appears to do a better job of predicting the North side deflections. At a load of 50 kips, the slope of the theoretical line starts to decrease, and by a load of 70 kips, the slope has decreased significantly. This same

behavior can also be seen in the North side wire pot, even though the first few data points are a little sporadic. The South side data, on the other hand, starts out with a lower slope than the other two, but a change in slope can still be seen around 50 kips. The change in slope of all the series indicates that cracking has occurred in the section. After a load of 70 kips, all three series exhibit the same behavior. The two measured series do have slightly lower slopes than the theoretical at these higher loads. This is probably due to the fact that shear deformations are occurring and were not accounted for in the theoretical data. Overall, it can be said that the effective width equation, the two effective moment of inertia equations, and the RISA-2D (1993) model predict the deflections very well.

4.2.3: Reinforcing Strains and Stresses

Figure 4.14 is a load vs. strain plot of steel strain gauge #13. The location of the gauge is shown in the plot. The slope of the plot is negative up to a load of 90 kips, indicating that the bar is initially below the neutral axis and is in compression. At this point the slope goes to infinity, then becomes positive at 110 kips. This indicates a crack in the section and the gradual lowering of the neutral axis. At 140 kips, the bar is in tension because the section has become so cracked that the neutral axis has now dropped below the bar.

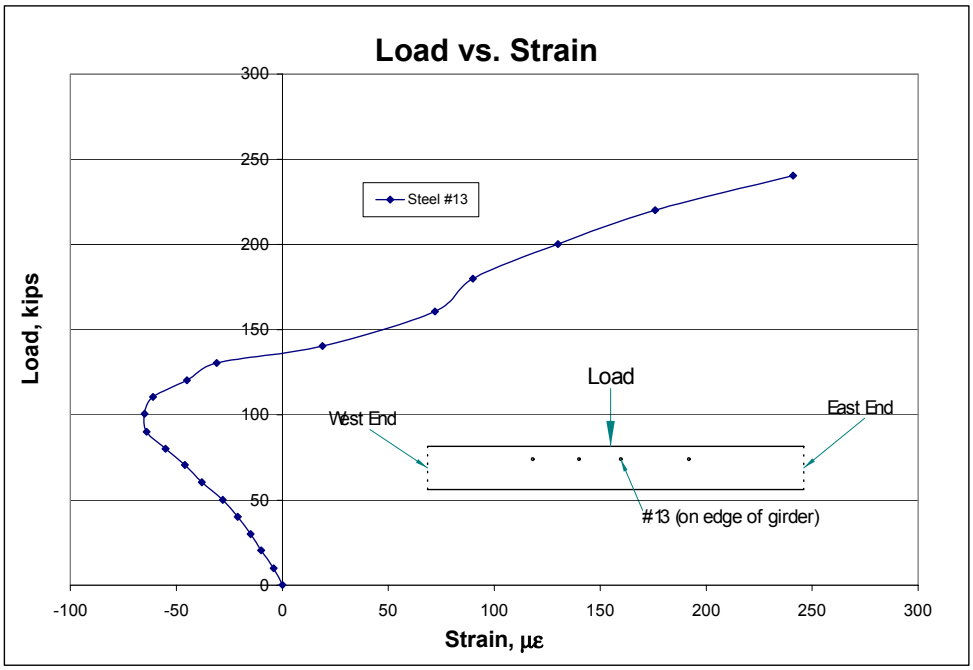

Figure 4.14: Load vs. Strain Plot for Interior Girder Test, Steel Bars

Figure 4.15 is a load vs. strain plot of GFRP strain gauges # 49 and #50. Gauge #49 is on the South side of the girder and #50 is on the North side of the girder. Both gauges exhibit the same behavior and have approximately the same values up to a load of 50 kips. Both also have a slight slope change at 40 kips. At 60 kips, the slope of #49 decreases greatly, indicating a crack in the section and a lowering of the neutral axis. Gauge #50 has the same behavior, except at a load of 90 kips, also indicating a cracked section and lowering of the neutral axis. Also at 90 kips, the slope of #49 increases up to a load of 120 kips is reached and the strain in #49 and #50 are almost equal. At this point, the slope of #49 decreases again and has the same slope of #50. What appears to be happening is that when one side cracks (at midspan due to positive moment or over the support due to negative moment), the opposite side stiffens up and takes a little more load. Next the opposite side cracks, but it is a little more cracked than the first side because it has taken on more load. At this point, the side that cracked first starts to stiffen

up and take on more load until both sides are equally cracked and are taking on equal load and the strain increase continues on both sides at a similar rate.

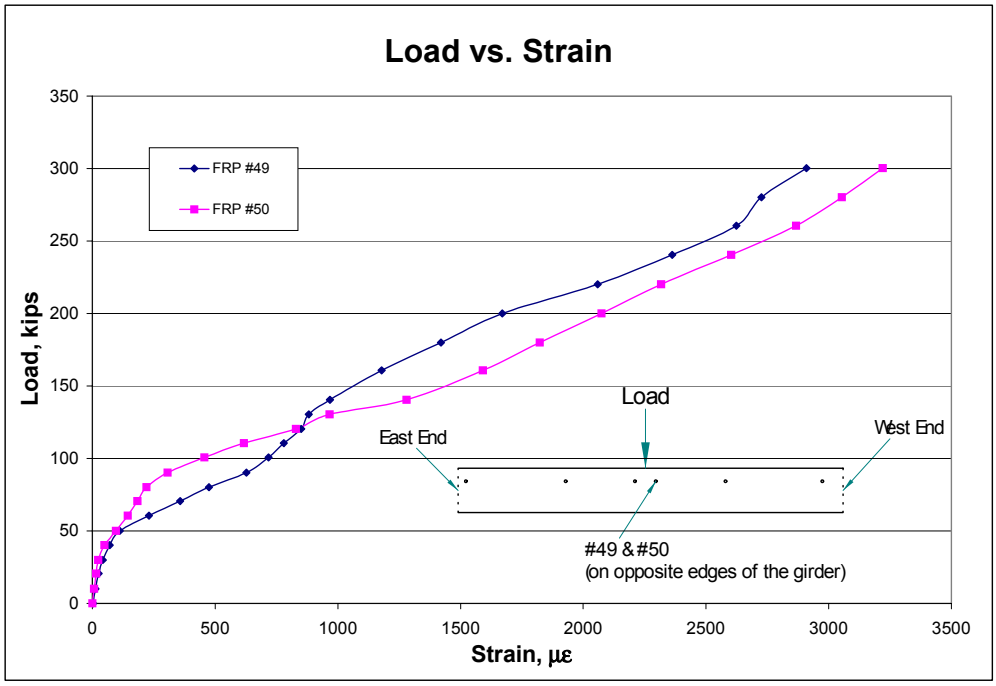

Figure 4.15: Load vs. Strain for Interior Girder Test, GFRP Bars

The stresses in the GFRP bars were obtained by multiplying the recorded strains by the modulus of elasticity of the GFRP bars, 6300 ksi. Stress profile curves were then created at various loads. These plots showed the stress in the bars relative to its distance from the load point. Figure 4.16 is a stress profile plot for loads of 10, 20, and 30 kips. As can be seen and as expected, the stresses are highest closer to the load and taper off as gauges get further away from the load.

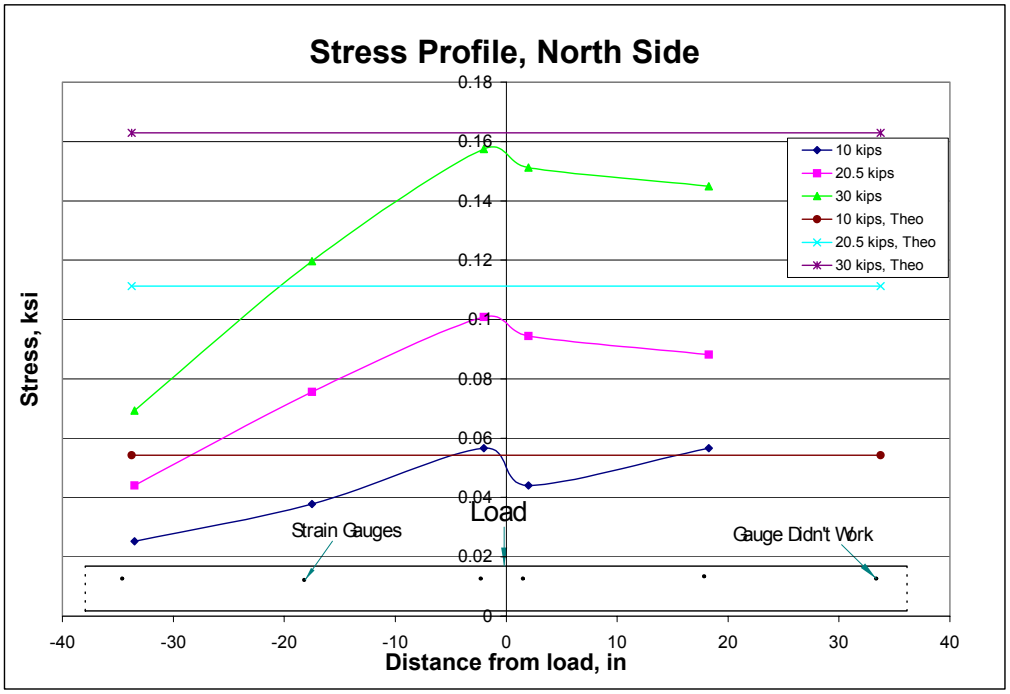

Figure 4.16: Stress Profile of Interior Girder Test, Pre-Cracking

Figure 4.16 also contains calculated theoretical values for the stresses in the bars. These were calculated by using the effective moment at the edge of the girder flange found in the previously mentioned RISA-2D (1993) analysis. Since the section was not cracked at these three loads, the moment was multiplied by y, the distance from the bar to the neutral axis, 1.65 in., and then divided by the transformed moment of inertia, I_t. The theoretical stress is plotted over the 5 ft 7 ½ in. effective width, and should match the peak stresses in the measured data, which it is doing pretty well. As can be seen, with the load increased from 20 kips to 30 kips, the predicted value is still over-predicting, but becoming more unconservative. Therefore, it is doing a better job of predicting stresses at lower loads before cracking, but is still slightly unconservative at the low loads closer to cracking.

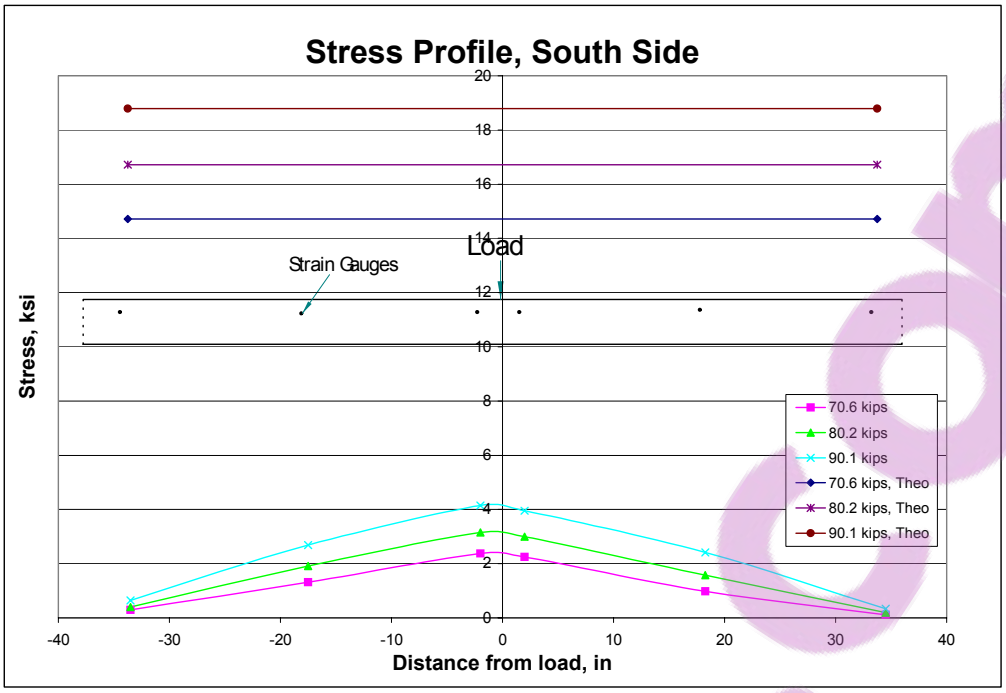

Figure 4.17: Stress Profile for Interior Girder Test, Post-Cracking

Figure 4.17 is the same type of stress profile, only this time on the South side and at higher loads of 70, 80, and 90 kips. This is considered to be after the section had cracked. The same pattern of higher stresses closer to the loads is again seen in this plot. The theoretical stresses were calculated in the same manner as before, only this time, the cracked moment of inertia, I_{cr}, was used and the y value increased to 4.23 in. Now, the theoretical values are conservative and greatly over-predicting the measured stresses. This is because the theoretical stresses are being calculated assuming that the section is completely cracked, when it is not. The section is only beginning to crack and as the load increases, the cracks in the section will propagate deeper and wider and the measured values should begin to approach the theoretical values, but unfortunately the section failed in punching shear before this could be seen.

4.2.4: Crack Widths and Cracking Loads

The first visible crack was seen at a load of 60 kips, 30 kips per patch. The cracks first appeared on the edge or near the edge of the interior girder flange close to the load. As the load increased, the cracks progressed along the edge of the flange towards either end of the deck. The progression and location of these cracks can be seen in Figure 4.18.

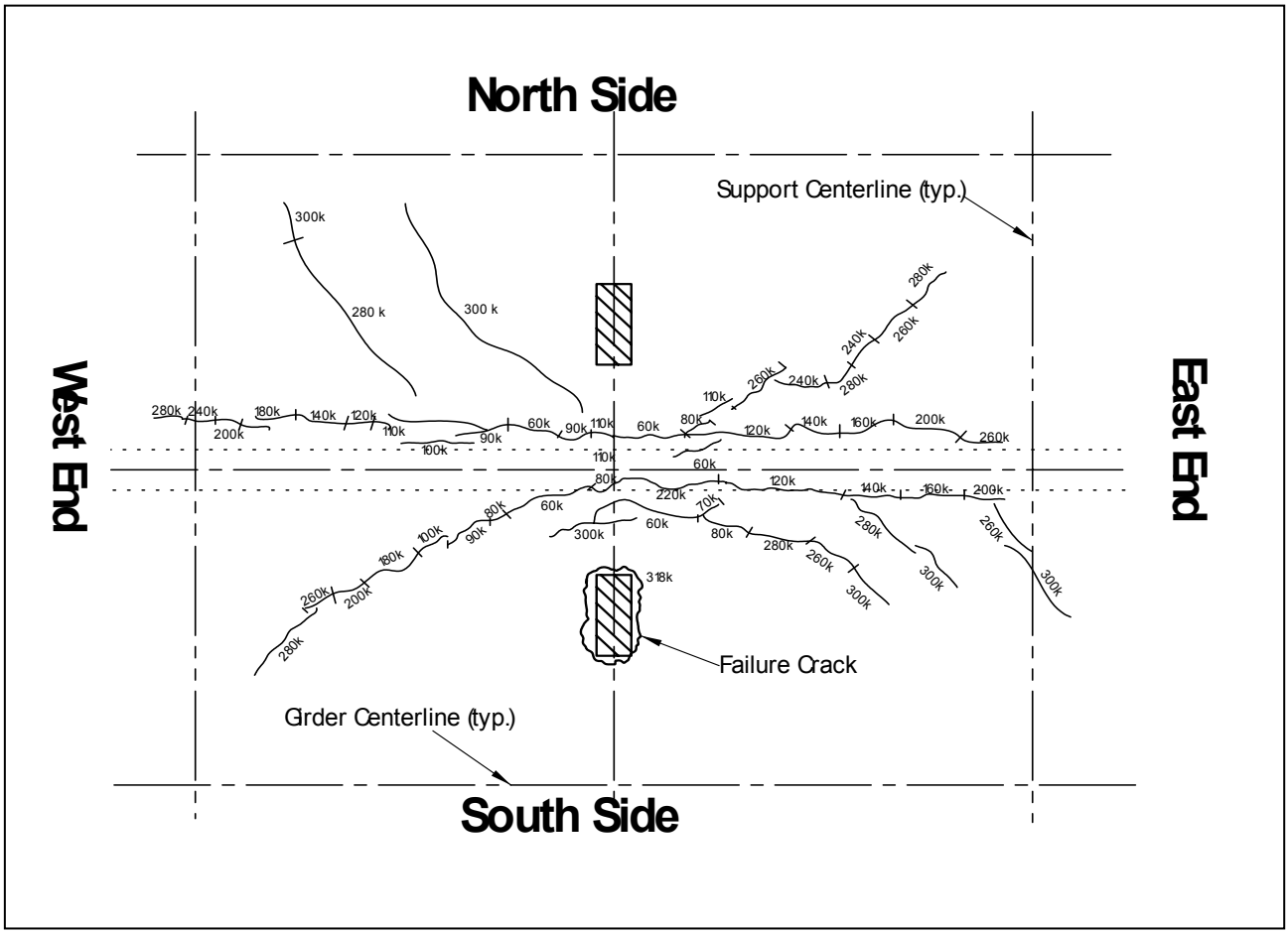

Figure 4.18: Crack Map for Interior Girder Test

As mentioned above, the first visible crack in the deck was seen at a load of 60 kips near the edge of the flange. This is consistent with the GFRP strain and deflection data which also indicated cracking at about 60 kips. The AASHTO LRFD effective width for overhangs and the cracking moment were used in conjunction to try to predict

this first cracking load. With the cracking moment over the support, $M_{cr(1)}$, previously calculated as 5.48 ft-kips and the effective width calculated as 5 ft 7 ½ in., the applied load to crack the section was calculated by dividing $M_{cr(1)}$ by the moment at the support from the output of the analysis program RISA-2D (1993) with 1 kip applied, ½ kip at each patch. That number was then multiplied by the effective width and this yielded a estimated cracking load of 50 kips, 25 kips per patch, which is close to the actual load considering load was applied in 10 kip increments, but it is still slightly conservative.

Table 4.3: Crack Widths

Interior Girder Crack Widths		
Load	Measured	Theoretical
kips	in.	in.
60	0.0024	0.0324
70	0.0024	0.0378
80	0.0039	0.0429
90	0.0047	0.0482
100	0.0055	0.0538
120	0.0063	0.0644
140	0.0087	0.0752
160	0.0102	0.086
180	0.0118	0.0963
200	0.0157	0.1068
220	0.0189	0.1178
240	0.0213	0.1287
260	0.0236	0.1394
280	0.026	0.15
300	0.0394	0.1607

The measured and theoretical crack widths for the interior girder test are presented in Table 4.3. The measured crack widths were measured using a crack microscope and are much more accurate than using a crack card. The theoretical values were calculated using Equation 4.5, the ACI 440 (2001) modified Gergely-Lutz equation as shown in Section 4.1.4.

As can be seen in Table 4.3, the ACI 440 equation for crack widths over-predicts the measured values, proving the equation to be extremely conservative. One factor that may make the equation so conservative is f_f. This stress in the GFRP bars is calculated using the AASHTO LRFD effective width. Previously in Section 4.2.3, it was shown that this method over-predicts the stresses. This would and does appear to lead to the crack widths being over-predicted as well.

4.2.5: Ultimate Load and Failure Mode

The failure mode of the interior girder test was two-way shear, commonly referred to as punching shear. The deck failed at a load of 318 kips, 159 kips per patch load. This was the failure mode that was expected, however, it failed at a much higher load than expected. The estimated failure load was calculated using the punching shear capacity Equation 4.7 in Section 4.1.5. With a d of 5.125 in., b_o was calculated as 76.5 in., and β_c was still 2.5. The concrete compressive strength, fc', used was equal to 5769 psi. This yielded a two-way shear strength of 107.2 kips per patch or a total load of 214 kips. So, the equation under-predicted the two-way shear capacity by 51.8 kips, and is considered to be very conservative for this test. One reason may be that the equation doesn't account for the amount of reinforcing used in the slab. This slab was heavily reinforced with GFRP bars and this may have lead to an increased two-way shear capacity.

4.2.6: Design Criteria

Table 4.4 below shows a comparison between allowable, calculated, and measured values for various design criteria.

Table 4.4: Design Criteria Comparison

	Interior Girder Test Values		
Design Criteria	Allowable	Measured	Calculated
Stresses, ksi	12.1	0.441	0.23
Crack Widths, in.	0.02	Not Cracked	0.022
Deflections, in.	0.0975	0.023/0.007*	0.0077
Nominal Moment Capacity, ft-k	-	197.2 #	257.7

*South Side/North Side

Failed in punching shear prior to flexural capacity

The allowable stresses were calculated in accordance with the ACI 440 (2001) guidelines. For cyclic stress limits in FRP reinforcement, the allowable stress is 20 percent of the design tensile strength, f_{fu}. The design tensile strength, f_{fu}, is equal to the guaranteed tensile strength, f^*_{fu}, times an environmental reductions factor, C_E, which is equal to 0.7 for GFRP bars. The guaranteed tensile strength, f^*_{fu}, is equal to the tested average, 106 ksi for the No. 5 bars, minus three standard deviations of 6.68 ksi. This yielded a design value of 12.1 ksi. The measured values were taken at service load, 32 kips plus an impact factor of 30 percent, for a total load of 42 kips on the deck. The actual measured value was 40 kips. As can be seen in the table, the measured value is well below the allowable design value. The measurement was taken before the section had cracked and is expected to be low. The section was cracked at 60 kips however, and the stress was 1.5 ksi, still well below the allowable. The allowable of 12.1 ksi was not reached until a load of 180 kips. This indicates that the design is conservative.

The calculated values for the crack widths were calculated using Equation 4.5, as presented in Section 4.1.4. The load used for the calculation was 42 kips, service load of 32 kips plus a 30 percent impact factor. ACI 440 (2001) recommends a maximum crack width of 0.02 in. In the test, the slab was not cracked until a load of 60 kips. After the slab became cracked at a load of 60 kips, the cracks measured were still very small, 0.0024 in. This indicates that the design method is conservative

AASHTO LRFD Bridge Design Specifications (1994) set the recommended, not mandatory, allowable deflections at service loads of a bridge deck as the spacing of the girders divided by 800. The spacing of the girders was 78 in. leading to an allowable deflection of 0.0975 in. at a service load of 42 kips. The measured data was for a load of

40 kips and was well below the allowable. Once again the section was not cracked and therefore the deflections are expected to be small. However, at 60 kips with a cracked sections, the deflection was still only 0.036 in. Allowable service deflections were not reached until a load of 130 kips. This indicates that the design is conservative.

The nominal moment capacity of the section was calculated following the same procedure described in Section 4.1.6. As in Section 4.1.6, the measured nominal moment capacity isn't the true nominal moment capacity because the section did not fail in flexure, it failed in punching shear. It is simply the moment over the interior support calculated by the RISA-2D (1993) analysis program at the failure load of 318 kips. As can be seen, the section failed well before the nominal moment capacity was reached. Therefore, the flexure design of the deck does not control.

4.3: Cantilever Test

4.3.1: Introduction

The cantilever test, which models a negative moment region over an interior support, was performed to obtain deflection information, GFRP reinforcing bar stresses, cracking loads, and crack widths. It was completed by following the procedures as presented in Chapter 3. The results of this test are presented in Section 3 of this chapter.

4.3.2: Deflections

The wire pots were attached to the bottoms of the girders with magnets. They were attached to the ends of the girders on the West end. The data was collected during the testing and load vs. deflection plots were created. Figures 4.19 and 4.20 below are two of the plots that were created.

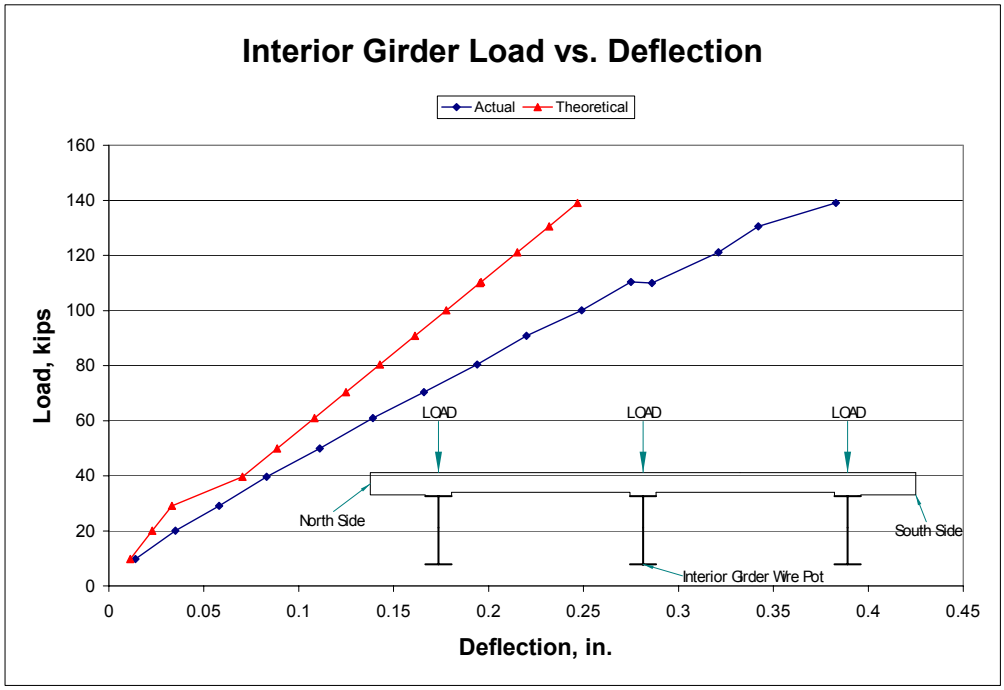

Figure 4.19: Load vs. Deflection Plot for Cantilever Test

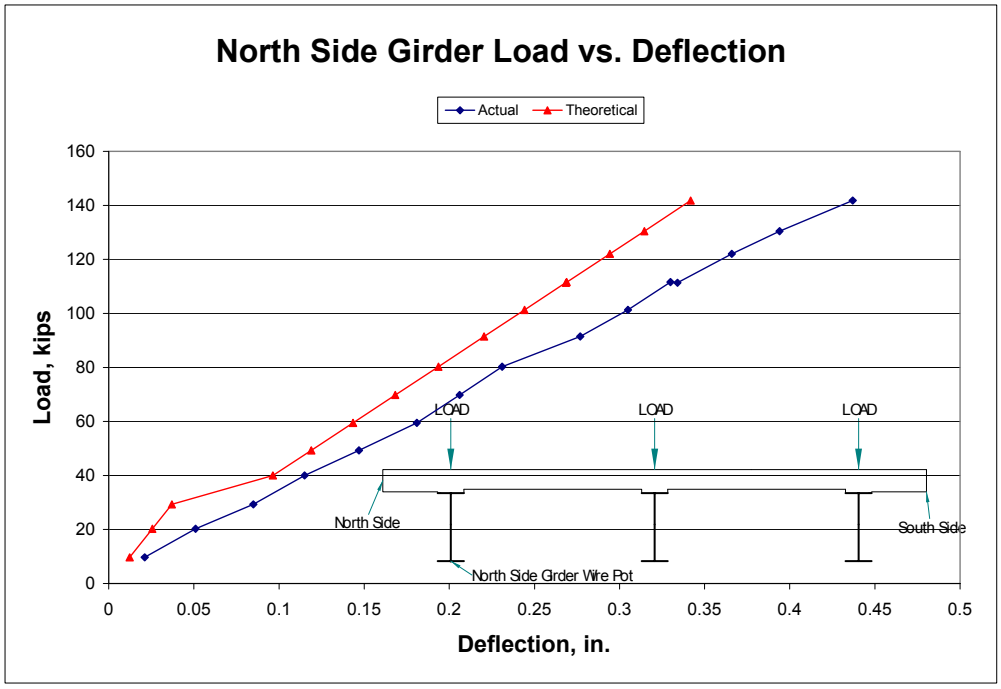

Figure 4.20: Load vs. Deflection Plot for Cantilever Test

Both plots contain an actual data series and a theoretical data series. The actual

data series for both are very similar. Both follow a fairly straight line and no significant slope change is seen. They both do have a small plateau at a load of 110 kips. This is because the bridge was loaded up to 110 kips, unloaded and cycled between 10 kips and 80 kips five times and then reloaded up to 110 kips. At the second load of 110 kips, the section had softened up a little and deflected a little more than the first time, leading to a plateau in the plot.

The theoretical data series for both were calculated the same way. They were both modeled as a beam element in RISA-2D (1993) and were loaded with the identical load as applied in the test. The only difference in the modeling was the supports. Both had roller supports 4 ft from the load and both had pin supports 20 ft. from the load. The two exterior girders had no other supports, however, the interior girder had a pin support 12 ft from the load where it was bolted down to the reaction floor. To model the sections as beams, the moments of inertia of each section were calculated considering the composite action between the slab and the girders. The effective flange widths of the slab were calculated for the interior and exterior beams using the Equation 4.13 and 4.14 as presented in the AASHTO LRFD Bridge Design Specifications (1994).

$$b_i \le \left\{ \begin{array}{l} \frac{1}{4}\, effective\ span \\ 12t_s + \frac{1}{2} b_f \\ ctr.\ to\ ctr.\ spacing\ of\ girders \end{array} \right\} \qquad \textbf{4. 13}$$

Where : b_i = effective width for interior girders, in.
t_s = thickness of slab, in.
b_f = width of top flange of girder, in.

$$b_e - \frac{b_i}{2} \le \begin{Bmatrix} 1/8\ effective\ span \\ 6t_s + 1/4\, b_f \\ width\ of\ overhang \end{Bmatrix} \qquad \textbf{4. 14}$$

Where : b_i = effective width for interior girders, in.
b_e = effective width for exterior girders, in.
t_s = thickness of slab, in.
b_f = width of top flange of girder, in.

For the interior girder, the center to center spacing of the girders governed and the effective width was calculated to be 78 in. For the exterior girders, the width of the overhang governed and the effective width was calculated to be 65 in. The transformed moments of inertia were calculated for both. The GFRP and concrete areas were transformed to steel by utilizing the materials' modular ratios. The cracked moments of inertia were also calculated for both, discounting the presence of any concrete and again transforming the GFRP to steel.

The transformed moment of inertia, I_t, for the interior girder was calculated to be 11,184 in.^{4}, with the neutral axis located 27.9 in. from the bottom of the girder. The cracked moment of inertia, I_{cr}, for the interior girder was calculated to be 4346 in.^{4}, with the neutral axis located 15.63 in. from the bottom of the girder. The exterior girders had a transformed moment of inertia of 10,797 in.^{4}, with the neutral axis located 27.5 in. from the bottom of the girder, and a cracked moment of inertia of 4273 in.^{4}, with the neutral axis located 15.5 in. from the bottom of the girder. See Appendix B for example calculations.

The transformed moments of inertia were used in the analysis program up to a load of 30 kips. At a load of 40 kips, the cracked moment of inertia was used because

based on observations, this is assumed to be the load at which the deck cracked. The deflections were recorded for each load in the analysis program. In order to calculate the actual deflections at the ends of the girders, shear deformations of the girders had to be accounted for because in short spans such as this, shear deformations tend to be large. In order to do this, the beam element in the RISA-2D (1993) model was modeled as just a W27x94 steel girder. The same exact support and loads were used. The model was run once at each load including shear deformations and once not including shear deformations. The second run was subtracted from the first run to obtain the deflections due to just shear deformations. These deflections were then added to the corresponding deflections using the transformed and cracked moments of inertia to obtain the total theoretical deflection.

As seen in the figures, the theoretical series do not identically match the actual deflections, but they are reasonably close. They are all less than the actual, which indicates that the theories and methods behind the calculations are unconservative. Both theoretical sections appear to be stiffer that their corresponding actual section up to a load of 30 kips because both have larger slopes. As mentioned above, at 40 kips, the sections are modeled as cracked and there is a significant change in their slopes. This change in slope is not seen at all in the actual section, which is quite unusual because the moment of inertia should be greatly reduced when the sections cracks causing a less stiff section that will deflect more with the same load increment. Another difference between the actual and theoretical series is that the theoretical series has a steeper slope after cracking as well. This shows once again that the model is stiffer than the actual section. This is seen more with the interior girder because it was modeled as having an interior support.

Overall, the theoretical values are unconservative but come close to predicting the actual values considering all the variables. This indicates that the model is stiffer that the actual section. This discrepancy in deflections and stiffness may be due to a number of different things. They include shear deformations in the slab, deflection at the support, and loss of composite action between the slab and the girder.

4.3.3: Reinforcing Strains and Stresses

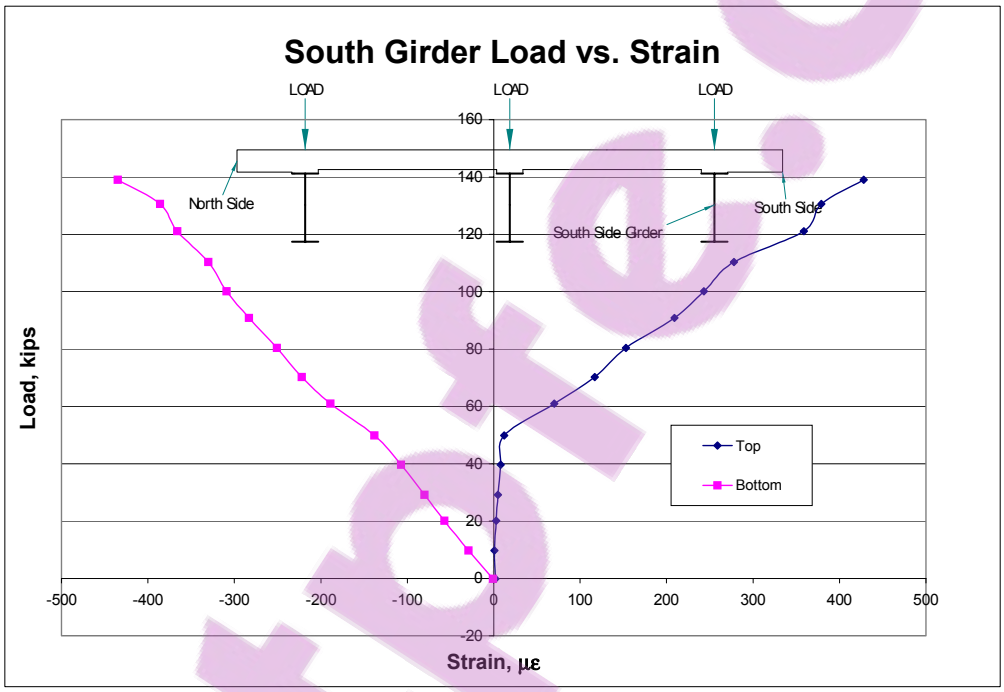

Figure 4.21: Load vs. Strain Plot for South Side Girder

The strains were recorded using the data acquisition system and load vs. strain plots were created. Figure 4.21 is a load vs. strain plot for the two strain gauges that were located on the South side girder close to the support. The data series labeled top was for the strain gauge located at the top of the girder and the data series bottom corresponds to the gauge located at the bottom of the girder. From the plot, it appears that the top strain gauge was located very close to if not on the neutral axis because it has zero or close to

zero strain up to a load of about 50 kips. The bottom gauge is well below the neutral axis because it is in compression. At 50 kips, in the top gauge, there is a very slight increase in the strain and by 60 kips the strain has increased significantly and is well into tension. This shows that the section above the girder may have begun to crack at 50 kips and by 60 kips the cracking had progressed. At this point, the neutral axis was significantly lowered and the top strain gauge was well above it.

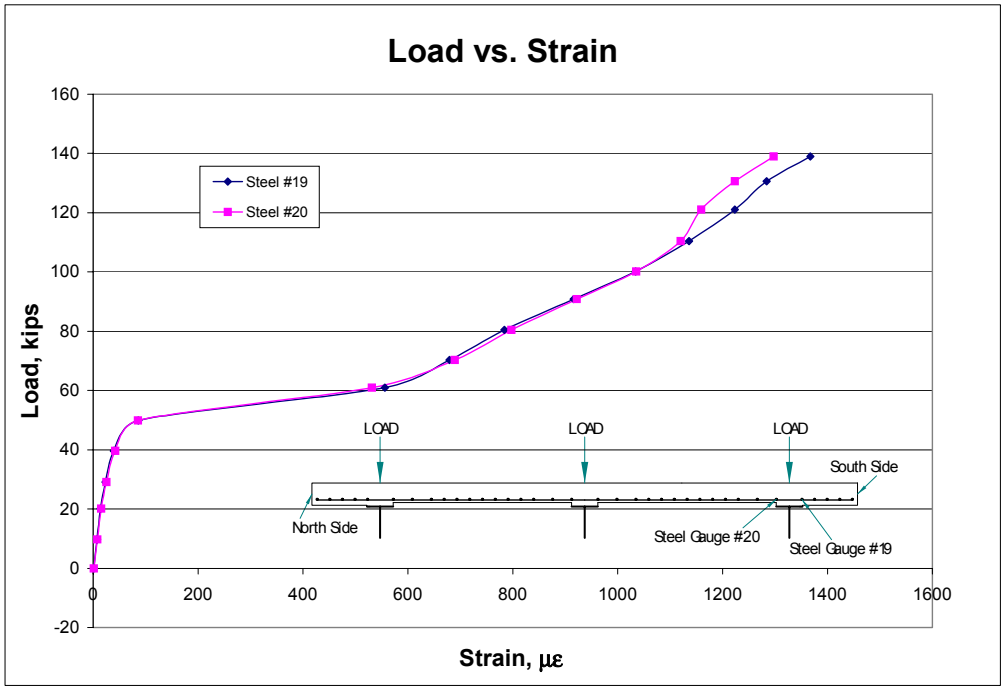

Figure 4.22: Load vs. Strain Plot for Steel Gauges

Figure 4.22 is a plot of load vs. strain for the two steel reinforcing bars located above the South side girder. They show exactly the same pattern as seen in the South side girder top gauge, only they are located above the neutral axis initially and have a more positive slope to begin with. As can be seen, there is a slight slope change and strain increase at 50 kips and then a significant slope change and strain increase at a load of 60 kips. Once again showing that the section may have begun to crack at 50 kips and

then totally cracked at 60 kips thus dropping the neutral axis and increasing the strains in the steel reinforcing bars.

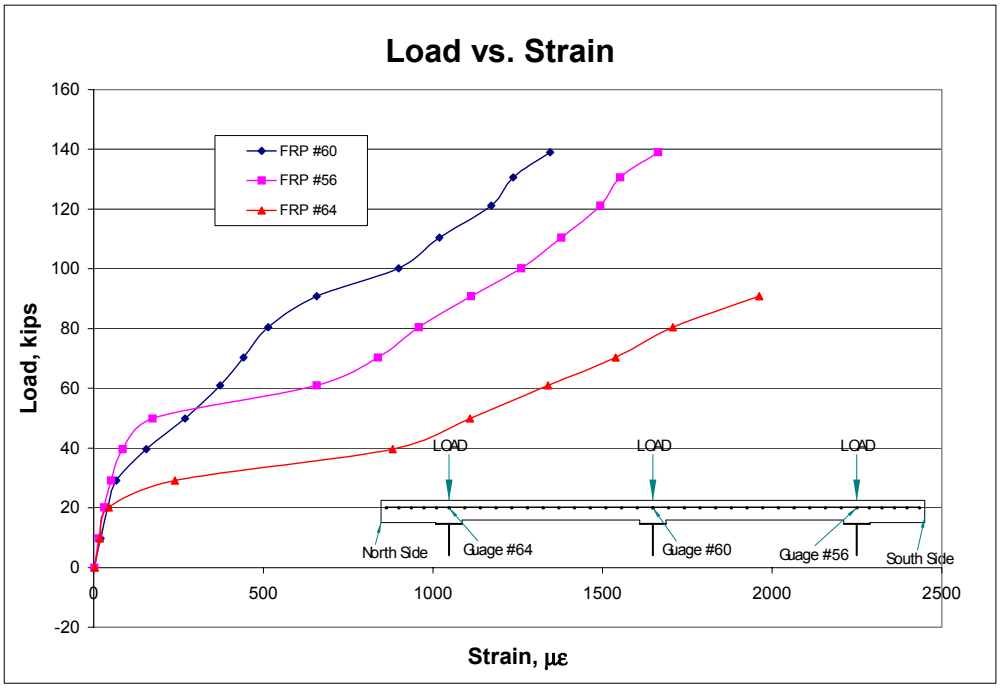

Figure 4.23: Load vs. Strain Plot for GFRP Gauges

Figure 4.23 is a load vs. strain plot for the GFRP stain gauges. The locations of the bars are shown on the plot, each is located directly over the centerline of the three girders. All three have positive slopes and are initially in tension because they are located above their respective neutral axes. All three also have almost identical slopes and values up to cracking. The North girder sections which contains gauge #64 appears to crack first at a load of 30 kips, followed by interior girder section containing gauge #60 cracking at 40 kips, and then the North side section beginning to crack at a load of 50 kips, as indicated by gauge #56. Gauge #56 is located above the South side girder and its load-strain behavior is almost identical to the steel gauges in Figure 4.22, which is expected because it is located just above the steel gauges. It shows the same pattern of

beginning to crack at 50 kips and then being almost totally cracked at 60 kips. The increase in strains and decrease in slopes indicates that the section has cracked, the neutral axis has lowered, and the bars are taking more strain at equal load increments.

The stresses in the GFRP bars were obtained by multiplying the recorded strains by the modulus of elasticity of the GFRP bars, 6300 ksi. Stress profile curves were then created at various loads. These plots showed the stress in the bars relative to its distance from the load points. Figure 4.24 is a stress profile plot for loads of 30 and 40 kips. As can be seen and as expected, the stresses are highest closer to the load and taper off as gauges get further away from the load.

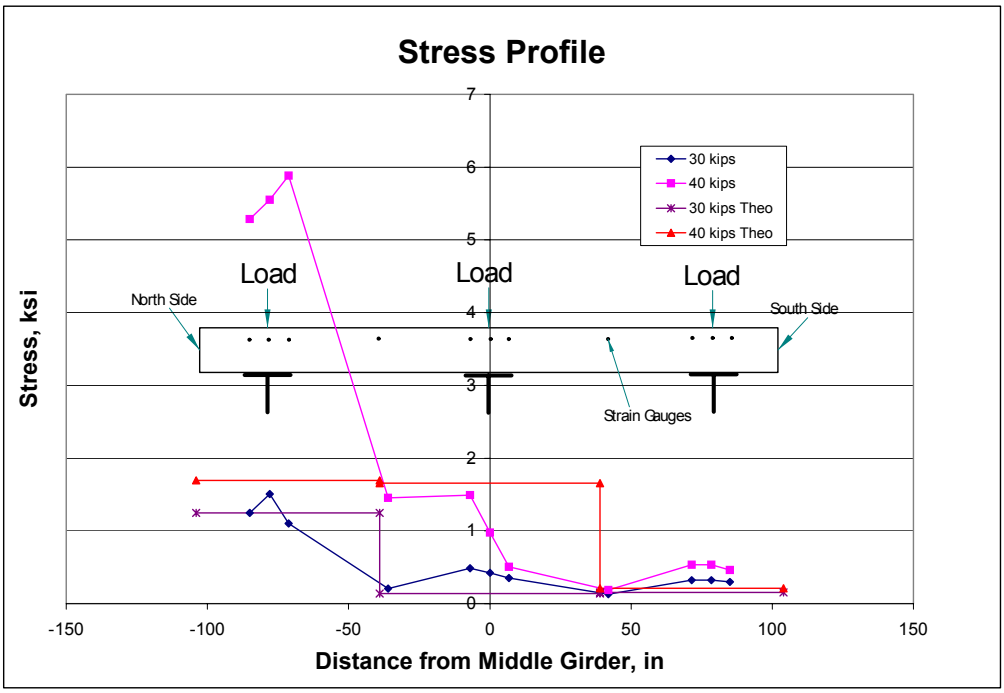

Figure 4.24: Stress Profile for Cantilever Test

The plot also contains calculated theoretical data for the stresses. These stresses were calculated by multiplying the moment at any given load by the appropriate distance

from the bar to the neutral, y, and then dividing by the appropriate moment of inertia, I. The moment was the applied load, 30 or 40 kips, times the moment arm of 48 in. A cracked moment of inertia and its corresponding y value was used for the North side girder at 30 and 40 kips and for the interior girder at 40 kips because the sections were determined, by observation, to be at least partially cracked at these loads. For the other cases, interior girder at 30 kips and South side girder and 30 and 40 kips, the transformed moment of inertia and its corresponding y value was used. These are the same I's and y's as calculated in Section 4.3.2.

The plot shows that the actual stresses are being under-predicted by the theoretical values everywhere except when the section first starts to crack. This first cracking occurred at a load of 30 kips for the North side section and 40 kips for the interior section. As can be seen on the plot, the theoretical stresses are very similar to the actual stresses for these two situations. However, at a load of 40 kips on the North side section, the actual stress got up to about 6 ksi and the theoretical only predicted a stress of about 1.7 ksi, which is only about 30 percent of the actual. For the uncracked sections, the theoretical values are slightly under-predicting the actual values, which is of little concern because cracked sections are usually used in design and the stresses at this level are well below allowable. This under-prediction proves this methodology for predicting stresses for this situation to be very unconservative. Some reasons for this large under-prediction may be loss of composite action between the slab and the girder and unconservative effective flange widths, but these alone would not account for the large differences between measured and predicted. The only other explanation at this time may

be faulty instrumentation readings, but it is unlikely that all the GFRP gauges would have the same high readings, yet still be accurately predicting when cracking occurs.

4.3.4 Crack Widths and Cracking Loads

The first visible crack was seen at a load of 40 kips per load ram, this was the first load at which the deck was visibly inspected, so a visible crack may have occurred at 30 kips, but the deck was not inspected. The first crack appeared directly over the first support spanning from the North side edge all the way to the interior girder. As the load increased, the crack progressed along the first support until it reached the South side edge of the slab. More cracks with the same pattern formed in the negative moment regions. The progression and location of these cracks can be seen in Figure 4.25.

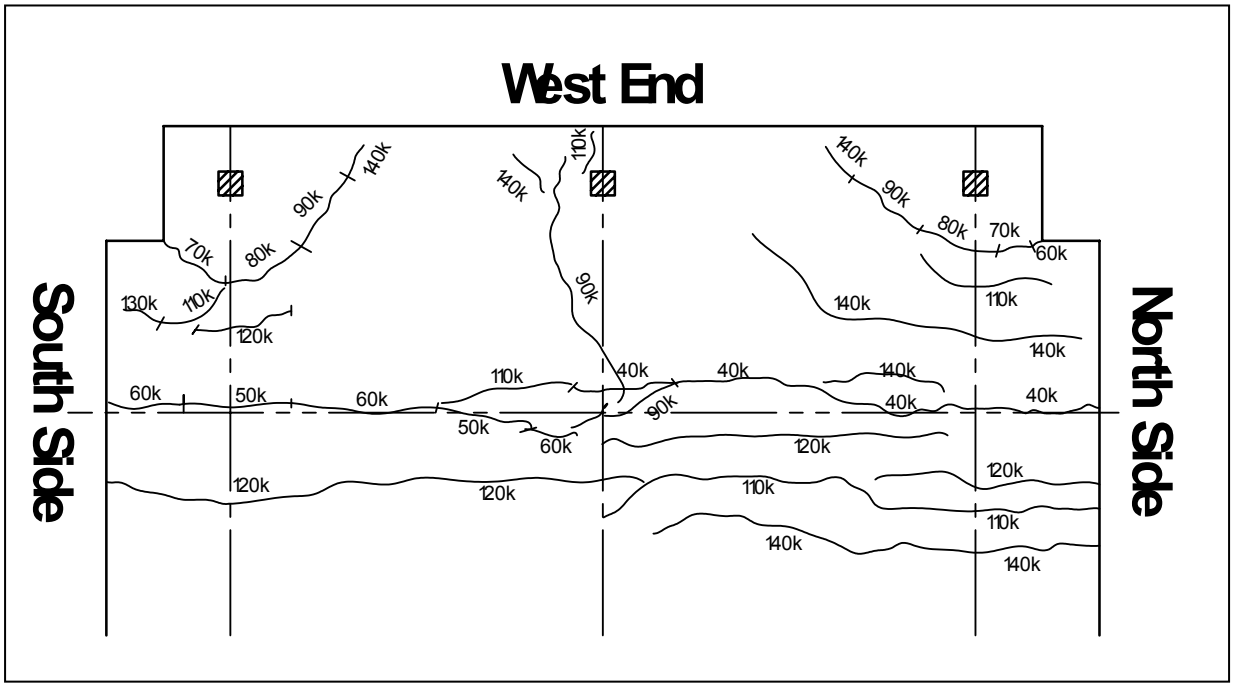

Figure 4.25: Crack Map for Cantilever Test

As stated above, the first visible crack was seen at a load of 40 kips over the North side and Interior girders. This corresponds with the strain data in which it was seen that the neutral axis lowered at a load of 40 kips indicating a crack. At a load of 50 kips, the slab above the South side girder was cracked which also corresponds to what was seen in the steel reinforcing bar, the girder, and the GFRP strain data presented in Section 4.3.3.

The estimated cracking load was calculated by dividing the cracking moment, M_{cr}, by the moment arm of 4 ft. Equation 4.4 in Section 4.1.2 was used to calculate the cracking moment. The concrete tensile strength had to be transformed to an equivalent steel tensile strength because the transformed moment of inertia and its corresponding y value were calculated by transforming everything to steel. To do this, the concrete tensile strength was divided by the 0.1556, the modular ratio of the concrete to the steel. A concrete compressive strength of 6267 psi was used for the calculation because this was the average strength of batch 2 at 61 days. For the interior girder, the cracking moment was calculated to be 443.8 ft-kips, which corresponds to a cracking load of 111 kips. For the exterior girder, the cracking moment was calculated to be 408 ft-kips, which corresponds to a cracking load of 102 kips. Both of these estimated cracking loads are over-predicting the actual cracking loads by more than 60 kips. This calculation is very unconservative. Some reasons for this large over-prediction may be loss of composite action between the slab and the girder and unconservative effective flange widths, but these alone would not account for 60 kips of error. So why it cracked so early cannot be explained.

The measured and theoretical crack widths for the interior girder test are presented in Table 4.5. The measured crack widths were measured using a crack microscope and are much more accurate than using a crack card. The theoretical values were calculated using Equation 4.5, the ACI 440 (2001) modified Gergely-Lutz equation as shown in Section 4.1.4.

Table 4.5: Crack Widths

Cantilever Test Crack Widths		
Load	Theoretical	Measured
kips	in.	in.
10*	0.0079	0.0102
40	0.0301	0.0079
50	0.0379	0.0102
60	0.0463	0.0118
70	0.0534	0.0142
80*	0.0610	0.0197
90	0.0689	0.0189
110	0.0835	0.0236
130	0.0992	0.0260
140	0.1055	0.0260

*Values measured during cyclic loading

As can be seen in Table 4.5, the ACI 440 equation for crack widths over-predicts the measured values, proving the equation to be extremely conservative, especially for the given cantilever situation. One interesting fact is that the equation is a function of the stress in the GFRP reinforcing bars and since the stress in the bars is being drastically under-predicted, it would be thought that the crack widths would be under-predicted as well, but they are not. This is very surprising. Overall, this equation is very conservative and may not be suited for this particular application of a composite girder and slab.

4.3.5: Design Criteria

Table 4.6 below shows a comparison between allowable, measured, and calculated values for various design criteria. For the measured values, all measurements were taken at an approximate service load on the bridge. The service load was calculated by finding the largest negative moment on the actual bridge. The actual bridge was modeled as a 3 span continuous structure, with each span being 45 ft in length. An influence function was created for the model and AASHTO LRFD (1994) design trucks

and lane loads were placed on the model to create the largest negative moment over a support. The resulting maximum negative moment due to a truck was 272 ft-kips and due to a lane load was 150 ft-kips, see Appendix C for calculations.

The service moment was then calculated by multiplying the moment due to the design truck by an impact factor of 1.33 and adding it to the lane load moment, giving a total service moment of 512 ft-kips. Distribution factors were then applied in accordance with AASHTO LRFD. The distribution factor for the exterior girder was 0.621, giving it a moment of 318 ft-kips, and 0.574 for the interior girder giving it a moment of 294 ft-kips. The prototype had two exterior and one interior girder, so the three moments were averaged to 310 ft-kips. This was divided by the moment arm of 4 ft and yielded a load of 78 kips per ram. The load was applied in 10 kip increments, so 80 kips per ram was used as the service load.

Table 4.6: Design Criteria Comparison

	Cantilever Test Values		
Design Criteria	Allowable	Measured	Calculated
Stresses, ksi	10.6	12.0	3.44
Crack Widths, in.	0.02	0.0197	0.061
Deflections, in.	0.2	0.32	0.19

The allowable stresses were calculated in accordance with the ACI 440 (2001) guidelines. For cyclic stress limits in FRP reinforcement, the allowable stress is 20 percent of the design tensile strength, f_{fu}. The design tensile strength, f_{fu}, is equal to the guaranteed tensile strength, f^*_{fu}, times an environmental reductions factor, C_E, which is equal to 0.7 for GFRP bars. The guaranteed tensile strength, f^*_{fu}, is equal to the tested average, 89.3 ksi for the No. 6 bars, minus three standard deviations of 4.56 ksi. This

yielded a design value of 10.6 ksi. As can be seen in the table, the measured value above the allowable design value. This indicates that the design is unconservative and the design needs to be reevaluated.

The calculated values for the crack widths were calculated using Equation 4.5, which was presented in Section 4.1.4. The load used for the calculation was 80 kips. ACI 440 (2001) recommends a maximum crack width of 0.02 in. The calculated value is well above the measured value indicating that the design is conservative or the equation needs to be changed. The measured is approximately equal to the allowable, indicating a good design.

AASHTO LRFD Bridge Design Specifications (1994) set the recommended, not mandatory, allowable deflections at service loads of a cantilever section as the length of the cantilever section divided by 300. The cantilever test had a length of 60 in. leading to an allowable deflection of 0.2 in. at a service load of 80 kips. The measured deflection of the overhang at service was 0.32 in. which is above the recommended value. This once again proves this to be an unconservative design of a cantilevered section.

CHAPTER V
CONCLUSIONS AND RECOMMENDATIONS

5.1: Introduction

This thesis had two objectives. The first objective was to build and test a full-scale prototype of a VDOT designed bridge deck containing GFRP reinforcing bars as the top mat of reinforcement. The tests examined aspects of bridge deck's behavior such as failure load, failure mode, cracking load, crack widths, deflections, and internal stresses. The second objective was to comment on the construction of a bridge deck reinforced with GFRP bars and to critique the state-of-the-art of designing bridge decks that utilize FRP reinforcement. Conclusions and recommendations are made in each section with final conclusions and recommendations for further research made at the end of the chapter.

5.2: General Conclusions and Recommendations

5.2.1: Cyclic Loading

As mentioned in Chapter 3, cyclic loads were applied in overhang test #1, overhang test #2, and the cantilever test. These cyclic loads were intended to represent cycling of vehicular loads on the bridge. However, the loads were only cycled a few times during each test, which is not a good representation of the load cycling the bridge will see due to traffic. The data for all tests showed that during the cycling of the loads, the crack widths, the reinforcing strains, and the deflections all did not increase at all. No conclusions about the effects of cyclic loading can be drawn from this data because the loads were not cycled enough to provide a good representation of actual conditions.

5.2.2: Deflections

For both overhangs, the two theoretical methods used fairly accurately predicted the deflections up to a load of 30 kips for overhang #1 and 16 kips for overhang #2. The effective moment of inertia method was more accurate in both cases of predicting the behavior of the deflections during cracking, but did not accurately predict the load at which this behavior occurred. The measured deflections at service were also below the recommended allowable. From this it can be concluded that the effective moment of inertia method accurately models deflections and it is recommended that it continue to be used. However, it is also recommended that the AASHTO LRFD (1994) effective width formula for overhangs, particularly short overhangs, be reevaluated.

The interior girder test utilized the same effective moment of inertia calculation as well as an additional effective moment of inertia calculation for continuous sections. These two formulas, in conjunction with the ASSHTO LRFD (1994) effective width formula for negative moment sections, predicted the deflections extremely well. The measured deflections at service were also below the recommended allowable. From this, it is concluded that this is a very good method and it is recommended that it continue to be used for similar situations.

The method used to predict deflections for the cantilever test reasonably predicted the deflections, but was still slightly unconservative and over-predicted the stiffness of the section. The measured deflections at service were also above the recommended allowable, proving the design to be unconservative in regards to deflections. In conclusion, the method is usable but needs some slight modifications. It is recommended

that this method still be used but some changes to the equations, such as the effective flange width equation, be made in order to more accurately predict the deflections.

5.2.3: Stresses

Overhang tests #1, #2, and the interior girder test all had similar results with respect to predicted stresses as compared to the actual stresses. All the theoretical values accurately predicted the measured stresses at low loads before cracking occurred. As cracking load was approached, the theoretical values began to under-predict the measured stress, becoming unconservative. After cracking, the theoretical values all over-predicted the measured values and are considered to be very conservative. However, all the measured stresses were still well below allowable at service loads. Because stresses calculated during design are based on a cracked section, it can be concluded that the current methods are very conservative for the above cases. It is recommended that a method be developed that utilizes an effective moment of inertia and a corresponding y value to more accurately predict stresses after cracking.

The theoretical values for stresses in the cantilever test did not adequately predict the actual measured stresses. Before cracking, the theoretical values were slightly unconservative, under-predicting the actual stresses. As the section began to crack, the theoretical values accurately predicted the actual, but after the section had become completely cracked, the theoretical values were very unconservative, under-predicting the stresses by a large amount. The stresses in the reinforcement at service were also above the allowable stresses as prescribed by ACI 440 (2001). In conclusion, the design for this particular section is very unconservative with respect to reinforcement stresses. It is recommended that better methods be developed for predicting stresses in FRP

reinforcement for cantilever sections such as this, or locations where the deck and girder are continuous over an interior support.

5.2.4: Crack Widths

Overhang tests #1, #2, and the interior girder test all had the same results with respect to their predicted crack widths as compared to the actual crack widths. The theoretical values for the crack widths over-predicted all the actual measured values. At service load for each test, the measured crack widths were well below the ACI 440 (2001) recommended value for allowable crack widths of 0.02 in., and in all three tests, the slab was not cracked when service load was first reached. Most of the reason for this over-prediction can be attributed to the fact that the stresses used for the crack width calculation were over-predicted as well. Another contributor to the over-prediction could be the bond factor, k_b. This is an arbitrary factor which increases the theoretical crack width by 30 percent. In conclusion, the design is conservative with respect to crack widths, but the equation used to predict theoretical crack widths too conservative. It is recommended that the ACI 440 (2001) equation for crack widths in conjunction with the method for predicting reinforcing stresses in bridge decks be studied more carefully in order to be able to more accurately predict crack widths.

Once again, the theoretical crack widths for the cantilever test were well above the actual measured values. This is surprising considering that the theoretical stresses used to calculate the crack widths were well below actual. The measured crack width at service was equal to the ACI 440 (2001) recommended allowable value. In conclusion, the section is adequate for crack width limitations, but the equation used to calculate

crack widths is inadequate. It is recommended that the equation used to calculate crack widths be researched further for composite sections.

5.2.5: Cracking Load

For both overhang tests, the effective width method over-predicted the cracking load and the moment influence method under-predicted the cracking load. From this, it can be concluded that neither method was accurate in its prediction for these particular tests, but the moment influence method should be used because it is the conservative one of the two. It is recommended that the equation for the effective width for overhangs be reevaluated and another equations for shorter overhangs, less than 2 ft, be produced.

The effective width method was again used to estimate the cracking load for the interior girder test. The predicted cracking load of 50 kips was very close to the actual cracking load of 60 kips. The load was applied in 10 kip increments, therefore cracking could have occurred at a load below 60 kips, but was not seen until 60 kips. In conclusion, the method is slightly conservative but very good. It is recommended that this method continue to be used for similar calculations.

The predicted cracking load for the cantilever test was very unconservative. The section cracked at a load well below the expected load. In conclusion, this method is not adequate for predicting cracking loads due to negative moment over an interior support. It is recommended that new methods and equations be developed that will accurately predict the cracking loads in negative moment regions over supports.

5.2.6: Failure Mode and Load

Both overhang tests failed at a much higher load than expected and by a different mode than expected. They were both expected to fail in one-way shear, but they both failed in two-way or punching shear. The predicted failure load for one-way shear was calculated using the ACI 440 (2001) modified equation and was very low. Even though the section did not fail in one-way shear, this equation is concluded to be too conservative and it is recommended that modifications be made to it. The equation used to predict the two-way shear capacities of the section was close to the failure loads, but was a little unconservative. In conclusion, the ultimate shear strength of the overhang sections is adequate and it is recommended that the mode of failure and their corresponding loads for overhangs be further investigated.

The interior girder test failed in punching shear which was expected. The slab failed at a much higher load than expected. The same punching shear capacity equation as used for the overhang tests was used for this test. The equation produced a very conservative failure load, much lower than the actual failure load. In conclusion, the deck has adequate shear strength, much higher than anticipated, and it is recommended that the punching shear capacity equation used be further evaluated for slabs containing FRP reinforcement.

5.3: Validity of Actual Design

The main objective of this project was to verify that the design of the deck would resist the loads for which it was designed. It was found that the deck has more than adequate strength to resist the design loads. The only area of major concern is the higher than allowable stresses found in the reinforcement over the interior support during the

cantilever test. This however is not a concern with the actual design because the bridge is designed as three simple spans and therefore no section is cantilevered or continuous over a support. The overhang sections were found to have more than adequate strength even though they will not receive live load on the actual bridge because a concrete barrier rail will be placed on them. The only test that resembles actual conditions that will exist on the bridge was the interior girder test, and this test proved the design to be adequate. Overall, the design is very conservative and there is no concern about failure of the GFRP reinforced deck.

5.4: Constructability

The construction of this deck was the first reinforced concrete construction performed by the researcher. The bottom mat of steel was laid and tied first. The steel bars were very heavy and could only be moved and lifted one or two at a time. The tying of the steel bars was quite simple. The top mat of GFRP reinforcing bars was laid second. The bars were very lightweight and were much less of a burden to carry around than the steel. The placing of the GFRP bars took a lot less time than the steel bars because of the weight and ability to lift more at a time. The only concerns with the construction were the plastic chairs used to support the bars, the flexibility and strength of the bars when stepped on by a 250 pound construction worker, and getting glass fibers in ones hands from handling the bars.

The plastic chairs used for this project were not ideal and are not recommended to be used. They were not designed very well and do not fit on top of the bottom mat at all. This will actually not be much of a problem at all in construction because contractors will more than likely used epoxy coated steel chairs. These are the same chairs that they

currently use for epoxy coated steel reinforcing bars. Having to tie the chairs to the bottom mat of steel was also not a problem at all. It took a little extra time to do, but not much at all especially in comparison to the time saved in placing the lighter GFRP bars. To avoid getting the fibers in ones hands, it is recommended that gloves be worn while handling the bars. This should not be a problem because construction workers usually wear gloves while placing steel bars.

The flexibility of the GFRP bars and the potential for shear strength loss due to flexural loads being applied by construction workers is a concern. The only way to prevent this problem from occurring is to either have the workers avoid stepping on the bars or only stepping on the bars close to where they are supported on chairs. This would only have to be done until the mat is mostly tied together and is not as flexible.

5.5: Recommendation for Further Research

Because there is still relatively little known about the behavior of FRP in concrete, there is still a lot of research to be done to insure optimal designs. If the designs stay the way they are now, overly conservative, no one will want to use FRP because the cost will exceed the benefits. This project was centered on the use of GFRP bars as the top mat of reinforcement in bridge decks and so will these recommendations for further research.

A major concern seen in the testing was the poor performance of the deck in negative moment over an interior support and the inability to accurately predict deflections, stresses, crack widths, or cracking load. This is a key area in bridge design because more and more bridges are being designed as continuous spans to eliminate joints in the bridge. It is recommended that further research be done in this area and that

methods and design procedures be developed that will insure conservative designs and will be able to accurately predict behavior.

It is also recommended that more research be done on the crack widths and shear strength, both one-way and two-way, of GFRP reinforced slabs. The current design equations appear to be extremely conservative in the areas of one-way shear and crack widths. Currently, there is no specific equation for the two-way shear capacity of a slab reinforced with FRP bars. The slab tested in this project was heavily reinforced with GFRP bars and this may be what contributed to its high two-way shear strength and more research should be done in this area.

Another research project that would be helpful is one that would develop effective moments of inertia and their centroids for cracked reinforced concrete sections. Currently, the stresses are being over-predicted because sections are being modeled using a cracked moment of inertia at the onset of cracking. This models the section as completely cracked which it is not, causing designs to be overly conservative.

More research should also be done in the area of cyclic loads on concrete slabs reinforced with FRP reinforcement. This would be very useful in studying the behavior of the decks, because these are the types of loads that an actual bridge deck receives while in service. The code currently has the maximum allowable stress in the reinforcing bars set at 20 percent of design tensile strength under cyclic loads to avoid failure due to fatigue. This is very conservative and does not allow designer to utilize the high strength of FRP.

REFRENCES

AASHTO. (1994). *AASHTO LRFD Bridge Design Specification,* Washington, D.C.

ACI Building Code Requirements for Structural Concrete and Commentary, ACI 318-99 (1999), American Concrete Institute Committee 318, Farmington Hills, MI.

ACI Control of Deflection in Concrete Structures, ACI 435R-95 (1995), American Concrete Institute Committee 435, Farmington Hills, MI.

ACI Guide for the Design and Construction of Concrete Reinforced with FRP Bars, ACI 440.1R-01 (2001), American Concrete Institute Committee 440, Farmington Hills, MI.

Bedard, Claude (1992). "Composite Reinforcing Bars: Assesing Their Use in Construction." *Concrete International: Design and Construction*, Vol. 14 No. 1, pp. 55-59.

Bradberry, T.E. (2001). "FRP-Bar-Reinforced Concrete Bridge Decks." *Transportation Research Board Proceedings, 80th Annual Meeting*., TRB, Washington, D.C.

Brown, V.L. and Bartholomew, C.L. (1993). "FRP Reinforcing Bars in Reinforced Concrete Members." *ACI Materials Journal*, Vol. 90 No. 1, pp. 34-39.

DeFreese, J.M. (2001). "Glass Fiber Reinforced Polymer Bars as the Top Mat Reinforcement for Bridge Decks." M.S. Thesis, Virginia Polytechnic Institute and State University, Blacksburg, U.S.

Deitz, D.H., Harik, I.E. and Gesund, H. (1999). "One-way Slabs Reinforced with Glass Fiber Reinforced Polymer Reinforcing Bars." *ACI Proceedings, 4th International Symp*., ACI, Detroit, pp. 279-286.

Erki, M.A. and Rizkalla, S.H. (1993). "FRP Reinforcement for Concrete Structures." *Concrete International: Design and Construction*, Vol. 15 No. 6, pp. 48-53.

Hassan, T., Abdelrahman, A., Tadros, G. and Rizkalla S. (2000). "Fibre Reinforced Polymer Reinforcing Bars For Bridge Decks." *Canadian Journal of Civil Engineering*, Vol. 27 No. 5, pp. 839-849.

Hyer, M. W. (1998). Stress Analysis of Fiber-Reinforced Composite Materials. Boston, McGraw-Hill.

Khalifa, M.A., Kuska, S.S.B. and Krieger, J. (1993). :Bridges Constructed Using Fiber Reinforced Plastics." *Concrete International: Design and Construction*, Vol. 15 No. 6, pp. 43-47.

Michaluk, C.R., Rizkalla, S., Tadros, G. and Benmokrane, B. (1998). "Flexural Behavior of One-way Concrete Slabs Reinforced by Fiber Reinforced Plastic Reinforcements." *ACI Structures Journal*, Vol. 95 No. 3, pp. 353-364.

Nanni, A., ed. (1993). Fiber-Reinforced-Plastic (FRP) Reinforcements for Concrete Structures: Properties and Applications. New York, Elsevier.

Pucher, A. (1977). *Einflufifelder Elastischer Platten – Influence Surfaces of Elastic Plates,* 5th ed. Vienna and New York: Springer-Verlag.

Rahman, A.H., Kingsley, C.Y. and Kobayashi, K. (2000). "Service and Ultimate Load Behavior of Bridge Deck Reinforced with Carbon FRP Grid." *Journal of Composites for Construction*, Vol. 4 No. 1, pp. 16-23.

RISA-2D (1993). *Educational RISA-2D (R) Version 3.00.* RISA Technologies, New York.

Tannous, F.E. and Saadatmanesh, H. (1998). "Environmental Effects on the Mechanical Properties of E-Glass FRP Rebars." *ACI Materials Journal*, Vol. 95 No. 9, pp. 87-100.

Thippeswamy, H. K., Franco, J. M. and GangaRao, H.V.S. (1998). "FRP Reinforcement in Bridge Deck." *Concrete International: Design and Construction*, Vol. 20 No. 6, pp. 47-50.

TTI FRP Reinforcing Bars in Bridge Decks: State of the Art Review, TTI Report 1520-2 (2000), Texas Transportation Institute, College Station, TX.

Yost, J.R., Gross, S.P. and Dinehart, D.W. (2001). "Shear Strength of Normal Strength Concrete Beams Reinforced with Deformed GFRP Bars." *Journal of Composites for Construction*, Vol. 5 No. 4, pp. 268-275.

APPENDIX A
INFLUENCE SURFACE METHOD

A.1: Calculation of Cracking Load Using Influence Surface Method

First, the cracking moment, M_{cr}, is calculated using Equation 4.4 in section 4.1.2.1.

$$M_{cr} = \frac{f_t I_t}{y}$$

$$f_t = 7.5\sqrt{f_c'} = 7.5\sqrt{5010} = 531.0\ psi$$

$$\Rightarrow M_{cr} = \frac{531 psi(629.9\ in.^4)}{4.31\ in.} = 77{,}605\ in.-lb$$

$$\Rightarrow 77{,}605\ in.-lb\left(\frac{1\ kip}{1000\ lb}\right)\left(\frac{1\ ft}{12\ in.}\right) = \underline{6.47\ ^{ft-kips}/_{ft.\,width}}$$

Next, the Pucher influence surface map, Figure A.1, is used with a 21 in. cantilever length and a load located 11 in. from the support. This corresponded to an influence surface value of 9.1. This is then used to calculate the cracking load, P_{cr}.

$$\frac{9.1 P_{cr}}{8\pi} = M_{cr} \Rightarrow P_{cr} = \frac{M_{cr} \cdot 8\pi}{9.1}$$

$$\Rightarrow P_{cr} = \frac{6.47\ ^{ft-kip}/_{ft} \cdot 8\pi}{9.1} = \underline{17.9\ kips = P_{cr}}$$

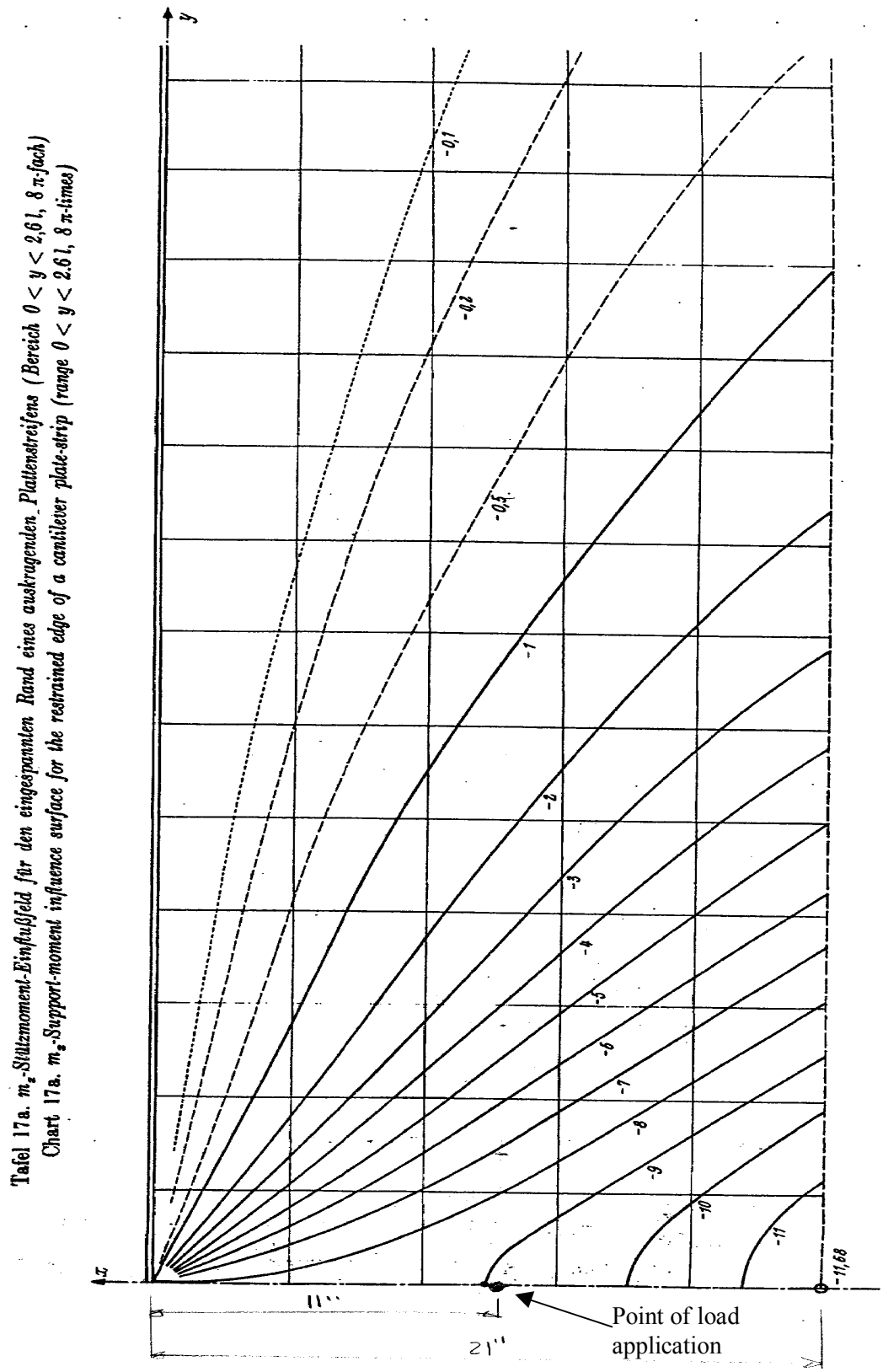

Figure A.1: Pucher Influence Surface Map

APPENDIX B
SAMPLE CALCULATIONS

B.1: Transformed Moment of Inertia for Cantilever Test

B.1.1: Uncracked Section, Interior Girder

The effective flange width of the slab was calculated to be 78 in. using Equation 4.13 from section 4.3.2. The W 27x94 girder has an area of 27.7 in.^{2} and a moment of inertia, I, of 3270 in.^{4}. The effective width of the slab contains 13 No. 6 GFRP bars each with an area of 0.44 in.^{2} and 13 No. 4 steel bars each with an area of 0.2 in.^{2}. The modulus of elasticity is 6300 ksi for the GFRP bars and 29,000 ksi for the steel bars and the steel girder. The concrete compressive strength is 6270 psi, corresponding to a modulus of elasticity of 4512 ksi. The girder is 26.92 in. tall and there is a 1 ½ in. concrete haunch on top of the girder. The slab is 7 ½ in. thick and is on top of the haunch. The centroid of the GFRP bars is 2 $^7/_8$ in. from the top of the slab and the centroid of the steel bars is 2 in. from the bottom of the slab.

First, the areas of the concrete and GFRP are transformed into equivalent steel areas. This is done by multiplying the areas by the modular ratios of concrete to steel, n_c, and of GFRP to steel, n_f.

$$n_c = \frac{4512\ ksi}{29000\ ksi} = 0.1556\,;\ n_f = \frac{6300\ ksi}{29000\ ksi} = 0.2172$$

$$A_t = 27.7\ in.^2 + 0.2\ in.^2(13) + 0.1556(1.5"\cdot 10" + 78"\cdot 7.5") + 0.2172(.44\ in.^2)(13) = \underline{124.9\ in.^2}$$

Next, the location of the centroid from the bottom of the girder, c_b, is calculated.

$$c_b = \frac{27.7\ in.^2(13.46") + 0.2\ in.^2(13)(30.42") + 0.1556(1.5"\cdot 10")(27.67")}{124.9\ in.^2}$$

$$+ \frac{(0.1556)(78"\cdot 7.5")(32.17") + 0.2172(.44\ in.^2)(13)(33.05")}{124.9\ in.^2} = \underline{27.9 \text{ in. from bottom of girder}}$$

Finally, the transformed moment of inertia for the section, I_t, is calculated.

$$I_t = 3270\,in.^4 + 27.7\,in.^2(27.9"-13.46")^2 + 0.2\,in.^2(13)(30.42"-27.9")^2 + 0.1556(1.5"\cdot 10")(27.9"-27.67")^2 + (0.1556)(78"\cdot 7.5")(32.17"-27.9)^2 + 0.2172(.44\,in.^2)(13)(33.05"-27.9")^2 + \tfrac{1}{12}(12.14")(7.5")^3 = \underline{11{,}182\,in.^4}$$

B.1.2: Cracked Section, Interior Girder

The transformed moment of inertia for the cracked section was calculated exactly the same way as for the uncracked section. The only difference between the two is that it is assumed that absolutely no concrete is present to add strength to the cracked section.

First, the area of the GFRP is transformed into an equivalent steel area. This is done by multiplying the area by the modular ratios of GFRP to steel, n_f.

$$n_f = \frac{6300\,ksi}{29000\,ksi} = 0.2172$$

$$A_t = 27.7\,in.^2 + 0.2\,in.^2(13) + 0.2172(.44\,in.^2)(13) = \underline{31.54\,in.^2}$$

Next, the location of the centroid from the bottom of the girder, c_b, is calculated.

$$c_b = \frac{27.7\,in.^2(13.46") + 0.2\,in.^2(13)(30.42") + 0.2172(.44\,in.^2)(13)(33.05")}{31.54\,in.^2} = \underline{15.63\,\text{in}}.$$

Finally, the cracked transformed moment of inertia for the section, I_{cr}, is calculated.

$$I_{cr} = 3270\,in.^4 + 27.7\,in.^2(15.63"-13.46")^2 + 0.2\,in.^2(13)(30.42"-15.63")^2 + 0.2172(.44\,in.^2)(13)(33.05"-15.63")^2 = \underline{4346\,in.^4}$$

B.2: Transformed Moment of Inertia of Overhang #1

B.2.1: Uncracked Section

The properties of the deck were calculated assuming the deck to be a 1 ft wide strip in the transverse direction. The depth of the overhang portion is 8 ½ in. The centroid of the GFRP bars is 2 $^3/_8$ in. from the top of the slab, the bars have an area of 0.93 in.^{2} per foot, and a modulus of elasticity, E_f, of 6300 ksi. The centroind of the steel bars is 6 $^1/_8$ in. from the top of the slab, the bars have an area of 0.66 in.^{2} per foot, and a modulus of elasticity, E_s, of 29,000 ksi. The concrete had a compressive strength, f_c', of 5010 psi, corresponding to a modulus of elasticity of 4036 ksi.

First, the areas of the steel and GFRP are transformed into equivalent concrete areas. This is done by multiplying the areas by the modular ratios of steel to concrete, n_s, and of GFRP to concrete, n_f.

$$n_s = \frac{29000\ ksi}{4036\ ksi} = 7.19\ ;\ n_f = \frac{6300\ ksi}{4036\ ksi} = 1.56$$

$$A_t = 12"\cdot 8.5" + 0.93\ in.^2(1.56-1) + 0.44\ in.^2(7.19-1) = \underline{106.6\ in.^2}$$

Next, the location of the centroid from the bottom of the slab, c_b, is calculated.

$$c_b = \frac{12"\cdot 8.5"(4.25") + 0.93\ in.^2(1.56-1)(6.125") + 0.44\ in.^2(7.19-1)(2.375")}{106.6\ in.^2} = \underline{4.19\ \text{in}}.$$

Finally, the transformed moment of inertia for the section, I_t, is calculated.

$$I_t = 12"\cdot 8.5"(4.25"-4.19")^2 + 0.93\ in.^2(1.56)(6.125"-4.19")^2 + 0.66\ in.^2(7.19-1)(4.19"-2.375")^2 + (1/12)\cdot 12"\cdot(8.5")^3 = \underline{629.9\ in.^4}$$

B.2.2: Cracked Section

Everything is the same for this calculation as for the uncracked calculation, except the fact that the concrete is now cracked. In order to calculate the cracked moment of inertia, I_{cr}, for the section, the centroid must first be located. The centroid is assumed to be below the steel reinforcement, and its location is measured to be a distance 'c' from the bottom of the slab. This assumption presumes that the steel is in tension after the section becomes cracked. To find the location of the centroid, 'c', the moment of area about the centroid due to tension is set equal to the moment af area about the centroid due to compression, and 'c' is solved for.

$$12"\cdot c\left(\frac{c}{2}\right) = 0.66\,in.^2\,(7.19)(2.375"-c) + 0.93\,in.^2\,(1.56)(6.125"-c)$$

$$\Rightarrow c^2 + 1.033c - 3.36 = 0$$

$$\Rightarrow c = \frac{-1.033 \pm \sqrt{1.033^2 - 4\cdot 1\cdot(-3.36)}}{2\cdot 1}$$

$$\Rightarrow \underline{c = 1.39"}$$

This proves the assumption of the centroid being below the steel correct. Finally, the cracked moment of inertia, I_{cr}, is calculated.

$$I_{cr} = (1/12)\cdot 12"(1.39")^3 + 12"\cdot 1.39"(0.695)^2 + 0.93\,in.^2\,(1.56)(6.125"-1.39")^2 + 0.66\,in.^2\,(7.19)(2.375"-1.39")^2 = \underline{47.9\,in.^4}$$

APPENDIX C
INFLUENCE FUNCTION

C.1: Negative Moment Over an Interior Support

In order to calculate the service moment needed for the cantilever test, an influence function was created using the program Microsoft Excel. The bridge that the lab prototype was modeled after is three spans with each span being a simple span. The span with the GFRP is 45 ft in length. Even though the bridge is three simple spans, the influence function is for a three span continuous bridge, each span being 45 ft in length, in order to create a negative moment over an interior support under service conditions. The program was created so that the negative moment would be produced over the first interior support, support B.

Five different truck loading arrangements along with a lane load were modeled in order to achieve the maximum service moment. The five different arrangements were; one HL-93 truck in either direction, two HL-93 trucks (train) in either direction, and a single tandem truck. The HL-93 trucks have three axles with the front axle having a load of 8 kips and the two rear axles having a load of 32 kips each. The tandem truck has two axles, each having a load of 25 kips. The lane load is a distributed load of 0.64 kips per ft length. The lane load was just applied in the influence regions that produced a negative moment, and produced a negative moment of 150 ft-kips. The maximum negative service moment was produced by a single HL-93 truck with its front, 8 kip, axle toward support A. The Excel sheet with the governing loading is shown below.

			One Design Truck Max Neg Moment W/ front facing A		Lane Load	
Support	Foot	Infl. Ord.	Truck Pos.	Moment	Position	Moment
A	0	0		0	0.32	0
	0.5	-0.00289		0	0.32	-0.0416
	1	-0.00578		0	0.32	-0.0832
	1.5	-0.00867		0	0.32	-0.1248
	2	-0.01156		0	0.32	-0.1664
	2.5	-0.01444		0	0.32	-0.208
	3	-0.01733		0	0.32	-0.2496
	3.5	-0.02022		0	0.32	-0.2912
	4	-0.02311	8	-8.32	0.32	-0.3328
	4.5	-0.026		0	0.32	-0.3744
	5	-0.02878		0	0.32	-0.4144
	5.5	-0.03156		0	0.32	-0.4544
	6	-0.03433		0	0.32	-0.4944
	6.5	-0.03711		0	0.32	-0.5344
	7	-0.03989		0	0.32	-0.5744
	7.5	-0.04267		0	0.32	-0.6144
	8	-0.04544		0	0.32	-0.6544
	8.5	-0.04822		0	0.32	-0.6944
	9	-0.051		0	0.32	-0.7344
	9.5	-0.05344		0	0.32	-0.7696
	10	-0.05589		0	0.32	-0.8048
	10.5	-0.05833		0	0.32	-0.84
	11	-0.06078		0	0.32	-0.8752
	11.5	-0.06322		0	0.32	-0.9104
	12	-0.06567		0	0.32	-0.9456
	12.5	-0.06811		0	0.32	-0.9808
	13	-0.07056		0	0.32	-1.016
	13.5	-0.073		0	0.32	-1.0512
	14	-0.07489		0	0.32	-1.0784
	14.5	-0.07678		0	0.32	-1.1056
	15	-0.07867		0	0.32	-1.1328
	15.5	-0.08056		0	0.32	-1.16
	16	-0.08244		0	0.32	-1.1872
	16.5	-0.08433		0	0.32	-1.2144
	17	-0.08622		0	0.32	-1.2416
	17.5	-0.08811		0	0.32	-1.2688
	18	-0.09	32	-129.6	0.32	-1.296
	18.5	-0.09111		0	0.32	-1.312
	19	-0.09222		0	0.32	-1.328
	19.5	-0.09333		0	0.32	-1.344
	20	-0.09444		0	0.32	-1.36
	20.5	-0.09556		0	0.32	-1.376
	21	-0.09667		0	0.32	-1.392
	21.5	-0.09778		0	0.32	-1.408
	22	-0.09889		0	0.32	-1.424
	22.5	-0.1		0	0.32	-1.44
	23	-0.10022		0	0.32	-1.4432

			One Design Truck Max Neg Moment W/ front facing A		Lane Load	
Support	Foot	Infl. Ord.	Truck Pos.	Moment	Position	Moment
	23.5	-0.10044		0	0.32	-1.4464
	24	-0.10067		0	0.32	-1.4496
	24.5	-0.10089		0	0.32	-1.4528
	25	-0.10111		0	0.32	-1.456
	25.5	-0.10133		0	0.32	-1.4592
	26	-0.10156		0	0.32	-1.4624
	26.5	-0.10178		0	0.32	-1.4656
	27	-0.102		0	0.32	-1.4688
	27.5	-0.10122		0	0.32	-1.4576
	28	-0.10044		0	0.32	-1.4464
	28.5	-0.09967		0	0.32	-1.4352
	29	-0.09889		0	0.32	-1.424
	29.5	-0.09811		0	0.32	-1.4128
	30	-0.09733		0	0.32	-1.4016
	30.5	-0.09656		0	0.32	-1.3904
	31	-0.09578		0	0.32	-1.3792
	31.5	-0.095		0	0.32	-1.368
	32	-0.093	32	-133.92	0.32	-1.3392
	32.5	-0.091		0	0.32	-1.3104
	33	-0.089		0	0.32	-1.2816
	33.5	-0.087		0	0.32	-1.2528
	34	-0.085		0	0.32	-1.224
	34.5	-0.083		0	0.32	-1.1952
	35	-0.081		0	0.32	-1.1664
	35.5	-0.079		0	0.32	-1.1376
	36	-0.077		0	0.32	-1.1088
	36.5	-0.07356		0	0.32	-1.0592
	37	-0.07011		0	0.32	-1.0096
	37.5	-0.06667		0	0.32	-0.96
	38	-0.06322		0	0.32	-0.9104
	38.5	-0.05978		0	0.32	-0.8608
	39	-0.05633		0	0.32	-0.8112
	39.5	-0.05289		0	0.32	-0.7616
	40	-0.04944		0	0.32	-0.712
	40.5	-0.046		0	0.32	-0.6624
	41	-0.04089		0	0.32	-0.5888
	41.5	-0.03578		0	0.32	-0.5152
	42	-0.03067		0	0.32	-0.4416
	42.5	-0.02556		0	0.32	-0.368
	43	-0.02044		0	0.32	-0.2944
	43.5	-0.01533		0	0.32	-0.2208
	44	-0.01022		0	0.32	-0.1472
	44.5	-0.00511		0	0.32	-0.0736
B	45	0		0	0.32	0
	45.5	-0.00433		0	0.32	-0.0624
	46	-0.00867		0	0.32	-0.1248

			One Design Truck Max Neg Moment W/ front facing A		Lane Load	
Support	Foot	Infl. Ord.	Truck Pos.	Moment	Position	Moment
	46.5	-0.013		0	0.32	-0.1872
	47	-0.01733		0	0.32	-0.2496
	47.5	-0.02167		0	0.32	-0.312
	48	-0.026		0	0.32	-0.3744
	48.5	-0.03033		0	0.32	-0.4368
	49	-0.03467		0	0.32	-0.4992
	49.5	-0.039		0	0.32	-0.5616
	50	-0.04178		0	0.32	-0.6016
	50.5	-0.04456		0	0.32	-0.6416
	51	-0.04733		0	0.32	-0.6816
	51.5	-0.05011		0	0.32	-0.7216
	52	-0.05289		0	0.32	-0.7616
	52.5	-0.05567		0	0.32	-0.8016
	53	-0.05844		0	0.32	-0.8416
	53.5	-0.06122		0	0.32	-0.8816
	54	-0.064		0	0.32	-0.9216
	54.5	-0.06544		0	0.32	-0.9424
	55	-0.06689		0	0.32	-0.9632
	55.5	-0.06833		0	0.32	-0.984
	56	-0.06978		0	0.32	-1.0048
	56.5	-0.07122		0	0.32	-1.0256
	57	-0.07267		0	0.32	-1.0464
	57.5	-0.07411		0	0.32	-1.0672
	58	-0.07556		0	0.32	-1.088
	58.5	-0.077		0	0.32	-1.1088
	59	-0.07733		0	0.32	-1.1136
	59.5	-0.07767		0	0.32	-1.1184
	60	-0.078		0	0.32	-1.1232
	60.5	-0.07833		0	0.32	-1.128
	61	-0.07867		0	0.32	-1.1328
	61.5	-0.079		0	0.32	-1.1376
	62	-0.07933		0	0.32	-1.1424
	62.5	-0.07967		0	0.32	-1.1472
	63	-0.08		0	0.32	-1.152
	63.5	-0.07944		0	0.32	-1.144
	64	-0.07889		0	0.32	-1.136
	64.5	-0.07833		0	0.32	-1.128
	65	-0.07778		0	0.32	-1.12
	65.5	-0.07722		0	0.32	-1.112
	66	-0.07667		0	0.32	-1.104
	66.5	-0.07611		0	0.32	-1.096
	67	-0.07556		0	0.32	-1.088
	67.5	-0.075		0	0.32	-1.08
	68	-0.07378		0	0.32	-1.0624
	68.5	-0.07256		0	0.32	-1.0448
	69	-0.07133		0	0.32	-1.0272

			One Design Truck Max Neg Moment W/ front facing A		Lane Load	
Support	Foot	Infl. Ord.	Truck Pos.	Moment	Position	Moment
	69.5	-0.07011		0	0.32	-1.0096
	70	-0.06889		0	0.32	-0.992
	70.5	-0.06767		0	0.32	-0.9744
	71	-0.06644		0	0.32	-0.9568
	71.5	-0.06522		0	0.32	-0.9392
	72	-0.064		0	0.32	-0.9216
	72.5	-0.06233		0	0.32	-0.8976
	73	-0.06067		0	0.32	-0.8736
	73.5	-0.059		0	0.32	-0.8496
	74	-0.05733		0	0.32	-0.8256
	74.5	-0.05567		0	0.32	-0.8016
	75	-0.054		0	0.32	-0.7776
	75.5	-0.05233		0	0.32	-0.7536
	76	-0.05067		0	0.32	-0.7296
	76.5	-0.049		0	0.32	-0.7056
	77	-0.04711		0	0.32	-0.6784
	77.5	-0.04522		0	0.32	-0.6512
	78	-0.04333		0	0.32	-0.624
	78.5	-0.04144		0	0.32	-0.5968
	79	-0.03956		0	0.32	-0.5696
	79.5	-0.03767		0	0.32	-0.5424
	80	-0.03578		0	0.32	-0.5152
	80.5	-0.03389		0	0.32	-0.488
	81	-0.032		0	0.32	-0.4608
	81.5	-0.03011		0	0.32	-0.4336
	82	-0.02822		0	0.32	-0.4064
	82.5	-0.02633		0	0.32	-0.3792
	83	-0.02444		0	0.32	-0.352
	83.5	-0.02256		0	0.32	-0.3248
	84	-0.02067		0	0.32	-0.2976
	84.5	-0.01878		0	0.32	-0.2704
	85	-0.01689		0	0.32	-0.2432
	85.5	-0.015		0	0.32	-0.216
	86	-0.01333		0	0.32	-0.192
	86.5	-0.01167		0	0.32	-0.168
	87	-0.01		0	0.32	-0.144
	87.5	-0.00833		0	0.32	-0.12
	88	-0.00667		0	0.32	-0.096
	88.5	-0.005		0	0.32	-0.072
	89	-0.00333		0	0.32	-0.048
	89.5	-0.00167		0	0.32	-0.024
C	90	0		0	0.32	0
	90.5	0.001222		0		0
	91	0.002444		0		0
	91.5	0.003667		0		0
	92	0.004889		0		0

			One Design Truck Max Neg Moment W/ front facing A		Lane Load	
Support	Foot	Infl. Ord.	Truck Pos.	Moment	Position	Moment
	92.5	0.006111		0		0
	93	0.007333		0		0
	93.5	0.008556		0		0
	94	0.009778		0		0
	94.5	0.011		0		0
	95	0.011889		0		0
	95.5	0.012778		0		0
	96	0.013667		0		0
	96.5	0.014556		0		0
	97	0.015444		0		0
	97.5	0.016333		0		0
	98	0.017222		0		0
	98.5	0.018111		0		0
	99	0.019		0		0
	99.5	0.019556		0		0
	100	0.020111		0		0
	100.5	0.020667		0		0
	101	0.021222		0		0
	101.5	0.021778		0		0
	102	0.022333		0		0
	102.5	0.022889		0		0
	103	0.023444		0		0
	103.5	0.024		0		0
	104	0.024222		0		0
	104.5	0.024444		0		0
	105	0.024667		0		0
	105.5	0.024889		0		0
	106	0.025111		0		0
	106.5	0.025333		0		0
	107	0.025556		0		0
	107.5	0.025778		0		0
	108	0.026		0		0
	108.5	0.025889		0		0
	109	0.025778		0		0
	109.5	0.025667		0		0
	110	0.025556		0		0
	110.5	0.025444		0		0
	111	0.025333		0		0
	111.5	0.025222		0		0
	112	0.025111		0		0
	112.5	0.025		0		0
	113	0.024667		0		0
	113.5	0.024333		0		0
	114	0.024		0		0
	114.5	0.023667		0		0
	115	0.023333		0		0

			One Design Truck Max Neg Moment W/ front facing A		Lane Load	
Support	Foot	Infl. Ord.	Truck Pos.	Moment	Position	Moment
	115.5	0.023		0		0
	116	0.022667		0		0
	116.5	0.022333		0		0
	117	0.022		0		0
	117.5	0.021556		0		0
	118	0.021111		0		0
	118.5	0.020667		0		0
	119	0.020222		0		0
	119.5	0.019778		0		0
	120	0.019333		0		0
	120.5	0.018889		0		0
	121	0.018444		0		0
	121.5	0.018		0		0
	122	0.017444		0		0
	122.5	0.016889		0		0
	123	0.016333		0		0
	123.5	0.015778		0		0
	124	0.015222		0		0
	124.5	0.014667		0		0
	125	0.014111		0		0
	125.5	0.013556		0		0
	126	0.013		0		0
	126.5	0.012333		0		0
	127	0.011667		0		0
	127.5	0.011		0		0
	128	0.010333		0		0
	128.5	0.009667		0		0
	129	0.009		0		0
	129.5	0.008333		0		0
	130	0.007667		0		0
	130.5	0.007		0		0
	131	0.006222		0		0
	131.5	0.005444		0		0
	132	0.004667		0		0
	132.5	0.003889		0		0
	133	0.003111		0		0
	133.5	0.002333		0		0
	134	0.001556		0		0
	134.5	0.000778		0		0
D	135	0		0		0
	Total Moment			-272		-150

VITA

Jason Cawrse was born to Patricia and Leonard Cawrse on February 3, 1978 in Columbia, SC and was raised in Charlotte, NC. He graduated from Providence Senior High School in June, 1996. He then attended Virginia Polytechnic Institute and State University (Virginia Tech) from 1996 to 2000, where he received his Bachelor of Science degree in Civil Engineering. He continued his studies at Virginia Tech from 2000 to 2002, where he received his Master of Science degree in Civil Engineering with and emphasis on Structural Engineering. Master Jason Cawrse accepted a job in bridge design with Michael Baker Jr., Inc. working in Blacksburg, VA with Dr. Gregor Wollmann out of their Charleston, WV office.